STEATOSIS IN NON ALCOHOLIC FATTY LIVER DISEASE

Adam Phillip Levene

Imperial College London

Department of Medicine

Division of Experimental Medicine

Centre for Pathology

MD (Res) Thesis

2009-2012

Statement of Originality

The work contained in the thesis is my own work and all other work has been appropriately referenced.

Abstract

Non-alcoholic fatty liver disease is the commonest cause of chronic liver disease in developed countries.

The accurate assessment of steatosis is central to the diagnosis of non-alcoholic fatty liver disease. I compared the assessment of steatosis by histology, biochemical triglyceride assays, digital image analysis, with and without Oil Red-O staining, in mouse livers and human liver biopsies. In each case Oil Red-O digital image analysis was the most reliable technique for quantitating steatosis.

I then investigated a potential, non-invasive technique for distinguishing steatosis from steatohepatitis as only the latter causes progressive liver disease. The liver contains fluorophores which can be detected by autofluorescence spectroscopy. The fluorophore levels vary depending on the levels of oxidative stress and fibrosis within the liver. Mouse and human livers, were assessed to measure the fluorescence intensity at different wavelengths and this was compared with the histology. The probe was able to accurately identify biopsies which had inflammation and fibrosis with a high degree of sensitivity and specificity.

Autophagocytosis has recently been suggested to play a role in fat metabolism. Using liver differentiated HUH7 cells grown in normal or oleate containing media with or without Rapamycin (an autophagocytosis activator) the role of autophagocytosis was investigated. This involved examining steatosis by Oil Red-O digital image analysis,

biochemical triglyceride assays, electron microscopy and confocal immunofluorescence. I concluded that activating autophagocytosis decreased the levels of steatosis within the cells.

This work has shown Oil Red-O digital image analysis is the most accurate way of assessing steatosis within the liver, that autofluorescence spectroscopy has the ability to distinguish, in real-time, isolated steatosis from steatohepatitis and that autophagocytosis has a role in fat metabolism within the liver which may be exploited therapeutically.

Abbreviations

ALT – Alanine aminotransferase

ATG – Autophagy related gene

AV – Annexin V

BMI – Body mass index

CRN – Clinical research network

DAPI – 4-6-Diamidino-2-phenylindole

DIA – Digital image analysis

DMEM – Dulbecco's modification of Eagle's medium

FACS – Fluorescence activated cell sorting

FAD – Flavin adenine dinucleotide

FITC – Fluorescein isothiocyanate

GGT – Gamma glutamyl transpeptidase

HBV – Hepatitis B virus

HbsAg – Hepatitis B surface antigen

HCV – Hepatitis C virus

H&E – Haematoxylin and eosin

HFD – High fat diet

MCD – Methionine choline deficient

MDA – Malondialdehyde

MTOR – Mammalian target of Rapamycin

NADH – Nicotinamide adenine dinucleotide

NADPH – Nicotinamide adenine dinucleotide phosphate

NAFLD – Non-alcoholic fatty liver disease

NAS – Non-alcoholic fatty liver disease activity score

NASH – Non-alcoholic steatohepatitis

OD – Optical density

ORO – Oil red-O

PBS – Phosphate buffered saline

PI – Propidium iodide

PS – Phosphatidyl serine

RNA – Ribonucleic acid

ROS – Reactive oxygen species

SMLR - Sparse multinomial logistic regression

TBARS - Thiobarbituric acid reactive substances

Table of Contents

STATEMENT OF ORIGINALITY **2**

ABSTRACT **3**

ABBREVIATIONS **5**

GENERAL INTRODUCTION **15**

1.1 NON-ALCOHOLIC FATTY LIVER DISEASE BACKGROUND 15
1.2 EPIDEMIOLOGY AND DISEASE NATURAL HISTORY OF NON-ALCOHOLIC FATTY LIVER DISEASE 17
1.3 PATHOGENESIS OF NON-ALCOHOLIC FATTY LIVER DISEASE 20
1.4 HISTOPATHOLOGY OF NON-ALCOHOLIC FATTY LIVER DISEASE 21

THE QUANTIFICATION OF STEATOSIS IN NON-ALCOHOLIC FATTY LIVER DISEASE: THE POTENTIAL USE OF OIL RED-O **28**

2.1. INTRODUCTION 28
2.2. AIMS 30
2.3. METHODOLOGY 30
2.3.1. Rationale *30*
2.3.2. Materials *31*
2.3.2.1. Animal husbandry 31
2.3.2.2. Liver tissue 31
2.3.2.3. Human liver tissue 32
2.3.2.4. Histopathology and special stains in mouse liver tissue 32
2.3.2.5. Histopathology and special stains in human liver tissue 33
2.3.2.6. Digital image analysis 34
2.3.2.7. Triglyceride quantification 36
2.3.2.8. Magnetic resonance imaging steatosis quantification 37
2.3.2.9. Statistical analysis 38
2.4. RESULTS 38
2.4.1. Mouse study *38*
2.4.1.1. Liver and body weights 38
2.4.1.2. Biochemical analysis of hepatic triglyceride content 40
2.4.1.3. Comparison of steatosis quantification methods with hepatic triglyceride content 41
2.4.1.3.1. H&E histopathologist steatosis assessment 44
2.4.1.3.2. ORO histopathologist steatosis assessment 45
2.4.1.3.3. H&E DIA steatosis assessment 46
2.4.1.3.4. ORO DIA steatosis assessment 46
2.4.1.4. The size of steatosis as assessed by ORO DIA 48
2.4.1.5. The zonation of steatosis as assessed by ORO DIA 51
2.4.2. Human liver biopsy study *53*
2.4.2.1. Comparison of steatosis quantification methods with hepatic triglyceride content 53
2.4.2.1.1. H&E histopathologist steatosis assessment 55
2.4.2.1.2. H&E DIA steatosis assessment 56
2.4.2.1.3. ORO DIA steatosis assessment 56
2.4.2.1.4. MRI Steatosis Assessment 56
2.5. DISCUSSION 57
2.5.1. The merits of the various techniques for steatosis assessment *57*
2.5.1.1. ORO use in human liver biopsies 58
2.5.2. The reasoning for triglyceride quantification *60*
2.5.3. Steatosis size assessment and comparison with previous studies *60*
2.5.4. Steatosis zonation assessment *62*
2.5.5. The future use of ORO DIA and NAS *62*
2.5.6. Conclusions *63*

EXPLORING THE USE OF MULTI-EXCITATION FLUORESCENCE SPECTROSCOPY IN THE DIAGNOSIS OF NON-ALCOHOLIC FATTY LIVER DISEASE. 65

3.1. INTRODUCTION 65
3.1.1. Diagnosis of NASH 65
3.1.2. Autofluorescence spectroscopy 66
3.1.2.1. Photobleaching phenomenon 70
3.1.3. Mouse models of NAFLD 70
3.2. AIMS 73
3.3. METHODOLOGY 73
3.3.1. Animal husbandry 73
3.3.2. Liver tissue and blood for MCD model of NAFLD 73
3.3.3. Liver tissue and blood for HFD/Fructose model of NAFLD 74
3.3.4. Human liver tissue 76
3.3.5. Histopathology and special stains 76
3.3.6. Malondialdehyde immunohistochemistry 76
3.3.6.1. Rationale 76
3.3.6.2. Deparaffinisation 76
3.3.6.3. Blocking of endogenous peroxidise activity 77
3.3.6.4. Antigen retrieval 77
3.3.6.5. Incubation with the primary antibody 77
3.3.6.6. Incubation with the secondary antibody 78
3.3.6.7. Application of the DAB/Chromogen detection system 78
3.3.6.8. Counterstaining and mounting 78
3.3.7. Thiobarbituric Acid Reactive Substances as a Marker of Oxidative Stress 78
3.3.8. Plasma Alanine AminoTransferase levels as a biochemical marker of hepatitis 79
3.3.9. Autofluorescence spectroscopy system 80
3.3.9.1. Autofluorescence data acquisition 82
3.3.9.2. Autofluorescence data processing and analysis 83
3.3.9.3. Photobleaching data acquisition 84
3.3.9.4. Photobleaching data processing and analysis 85
3.3.10. Statistical analysis 85
3.4. RESULTS 86
3.4.1. MCD study results 86
3.4.1.1. Phenotypic differences in experimental groups 86
3.4.1.2. H&E and Sirius Red stains 87
3.4.1.3. MDA immunohistochemistry 90
3.4.1.4. TBARS assay 91
3.4.1.5. ALT biochemistry 93
3.4.1.6. Autofluorescence spectroscopy 95
3.4.2. HFD/Fructose study results 100
3.4.2.1. Phenotypic differences in experimental groups 100
3.4.2.2. H&E & Sirius Red stains 100
3.4.2.3. ALT biochemistry 103
3.4.2.4. Autofluorescence spectroscopy results 104
3.4.2.5. Photobleaching results 109
3.4.3. Human liver biopsies 110
3.4.3.1. H&E & Sirius Red stains 110
3.4.3.2. ALT biochemistry 111
3.4.3.3. Autofluorescence spectroscopy results 112
3.5. DISCUSSION 114

THE ROLE OF AUTOPHAGOCYTOSIS IN NON-ALCOHOLIC FATTY LIVER DISEASE 122

4.1. INTRODUCTION 122
4.2. AIMS 126
4.3. METHODOLOGY 126
4.3.1. Overall cell culture methods 126
4.3.2. Confocal immunofluorescence experiment 127
4.3.2.1. Cell culture methods for confocal immunofluorescence experiment 127

4.3.2.1.1. Cell preparation for confocal immunofluorescence DMEM ± Rapamycin experiment 128
4.3.2.1.2. Cell preparation for confocal immunofluorescence Oleate DMEM ± Rapamycin experiment 129
4.3.2.1.3. Protocol for the addition of BODIPY and LAMP1 immunofluorescent markers 129
4.3.2.2. Confocal immunofluorescence microscopy 130
4.3.2.3. Confocal immunofluorescence digital image analysis 131
4.3.3. Electron microscopy experiment *132*
4.3.3.1. Cell culture methods for electron microscopy experiment 132
4.3.3.1.1. Cell preparation for electron microscopy DMEM ± Rapamycin experiment 133
4.3.3.1.2. Cell preparation for electron microscopy Oleate DMEM ± Rapamycin experiment 134
4.3.3.2. Electron microscopy and analysis 134
4.3.4. Oil Red-O digital image analysis experiment *135*
4.3.4.1. Cell culture methods for Oil Red-O digital image analysis experiment 135
4.3.4.1.1. Cell preparation for Oil Red-O DMEM ± Rapamycin experiment 136
4.3.4.1.2. Cell preparation for Oil Red-O Oleate DMEM ± Rapamycin experiment 137
4.3.4.2. Oil Red-O digital image analysis 137
4.3.5. Triglyceride assay *139*
4.3.5.1. Cell culture methods for triglyceride assay 139
4.3.5.1.1. Cell preparation for triglyceride DMEM and Oleate DMEM ± Rapamycin assay 140
4.3.5.2. Triglyceride quantification 140
4.3.6. Fluorescence activated cell sorting experiments *142*
4.3.6.1. Cell culture methods for fluorescence activated cell sorting for reactive oxygen species detection 142
4.3.6.1.1. Cell preparation for fluorescence activated cell sorting reactive oxygen species detection DMEM ± Rapamycin experiment 143
4.3.6.1.2. Cell preparation for fluorescence activated cell sorting reactive oxygen species detection Oleate DMEM ± Rapamycin experiment 145
4.3.6.2. Cell culture methods for fluorescence activated cell sorting for apoptosis detection 145
4.3.6.2.1. Cell preparation for fluorescence activated cell sorting apoptosis detection DMEM ± Rapamycin experiment 146
4.3.6.2.2. Cell preparation for fluorescence activated cell sorting apoptosis detection Oleate DMEM ± Rapamycin experiment 147
4.3.6.2.3. Protocol for the addition of Annexin V and Propidium Iodide immunofluorescent markers 147
4.3.6.3. Fluorescence activated cell sorting 148
4.4. RESULTS 149
4.4.1. Confocal immunofluorescence *149*
4.4.1.1. Lipid droplet number & area 149
4.4.1.2. Co-localisation of lysosomes and lipids 154
4.4.2. Electron microscopy *160*
4.4.3. Oil Red-O digital image analysis *169*
4.4.4 Triglyceride assay analysis *171*
4.4.5. Fluorescence activated cell sorting analysis *173*
4.5. DISCUSSION 183
OVERALL CONCLUSIONS 189
5.1. FUTURE WORK 190
PUBLICATIONS & PRESENTATIONS DERIVED FROM THE THESIS 192
ACKNOWLEDGEMENTS 195

List of Figures

Figure 1: Definition of the metabolic syndrome 15
Figure 2: The natural history of NAFLD 19
Figure 3: Scatter graph of the three colour differentiation used in ORO DIA (red = fat, white = cytoplasm, blue = nuclei) 35
Figure 4: Graph showing mean body weights of the mice in each study group over the course of the HFD/Fructose experiment ± 1 standard error of the mean 40
Figure 5: The mean triglyceride concentration for each mouse study group and the mean percentage steatosis for each mouse study group using H&E DIA, H&E expert pathologists and ORO DIA ± 1 standard error of the mean 43
Figure 6a: H&E stained slide from mouse liver with no steatosis. Figure 6b: ORO stained slide of the same mouse liver showing mainly microvesicular steatosis. x400 original magnification 46
Figure 7a: H&E stained slide from mouse liver with marked mainly macrovesicular steatosis. Figure 7b: ORO stained slide of the same mouse liver showing mainly macrovesicular steatosis. x400 original magnification 47
Figure 8: The mean percentage of microvesicular and macrovesicular steatosis present in each zone of the liver for each experimental group 52
Figure 9: Scatter graphs showing percentage steatosis by a)ORO DIA, b)H&E pathologist, c)H&E DIA and d)MRI compared to triglyceride concentration in the five human patients including the best fit line and R^2 value 55
Figure 10: Emission spectra of endogenous fluorophores at 375nm excitation 67
Figure 11: Experimental set-up of multi excitation wavelength fluorescence spectroscopy probe 81
Figure 12: Graph showing mean body weights of the mice in each experimental group over the course of the study ± 1 standard error of the mean 87
Figure 13: H&E stained sections of mouse livers. a) Db/Db mouse fed MCD showing steatosis, lobular inflammation and hepatocyte ballooning, b) Db/Db mouse fed standard Chow showing steatosis only, c) Db/m mouse fed standard Chow. x400 original magnification 89
Figure 14: Sirius Red stained sections of mouse livers. a) Db/Db mouse fed MCD showing mild, zone 3, perisinusoidal fibrosis, stage 1A. b) Db/Db mouse fed standard Chow showing a normal architecture with no fibrosis. x400 original magnification 90
Figure 15: MDA immunohistochemistry on mouse livers. a & b) Db/Db mice fed an MCD diet, showing positive brown granular staining in the cytoplasm of hepatocytes. c) Db/Db mice fed a standard Chow diet showing no staining. d) Db/m mice fed a standard Chow diet showing no staining, x400 original magnification 91
Figure 16: Mean malondialdehyde concentration in the livers of the MCD study group mice ±SEM 93
Figure 17: Mean ALT levels in the plasma of the MCD study group mice ±SEM 95

Figure 18: Mean spectra at 375 nm excitation ± SEM for the MCD study ……..... 96
Figure 19: Mean spectra at 405 nm excitation ± SEM for the MCD study 97
Figure 20: Posterior probability of fluorescence spectra from the sites of probe readings to belong to their correct (as classified by histopathology) disease group in the MCD study 99
Figure 21: H&E stained sections of mouse liver. a) Mice fed HFD and fructose showing steatosis, lobular inflammation and ballooned hepatocytes. b) Mice fed HFD and water showing steatosis and an occasional ballooned hepatocyte. c) Mice fed chow and water (same with fructose) showing normal liver histology. x400 original magnification 102
Figure 22: Mean ALT levels in the plasma of the HFD/Fructose study mice ±SEM 104
Figure 23: Mean spectra at 375 nm excitation ± SEM in the HFD/Fructose study ……..... 105
Figure 24: Mean spectra at 405 nm excitation ± SEM in the HFD/Fructose study ……..... 106
Figure 25: Posterior probability of fluorescence spectra from the sites of probe readings to belong to their correct (as classified by histopathology) disease group in the HFD/Fructose study ……..... 108
Figure 26: Mean photobleaching rates at 375nm excitation in the HFD/Fructose study ……..... 109
Figure 27: Photomicrograph showing steatosis, hepatocyte ballooning, lobular inflammation and nuclear vacuolation in a patient with NASH. Original magnification x400 111
Figure 28: Mean spectra at 375 nm excitation ± SEM in the HFD/Fructose study ……..... 113
Figure 29: Schematic diagram of autophagocytosis in lipid metabolism 123
Figure 30: Schematic chamber slides for the confocal immunofluorescence experiment 127
Figure 31: Schematic chamber slides for the electron microscopy experiment 132
Figure 32: Schematic 6 well plates for the Oil Red-O digital image analysis experiment 135
Figure 33: Scatter graph of the three colour differentiation used in ORO DIA (red =fat, blue=cells, white=background) 139
Figure 34: Schematic 6 well plates for the triglyceride assay experiment 140
Figure 35: Schematic 6 well plates for the fluorescence activated cell sorting reactive oxygen species experiment 143
Figure 36: Schematic 6 well plates for the fluorescence activated cell sorting apoptosis detection experiment 146
Figure 37: Confocal immunofluorescence images with BODIPY staining in HUH7 cells grown in Oleate DMEM with and without Rapamycin 149
Figure 38: Confocal immunofluorescence images with BODIPY staining in HUH7 cells grown in DMEM with and without Rapamycin 150
Figure 39: Mean number of lipid droplets ± SEM per HUH7 cell in different growth mediums 152
Figure 40: Mean lipid droplet area (pixels^2) ± SEM per HUH7 cell in different growth mediums 153
Figure 41: Confocal immunofluorescence in HUH7 cells grown in Oleate DMEM without Rapamycin . 155
Figure 42: Confocal immunofluorescence in HUH7 cells grown in Oleate DMEM with Rapamycin 156
Figure 43: Confocal immunofluorescence in HUH7 cells grown in DMEM without Rapamycin 157

Figure 44: Confocal immunofluorescence in HUH7 cells grown in DMEM with Rapamycin 158
Figure 45: Mean percentage area co-localisation ±SEM between LAMP1 and BODIPY in HUH7 cells grown in different growth mediums 160
Figure 46: Electron microscopy photomicrograph, original magnification x25000 from an HUH7 cell grown in DMEM only 161
Figure 47: Electron microscopy photomicrograph , original magnification x3000 from an HUH7 cell grown in DMEM only 162
Figure 48: Electron microscopy photomicrograph, original magnification x5000 from an HUH7 cell grown in DMEM with Rapamycin 163
Figure 49: Electron microscopy photomicrograph, original magnification x25000 from an HUH7 cell grown in DMEM with Rapamycin 164
Figure 50: Electron microscopy photomicrograph , original magnification x6000 from an HUH7 cell grown in Oleate DMEM 165
Figure 51: Electron microscopy photomicrograph, original magnification x15000 from an HUH7 cell grown in Oleate DMEM 166
Figure 52: Electron microscopy photomicrograph , original magnification x3000 from an HUH7 cell grown in Oleate DMEM with Rapamycin 167
Figure 53: Electron microscopy photomicrograph, original magnification x12000 from an HUH7 cell grown in Oleate DMEM with Rapamycin 168
Figure 54: Oil Red-O staining in HUH7 cells grown in Oleate DMEM or Normal DMEM ± Rapamycin 169
Figure 55: Oil Red-O digital image analysis mean percentage steatosis ± SEM in HUH7 cells grown in Oleate DMEM ± Rapamycin or DMEM ± Rapamycin 170
Figure 56: Mean triglyceride concentration (nmol per well) ± SEM for HUH7 cells grown in Oleate DMEM ± Rapamycin or DMEM ± Rapamycin 172
Figure 57: A contour diagram of AV/PI obtained by flow cytometry of HUH7 cells grown in DMEM only. AV fluorescence is presented on the horizontal axis and PI fluorescence on the vertical axis 175
Figure 58: A contour diagram of AV/PI obtained by flow cytometry of HUH7 cells grown in DMEM with Rapamycin. AV fluorescence is presented on the horizontal axis and PI fluorescence on the vertical axis 176
Figure 59: A contour diagram of AV/PI obtained by flow cytometry of HUH7 cells grown in an oleate DMEM only. AV fluorescence is presented on the horizontal axis and PI fluorescence on the vertical axis 177
Figure 60: A contour diagram of AV/PI obtained by flow cytometry of HUH7 cells grown in an oleate DMEM with Rapamycin. AV fluorescence is presented on the horizontal axis and PI fluorescence on the vertical axis 178

Figure 61: A contour diagram of carboxy-H2DFFDA obtained by flow cytometry of HUH7 cells grown in DMEM only. FITC fluorescence is presented on the horizontal axis and forward scatter on the vertical axis 179
Figure 62: A contour diagram of carboxy-H2DFFDA obtained by flow cytometry of HUH7 cells grown in DMEM with Rapamycin. FITC fluorescence is presented on the horizontal axis and forward scatter on the vertical axis 180
Figure 63: A contour diagram of carboxy-H2DFFDA obtained by flow cytometry of HUH7 cells grown in an Oleate DMEM only. FITC fluorescence is presented on the horizontal axis and forward scatter on the vertical axis 181
Figure 64: A contour diagram of carboxy-H2DFFDA obtained by flow cytometry of HUH7 cells grown in an Oleate DMEM with Rapamycin. FITC fluorescence is presented on the horizontal axis and forward scatter on the vertical axis 182

List of Tables

Table 1: NASH CRN scoring system 25
Table 2: Fibrosis staging for NAFLD 25
Table 3: Mouse study groups for steatosis assessment 31
Table 4: Body and liver weights for each mouse in the steatosis assessment study 39
Table 5: Mean percentage steatosis by various methods and mean triglyceride concentration within the liver ±1 standard error of the mean in each study group 42
Table 6: The percentage of hepatocytes involved by steatosis and NAS for each mouse as assessed by the two expert pathologists on H&E 45
Table 7: The percentage steatosis and NAS for each mouse using the mean expert pathologists on H&E and ORO DIA 48
Table 8: Fat size distribution in the experimental groups using ORO DIA 49
Table 9: Fat droplet numbers in the experimental groups using ORO DIA 50
Table 10: The mean percentage of microvesicular and macrovesicular steatosis present in each study group identified by ORO DIA 50
Table 11: Mean percentage steatosis by various methods within the liver ±1 standard error of the mean in each NAFLD patient 54
Table 12: MCD study groups 74
Table 13: HFD/Fructose study groups 75
Table 14: The number of emission spectra for each disease model in the MCD study 82
Table 15: The number of emission spectra for each disease model in the HFD/Fructose study 82
Table 16: The number of emission spectra for each diagnosis in the human liver biopsies 83
Table 17: Median NAFLD activity score and fibrosis stage for the MCD study mice with the range in brackets. 88
Table 18: Mean malondialdehyde concentration in the livers of the MCD study group mice ±SEM 92
Table 19: Mean ALT levels in the plasma of the MCD study group mice ±SEM 94
Table 20: Confusion matrix demonstrating the ability of fluorescence spectroscopy to distinguish between control, steatosis and fibrosing steatohepatitis disease groups in the MCD study 98
Table 21: Median NAFLD activity score for the HFD/Fructose study mice with the range in brackets 101
Table 22: Mean ALT levels in the plasma of the HFD/Fructose study mice ±SEM 103
Table 23: Confusion matrix demonstrating the ability of fluorescence spectroscopy to distinguish between control, steatosis and steatohepatitis disease groups in the HFD/Fructose study 107
Table 24: Median NAFLD activity score for the suspected NAFLD patients undergoing liver biopsy with the range in brackets. 110

Table 25: Mean ALT levels in the plasma of the suspected NAFLD patients undergoing liver biopsy ±SEM 112
Table 26: Confusion matrix demonstrating the ability of fluorescence spectroscopy to distinguish between control, steatosis and NASH in human liver biopsies 114
Table 27: Mean number of lipid droplets and lipid droplet area ± SEM per HUH7 cell, grown in DMEM ± Rapamycin or Oleate DMEM ± Rapamycin 151
Table 28: Mean percentage area co-localisation between LAMP1 and BODIPY in HUH7 cells grown in different growth mediums 159
Table 29: Oil Red-O digital image analysis mean percentage steatosis ± SEM in HUH7 cells grown in Oleate DMEM ± Rapamycin or DMEM ± Rapamycin 170
Table 30: Mean triglyceride concentration (nmol per well) ± SEM for HUH7 cells grown in Oleate DMEM ± Rapamycin or DMEM ± Rapamycin 171
Table 31: The percentage of viable, early apoptotic, late apoptotic and necrotic cells and the intracellular ROS levels (median fluorescence intensity) in HUH7 cells grown in Oleate DMEM ± Rapamycin or DMEM ± Rapamycin 173

Chapter 1.

General Introduction

1.1 Non-Alcoholic Fatty Liver Disease Background

Non alcoholic fatty liver disease (NAFLD) encompasses a spectrum of steatosis, non-alcoholic steatohepatitis (NASH) and cirrhosis. It is the leading cause of chronic liver disease in the developed world.[1]

The increasing prevalence of obesity and diabetes and the associated metabolic syndrome (**Figure 1**) in the population is leading to an increased prevalence of NAFLD and it is estimated that 30% of the population of the USA has NAFLD.[2] This figure is expected to rise with increasing obesity in the USA and other Western countries.

The Metabolic Syndrome
1. Obesity: BMI≥30 kg/m² or waist: hip ratio >0.9 (males), >0.85 (females)
2. Hypertension: blood pressure ≥140/90 mmHg
3. Dyslipidemia: low HDL <0.9 mmol/L and/or hypertriglyceridemia: >1.7 mmol/L
4. Microalbuminuria: urinary albumin excretion >20µg/min
At least two of 1-4 above plus:
5. Type 2 diabetes mellitus OR insulin resistance OR impaired glucose tolerance.

Figure 1. Definition of the metabolic syndrome.[3]

The increasing prevalence of NAFLD is particularly worrying as patients appear to have a higher mortality from non-liver related causes of death in addition to liver-related cause of death and recent data has highlighted an increased risk for cardiovascular disease.[4-6] It is not clear if this simply reflects shared risk factors or if NAFLD, per se, increases the risks of cardiovascular disease.

Many of the risk factors for NAFLD are known but the underlying pathogenesis is still incompletely understood. The majority of patients with NAFLD have a stable disease with isolated steatosis and an indolent course with no clinical sequelae or progression to advanced liver disease. However, a subset develops NASH and is at risk of progressive fibrosis, cirrhosis and liver failure or hepatocellular carcinoma. The distinction between isolated steatosis and NASH is important as their prognoses and management are different.

Histological analysis of a liver biopsy remains the "gold standard" and only accurate way of assessing the degree of steatosis, necro-inflammatory changes and fibrosis, and therefore to distinguish NASH from isolated steatosis.[7]

1.2 Epidemiology and Disease Natural History of Non-Alcoholic Fatty Liver Disease

Estimates of NAFLD prevalence based on "cryptogenic" abnormal liver function tests, autopsy samples, ultrasound and magnetic resonance spectroscopy vary between 3% and 37% with the usual figure quoted being around 30%.[8-11]

In a large US based study using magnetic resonance spectroscopy to look at hepatic steatosis a third of the population were found to have hepatic steatosis. This was not distributed evenly amongst ethnic groups with 45% of Hispanics, 33% of Caucasians and 24% of African Americans affected.[11] Further data suggesting ethnic background plays a role in the incidence of NAFLD was shown in a study which revealed a significantly higher prevalence of NAFLD in Hispanic's compared with non-Hispanic whites, even after controlling for obesity and body fat distribution.[12]

The Italian Dionysos study looked at the prevalence of NAFLD in the general population using ultrasound and found it to be similar in individuals with and without suspected liver disease (25% vs. 20%). This study confirmed the high prevalence of NAFLD in the general population and showed that NAFLD is not associated with suspected liver disease (raised ALT, GGT, HbsAg or HCV RNA positivity). They also showed NAFLD was more likely in the presence of obesity, hyperglycaemia, hyperinsulinaemia, hypertriglyceridemia and systolic hypertension; all features of the metabolic syndrome.[10]

The prevalence of NASH is difficult to determine as large population based studies are not possible because a liver biopsy is required for diagnosis. A review looking at the

epidemiology of NAFLD, found that in studies of bariatric surgery patients 76% have steatosis (range 33 to 99%), 37% have NASH (range 9.8 to 72.5%), 23% fibrosis (range 7.3 to 49%), and 5.8% cirrhosis (range 1.6 to 10%).[13] An autopsy study found NASH in 18.5% of markedly obese patients and 2.7% of lean patients.[9] This highlights the possible effect weight has on the incidence of NASH and may help to explain why clinical studies have shown a ratio of patients with NASH to those with NAFLD varying from 1:1 to 1:3.[14-16]

In NAFLD approximately 30% of patients with isolated steatosis will progress to NASH. Of those with NASH, approximately 20% develop cirrhosis and of those with cirrhosis, 30–40% decompensate and succumb to liver-related death within 10-years **(Figure 2)**.[17]

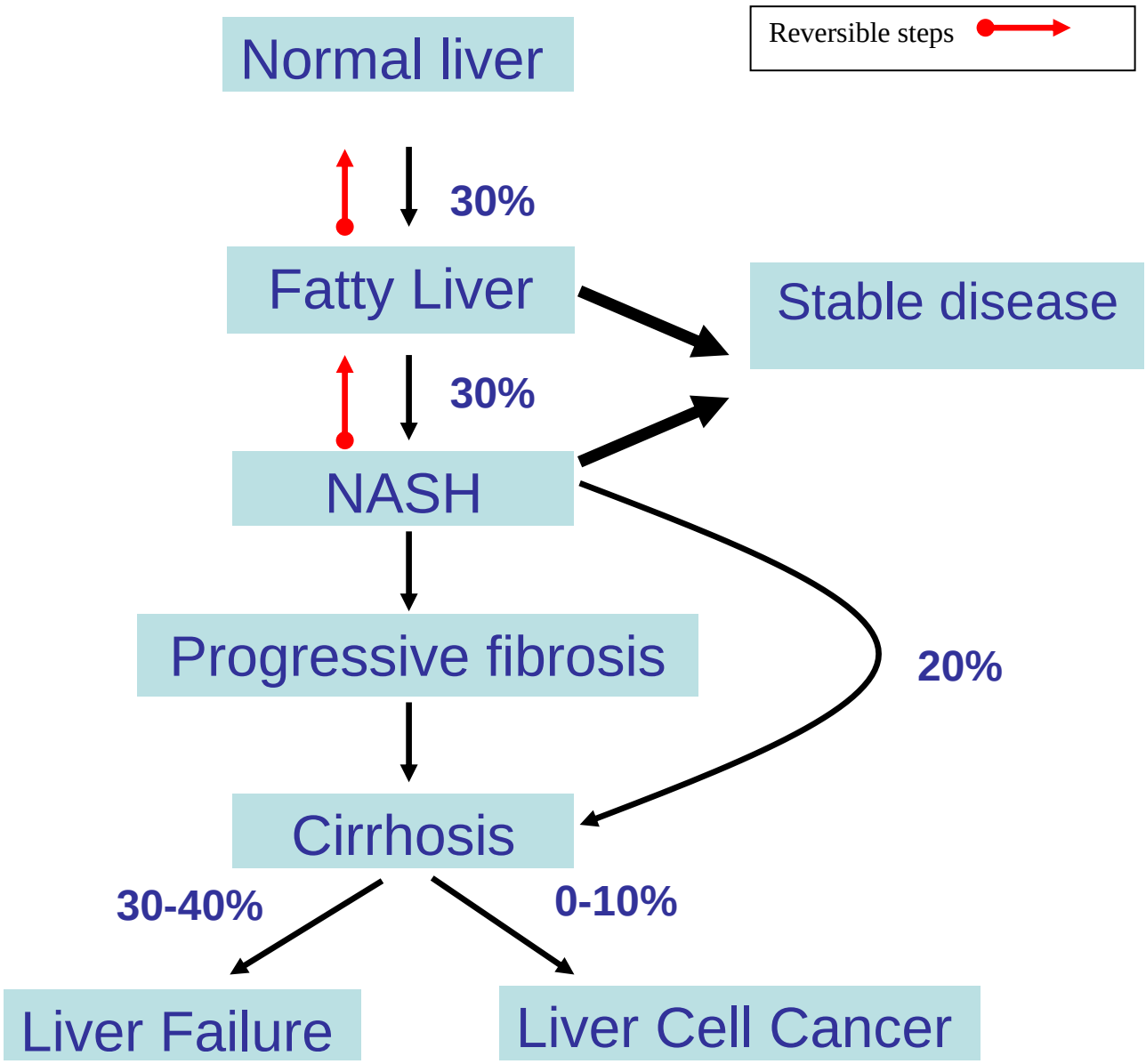


Figure 2. The natural history of NAFLD**.** Adapted from[17]

A long term follow up study of Swedish patients with biopsy proven NAFLD compared survival and cause of death with a matched reference population. The mean follow up was 13.7 years (all more than 10 years). Patients with simple fatty change had no increase in mortality. Patients with NASH had a reduced survival and more died from cardiovascular disease (15.5% vs. 7.5%) and liver related disease (2.8% vs. 0.2%). A subset of patients without cirrhosis at presentation developed end stage liver disease.

Progression of liver fibrosis was identified in 41% of patients on repeat biopsy with no fibrosis or early stage fibrosis on their initial biopsy. Interestingly the absence of periportal fibrosis at baseline had a negative predictive value of 100% in predicting liver related complications.[18] A similar long term follow up study in Minnesota, USA of 420 patients in the community with NAFLD (only 17% biopsy proven) showed an increased mortality compared to the general population (standardised mortality ratio, 1.34; 95% CI 1.003-1.76, p=0.03). The increased mortality was associated with impaired fasting glucose and cirrhosis. Liver related death was also much higher than in the general population (13% vs. <1%) although the absolute risk was still low (1.7% of the patients).[4]

A well recognised complication of cirrhosis due to NAFLD is hepatocellular carcinoma (HCC).[19-23] HCC has also been noted as a rare complication of NAFLD prior to cirrhosis.[24] This may be explained by the association of diabetes and obesity with the development of HCC as well as the carcinogenic factors associated with cirrhosis in general.[19, 20, 25] Less commonly other primary liver cancers, mainly cholangiocarcinoma, are being increasingly linked with NAFLD.[26]

1.3 Pathogenesis of Non-Alcoholic Fatty Liver Disease

NAFLD is closely linked to obesity, insulin resistance and the metabolic syndrome.[27] The initial theory for the pathogenesis of NAFLD was the 'two-hit' hypothesis.[28] The first hit, steatosis, sensitises the liver to the induction of inflammation by a second pathogenic insult that promotes oxidative stress and hence steatohepatitis. This model has subsequently been revised in recognition that a combination of 'second hits' (both

environmental and genetic) may lead to the development of steatohepatitis.[29] There have since been studies suggesting that steatosis is actually a protective mechanism within the liver to prevent the development of steatohepatitis.[30]

Currently it is not fully understood why some patients develop isolated steatosis and others develop steatohepatitis. However, it appears that insulin resistance and increased free fatty acids in the liver are strongly associated with NASH.[31, 32] Insulin causes esterification of free fatty acids and triglyceride fat storage in adipose tissues. When insulin resistance develops, free fatty acids are inappropriately moved to non adipose tissues such as the liver. Insulin resistance increases free fatty acid movement to the liver by decreased inhibition of lipolysis and increased *de novo* lipogenesis.[33]

There is currently increasing work on the interaction between cytokines and adipokines (cytokines secreted by adipose tissue) to try and understand the mechanisms involved in NAFLD development. Insulin resistance is thought to be regulated by pro-inflammatory cytokines, such as tumour necrosis factor-alpha, and adipokines such as adiponectin and leptin.[34, 35] Oxidative stress and apoptosis also appear to contribute to the development and progression of NASH.[36, 37]

1.4 Histopathology of Non-Alcoholic Fatty Liver Disease

Histological analysis of a liver biopsy remains the only accurate way of assessing the degree of steatosis, necro-inflammatory changes and fibrosis of NASH, and therefore to

distinguish NASH from isolated steatosis.[7] The diagnosis of NAFLD should only be made if the alcohol intake of the patient is <20g/day.[38]

In 2002 a multicentre cooperative Clinical Research Network (CRN) for NASH was developed. [39] One of its main aims was to develop and validate a system of histological evaluation that would encompass the spectrum of NAFLD, that could be applied to paediatric NAFLD, and that would allow for assessment of changes with therapy. This was based on the earlier Brunt scoring system for NASH.[40]

The pathology committee of the NASH CRN group developed and validated the NAS, a histological scoring system which is now widely used in NAFLD.[41] The NAS is a pragmatic, semi-quantitative scoring system for determining the severity of NAFLD. For each case a NAS and a separate fibrosis stage is given. **(Tables 1 & 2)**. The NAS comprises 14 histological features (9 of which are recorded as present or absent, such as Mallory Denk bodies), 3 of which are evaluated semi-quantitatively: steatosis (0-3), lobular inflammation (0-3) and, hepatocellular ballooning (0-2) to give a score of between 0 and 8. The higher the NAS score the more severe NAFLD the patient has. Many clinicians inappropriately use a NAS of ≥ 5 to diagnose NASH and a score ≤ 2 to determine that a diagnosis of NASH is unlikely. The fibrosis is scored separately to give a fibrosis stage of between 0-4. The lobular inflammatory infiltrate is usually composed predominantly of neutrophils but lymphocytes and macrophages are commonly seen. In practice, the presence of ballooned hepatocytes is a *sine qua non* for the diagnosis of NASH rather than steatosis.

Staging and grading of liver biopsies is used in the evaluation of a wide range of liver diseases to assess the severity of the disease. The grade relates to the severity of the disease, in the case of NAFLD this is the NAS score, and the features assessed vary depending on the pathogenesis of the disease. The stage is a measure of how far the disease has progressed and in the liver this involves assessing the degree of fibrosis with the end stage being cirrhosis. The intention of grading and staging is that this will help clinicians predict patient outcome and therefore guide treatment options.[42] Chronic viral hepatitis have been the diseases with the most widespread staging and grading using systems such as Metavir, and the Modified Histology Activity Index but other systems such as the NAS in NAFLD have been more recently developed.[41, 43, 44]

Semi quantitative scoring systems such as the NAS are useful for assessing disease severity and changes due to therapy as this is what they were designed for; however, they are often inappropriately used in clinical practice for making a diagnosis of NASH. The NAS is prone to sampling variability, one study showed discordance in the presence of hepatocyte ballooning, fibrosis stage and lobular inflammation between paired biopsy specimens for the same patient. The same study also showed intraobserver variability, although this was lower than sampling variability.[45]

As well as intraobserver variability there is also the problem of interobserver variability. The most problematic areas in the NAS are steatosis and hepatocyte ballooning. As well as assessment on routine H&E stained sections, ballooning can be assessed by using immunohistochemical stains for Mallory Denk bodies. In NAFLD Mallory Denk bodies

are often small and poorly formed and may be difficult to detect in routinely stained sections. Immunohistochemistry for ubiquitin, p62 and cytokeratins 8 and 18 can be used to demonstrate antigens associated with Mallory Denk bodies and ballooned hepatocytes. [46-48]

A limitation with a semi quantitative system such as the NAS, is that a small change in the percentage of steatosis or foci of lobular inflammation can change the score by 2 points, which in a scoring system comprised of only 8 points is a large change. If clinicians use the score as the basis for diagnosis and treatment options they need to be aware of this limitation as well as those of sampling variability and observer variability.

Steatosis grade (0-3)	Lobular inflammation (0-3)	Hepatocyte ballooning (0-2)
+	+	
0: <5% 1:5-33% 2: 34-66% 3: >66%	0: None 1:<2 foci/20x field 2: 2-4 foci/20x field 3: >4 foci/20x field	0: None 1: Mild, few 2: Moderate – Many
NAFLD activity score: **(NAS): 0-8**		

Table 1 NASH CRN scoring system for assessing NAFLD disease severity[41]

Stage 1: Perisinusoidal or periportal **1A:** Mild, zone 3, perisinusoidal **1B:** Moderate, zone 3, perisinusoidal **1C:** Portal/periportal fibrosis only
Stage 2: Perisinusoidal and portal/periportal fibrosis
Stage 3: Bridging fibrosis
Stage 4: Cirrhosis

Table 2. Fibrosis staging for NAFLD[41]

Changes from the initial scoring system devised by Brunt included, firstly, subdivisions within stage 1 fibrosis to include a distinction between delicate (1A) and dense (1B) perisinusoidal fibrosis, and the recognition of portal-only fibrosis, without perisinusoidal fibrosis (stage 1C).[49] Secondly, the introduction of a minimal steatosis category (score 0 for under 5%) to avoid giving weight to this feature when minimal steatosis is present.

The histological features recorded but not scored in the NAS include Mallory Denk bodies, megamitochondria and glycogenated nuclei.[50]

A study looking at liver biopsies in morbidly obese patients found a third of patients with isolated portal fibrosis in the absence of NASH but associated with the metabolic syndrome. Therefore, they suggested that isolated portal fibrosis should be considered as part of the spectrum of NAFLD that may precede NASH in the morbidly obese.[51] There is an increasing recognition that mild portal inflammation and bile ductular reaction can also often be present in NAFLD. A recent study by the NASH CRN concluded that more than mild portal chronic inflammation is associated with many clinical and pathologic features of progressive NAFLD in both adults and children. If the patient is untreated it may be considered a marker of advanced disease.[52] A postulated mechanism for periportal fibrosis in NASH is that cellular injury, often associated with portal inflammation, is thought to attract periportal, hepatic progenitor cells that when activated induce a periportal ductular reaction that induces progressive periportal fibrosis.[53]

In summary, the histological spectrum of NAFLD is characterised by steatosis, lobular inflammation, ballooning of hepatocytes, fibrosis and other features which may or may not be present such as Mallory Denk bodies and portal inflammation. The NASH clinical research network has developed a grading and staging system of NASH based on the use of Haematoxylin and Eosin (H&E) and Masson's trichrome stain so it can be used routinely by histopathologists.[41]

Chapter 2.

The Quantification of Steatosis in Non-Alcoholic Fatty Liver Disease: The Potential Use of Oil Red-O

2.1. Introduction

The majority of patients with NAFLD have isolated steatosis and an indolent course with no clinical sequelae or progression to advanced liver disease. A smaller number have NASH and are at risk of progressive fibrosis, cirrhosis and liver failure or hepatocellular carcinoma. The distinction between isolated steatosis and NASH is therefore important, as their prognoses and management are different.

As described earlier, histological analysis of a liver biopsy is still the only accurate method of assessing the degree of steatosis, lobular inflammation, hepatocytes ballooning and fibrosis, and therefore to distinguish NASH from isolated steatosis.[7] Radiological techniques, especially MRI, are supposedly improving for the detection of steatosis with a quoted sensitivity ranging from 80 to 95%.[54] However, they and biochemical indices are currently still unable to reliably distinguish between the different types of NAFLD.[55, 56]

The primary histological scoring system, the NAS, was developed by the pathology committee of the NASH CRN, **see Table 1**.[41] Whilst there is some interobserver variability, a NAS ≥5 consistently implies a diagnosis of NASH and a score ≤2 is not NASH.

As was intended by the original authors, in many NAFLD studies the NAS is part of the inclusion criteria. However, it has frequently also been adopted as an endpoint to define treatment response.[57] Given the degree of steatosis contributes up to 3 of the 8 points to this score and hepatocyte ballooning (which may be confused with small fat droplets) a further 2 points, it is important to correctly identify steatosis in a liver biopsy.

Accurately determining the amount and type (macrovesicular or microvesicular) of steatosis on H&E staining can be extremely challenging, especially when the fat droplets are small. There can also be processing artefacts present which appear similar to steatosis. Similarly hepatocyte ballooning may be difficult to differentiate from steatosis. The need for accurate hepatic steatosis quantification is equally important in the clinical trial setting and in the laboratory for assessing NAFLD models.

Murine dietary models of NAFLD, widely used to study disease pathogenesis, provide a reproducible and predictable distribution and degree of steatosis.[58, 59] To study the accuracy of histological steatosis quantification, we used mouse models of NAFLD induced by a high fat diet and/or high fructose consumption to reproduce the range of histological steatosis extending from normal tissue through to microvesicular and macrovesicular steatosis alone or in combination. Steatosis was quantified on H&E slides by myself and my supervisor Professor Goldin and also digital image analysis (DIA). An alternative approach was explored using Oil Red-O (ORO) stained slides, a histochemical stain which specifically identifies lipids.[60]

Based on the results from the mouse study and to assess the validity of these techniques in clinical practice, steatosis in human liver biopsies was quantified on H&E slides by visual assessment from liver pathologists and DIA and compared with ORO stained slides DIA and MRI steatosis quantification.

2.2. Aims

The aim was to use liver tissue from a mouse model of NAFLD exhibiting a reproducible spectrum of steatosis to study the accuracy of histological steatosis quantification. Steatosis was quantified on H&E by two liver pathologists and also by DIA quantification. An alternative approach using ORO stained sections was explored to assess the degree and type of steatosis. The results from this study were then validated using the same techniques in human liver biopsies.

2.3. Methodology

2.3.1. Rationale

ORO staining was used to stain liver tissue sections for lipids. This method allows for accurate assessment of neutral lipids within frozen tissue sections. Hepatic triglyceride levels were quantified in the same tissues.

2.3.2. Materials

2.3.2.1. Animal husbandry

The research was approved by the local ethics committee and was carried out under Home Office supervision in accordance with the Animal (Scientific Procedures) Act 1986 taking care to minimise any distress caused to the animal. Procedures were performed under the authority of licence 30/2505 'Mouse Models of Steatohepatitis for Basic Science & Therapeutics Investigation'. Animals were housed under standard conditions (12 hour light/dark cycle, temperature 21 ± 2°C, humidity 55 ± 10%).

2.3.2.2. Liver tissue

Twenty male C57BL/6J (Charles River, UK) mice were housed under standard conditions. From 8 weeks of age the mice were randomly divided into four groups and fed a standard pelleted commercial chow containing 11.5 kcal% fat (#801722, SDS, UK), or a nutritionally replete pelleted high fat diet (45%kcal fat derived from lard; D12451, Research Diets Inc, USA) with or without 30% fructose w/v (Sigma-Aldrich, UK) in drinking water according to a 2x2 factorial design. (**Table 3**)

	Water	30% Fructose
Standard Chow	N=5	N=5
45% High Fat Diet	N=5*	N=5

* One of the mice in the high fat diet and water group became unwell during the study and was excluded from the analysis

Table 3. Mouse study groups for steatosis assessment

After 15 weeks the mice were culled by overdose of anaesthetic administered by intraperitoneal injection (0.2ml Sagatal, Pentobarbitone sodium 60mg/ml, Merial Ltd., UK). Cardiac puncture and exsanguination were then performed to collect blood for biochemical analysis. The liver was explanted and bisected, half was placed in 10% formalin and half was snap frozen in liquid nitrogen and stored at -80°C for subsequent ORO staining and triglyceride assessment.

2.3.2.3. Human liver tissue

Percutaneous liver biopsies from five patients with NAFLD had at least 5mm length of tissue removed immediately after biopsy and snap frozen. The remainder of the tissue was placed in formalin and processed as normal. The five patients were male with an age range of 36-55.

2.3.2.4. Histopathology and special stains in mouse liver tissue

Formalin fixed liver tissue was processed into paraffin wax and sections were stained with H&E. H&E stained sections were assessed by myself and my supervisor Professor Goldin to identify the percentage of hepatocytes involved by steatosis and subsequently the steatosis score using the NAS system (**Table 1**). The percentage of hepatocytes involved by steatosis was assessed by counting hepatocytes in six photomicrographs at x400 magnification in six randomly selected fields, both Professor Goldin and I used the same photomicrograph. Between 297 and 423 hepatocytes were counted per sample.

Frozen fresh liver tissue sections were cut on the cryostat and stained with ORO by Mr Suresh Ladva, senior biomedical scientist at St Mary's Hospital, Imperial College London. ORO solution for staining the tissue was made up using 0.9g of ORO and 180ml absolute isopropyl alcohol. The solution was stirred and allowed to stand overnight. The ORO solution was then mixed with 1.2g Dextrin and 120ml distilled water and allowed to stand for at least 1 day. The slides were then placed into the filtered 0.5% ORO in Dextrin, left to stain for 20 minutes and then rinsed briefly with running water. The tissue was counterstained with Gill II haematoxylin for 20-30 seconds. Finally, the slide was rinsed with tap water and coverslipped with aqueous mounting media.

The ORO stained sections of frozen liver were assessed in the same way as the H&E stained sections to identify the percentage of hepatocytes involved by steatosis and subsequently the steatosis score using the NAS system.

2.3.2.5. Histopathology and special stains in human liver tissue

Formalin fixed liver tissue was processed into paraffin wax and sections were stained with H&E. H&E stained sections were assessed by myself to identify the percentage of hepatocytes involved by steatosis and subsequently the steatosis score using the NAS system. The percentage of hepatocytes involved by steatosis was assessed by counting every hepatocyte in the biopsy at x400 magnification (2795 – 4818 hepatocytes).

Frozen fresh liver tissue sections were cut on the cryostat and stained with ORO as detailed in section 2.3.2.4. ORO stained sections of frozen human liver were assessed by digital image analysis.

2.3.2.6. Digital image analysis

DIA was performed using Nikon NIS-Elements BR Software Basic Research. Six random images at x400 magnification for each mouse and liver biopsy were taken to ensure a representative sample for each specimen. The percentage steatosis by area in the liver for each mouse and human liver biopsy was calculated on H&E stained slides using the same three colour differentiation system for each case. Prior to starting the analysis 50 points on a representative H&E stained slide were identified for each colour (pink-cytoplasm, blue-nuclei, white-fat) by the investigator so that the DIA system learnt how to classify an H&E stained slide. The same procedure was performed on ORO stained slides using different colour differentiation (white-cytoplasm, blue-nuclei, and red-fat). This approach is different to the scoring system in the NAS as that uses the percentage of hepatocytes involved by steatosis rather than the percentage area of steatosis.

Figure 3 shows the colour differentiation scatter graph used for the ORO stained slides, each dot on the graph represents a point on the slide that the investigator has identified so the DIA system learnt how to classify an ORO stained slide. This shows that the fat, nuclei and cytoplasm on an ORO stained slide can be differentiated into three distinct categories with no overlap between them.

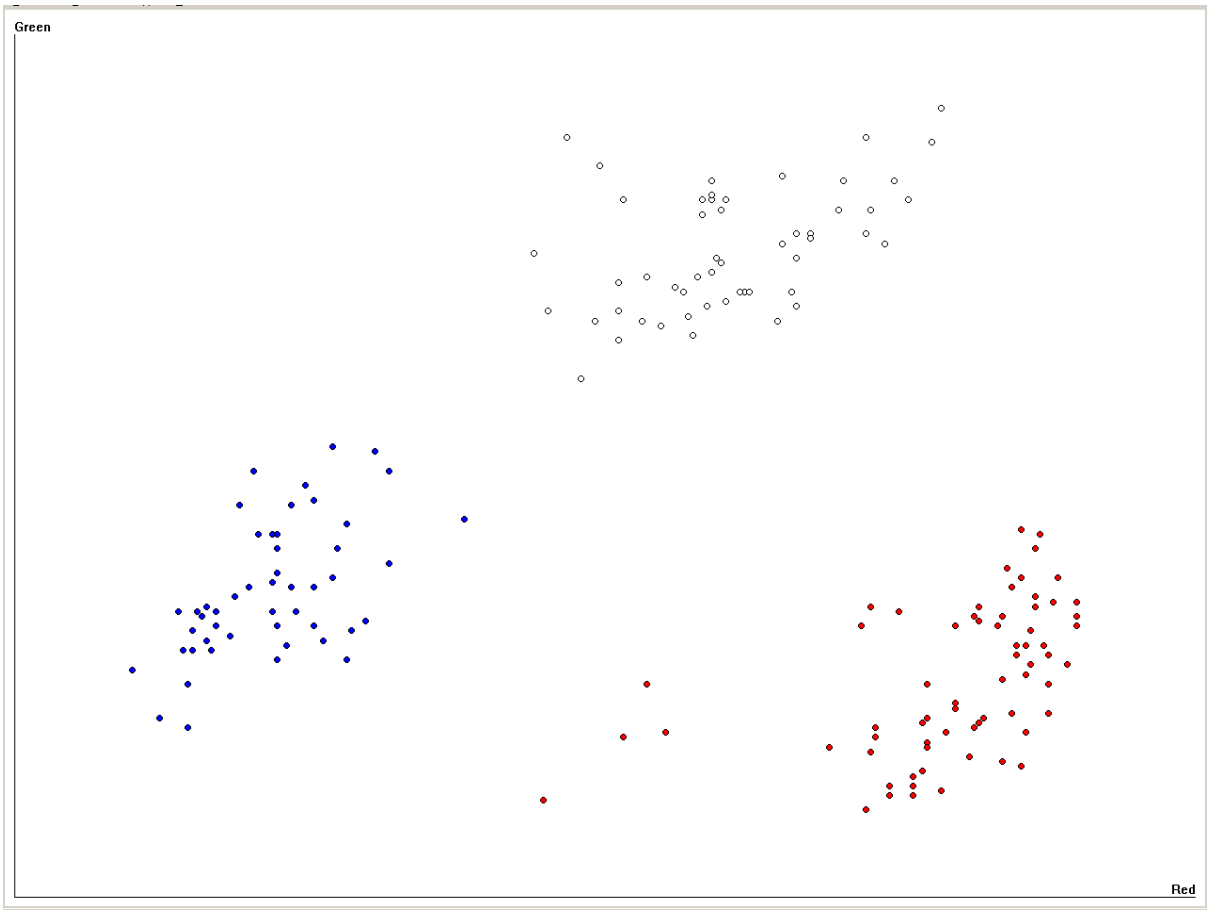


Figure 3. Scatter graph of the three colour differentiation used in ORO DIA (red = fat, white = cytoplasm, blue = nuclei)

In addition to the percentage of steatosis, the size of the fat droplets was calculated to identify the percentage of microvesicular and macrovesicular steatosis. Microvesicular steatosis was defined as ≤15um.[61]

Using the ORO stained sections of mouse liver, two images at x400 magnification from each zone of each liver were taken to ensure a representative sample of the liver from each mouse. The percentage area occupied by steatosis and its breakdown into microvesicular and macrovesicular steatosis by liver zone were calculated using DIA.

The same three colour differentiation system and size parameters described above were used.

2.3.2.7. Triglyceride quantification

Triglyceride concentrations within the mouse and human tissue were measured using a commercially available assay by spectrophotometry (Abcam; ab65336). The triglyceride quantification assay gives a sensitive measure of triglyceride concentration using a colourimetric (spectrophotometry at an optical density (OD) of 570 nm) method. In the assay, triglycerides are converted to free fatty acids and glycerol. The glycerol is then oxidised to generate a product which reacts with a probe to produce colour.

Approximately 100mg of previously frozen mouse liver tissue was homogenised in 600µl 5% Triton-X100 in water, then the sample was slowly heated to 80°C for five minutes. Then the sample was slowly cooled down to room temperature. The heating was repeated once more to solubilise all the triglyceride into solution. The sample was then centrifuged at 14,000rpm for five minutes and any insoluble material removed. Finally the sample was diluted prior to each assay either 50 fold, 100 fold or 200 fold with distilled H_2O.

For the human tissue the remainder of the previously frozen sample (0.4-1.8mg) was homogenised in 600µl 5% Triton-X100 in water, then the sample was slowly heated to 80°C for five minutes. Then the sample was slowly cooled down to room temperature. The heating was repeated once more to solubilise all the triglyceride into solution. The sample was then centrifuged at 14,000rpm for five minutes and any insoluble material

removed. Finally the sample was either not diluted or diluted prior to the assay 2.5 fold, 5 fold, 10 fold or 20 fold with distilled H_2O.

Using a 96 well plate 50µl of each sample was placed into a well, this was performed in duplicate. A standard curve was calculated using the triglyceride standard provided with the assay, and this was again performed in duplicate. 2 µl of lipase was added to each standard and sample well. This was mixed and incubated for 20 minutes at room temperature to convert triglyceride to glycerol and fatty acid. 50µl of triglyceride reaction mix (46 µl Triglyceride Assay Buffer, 2 µl Triglyceride Probe, 2 µl Triglyceride Enzyme Mix) was added to each standard and sample well. This was mixed and incubated for 60minutes at room temperature and protected from the light. Spectrophotometry at an OD of 570nm was measured using a plate reader. Using the absorbance values and standard curve the triglyceride concentration in nmol/mg of liver of the samples was calculated.

2.3.2.8. Magnetic resonance imaging steatosis quantification

The five NAFLD patients who had liver biopsies underwent a liver MRI scan within 1 week of the biopsy. The images from each patient were assessed in conjunction with Professor Gedroyc, Professor of Radiology at Imperial College Healthcare NHS Trust using a modified three-point Dixon suppression technique to assess fat.[62] Four steatosis percentage readings were taken from the right lobe of the liver. The right lobe of the liver was chosen to minimise sampling error when comparing results with those from the liver biopsy as the biopsy is also taken from the right lobe.

2.3.2.9. Statistical analysis

Data were collated in Microsoft Excel (Microsoft Inc, USA) and statistical analysis performed using SPSS version 17 (SPSS, USA). Values are presented as mean±SEM for continuous variables. Parametric data was analysed using ANOVA with post-hoc Bonferroni correction. Two-tailed p-values are shown throughout with $p<0.05$ taken as significant. Statistical comparison looking at inter-observer variation in identifying the percentage of hepatocytes involved by steatosis and comparing triglyceride quantification with other methods of quantifying steatosis was performed using Pearson Correlation. Intraclass correlation coefficient was used to compare NAS scores between expert pathologists.

2.4. Results

2.4.1. Mouse study

2.4.1.1. Liver and body weights

After 15 weeks on different diets, phenotypic differences were apparent between groups (**Table 4**). Whilst fructose consumption made only minor contributions to body weight, mice fed a high fat diet (with or without fructose) were significantly heavier than those fed a standard chow diet (45.82±0.60g vs. 36.34±1.13g, $p<0.001$, see **Figure 4**). This effect was attributed to the diet consumed as the body weights at the start of the experiment were not significantly different (25.41±0.81g vs. 25.65±0.41g respectively). The mice receiving a high fat diet, with or without fructose, also had a heavier mean liver weight (2.31±0.18g) compared to those receiving a standard chow diet, with or without

fructose (1.54±0.08g). The liver to body weight ratio did not show any significant difference between groups.

	Body Weight (g)		Liver Weight (g)
Experimental Group	Start of Experiment	End of experiment	End of Experiment
Chow & Water 1	25.3	36.6	1.5
Chow & Water 2	25.6	38.9	1.5
Chow & Water 3	24.5	33.6	1.3
Chow & Water 4	25.8	39.8	1.4
Chow & Water 5	23.2	30.9	1.1
High Fat Diet & Water 1	23.2	46.5	1.9
High Fat Diet & Water 2	25.4	48.6	2.8
High Fat Diet & Water 4	23.1	44.6	1.8
High Fat Diet & Water 5	22.6	45.0	2.2
Chow & Fructose 1	26.8	38.5	1.9
Chow & Fructose 2	27.6	41.5	1.9
Chow & Fructose 3	25.3	35.5	1.6
Chow & Fructose 4	25.2	31.2	1.5
Chow & Fructose 5	27.2	36.9	1.7
High Fat Diet & Fructose 1	24.7	42.9	1.9
High Fat Diet & Fructose 2	27.4	47.5	3.5
High Fat Diet & Fructose 3	30.2	47.2	2.3
High Fat Diet & Fructose 4	26.9	45.8	2.4
High Fat Diet & Fructose 5	25.2	44.3	2.0

Table 4. Body and liver weights for each mouse in the steatosis assessment study

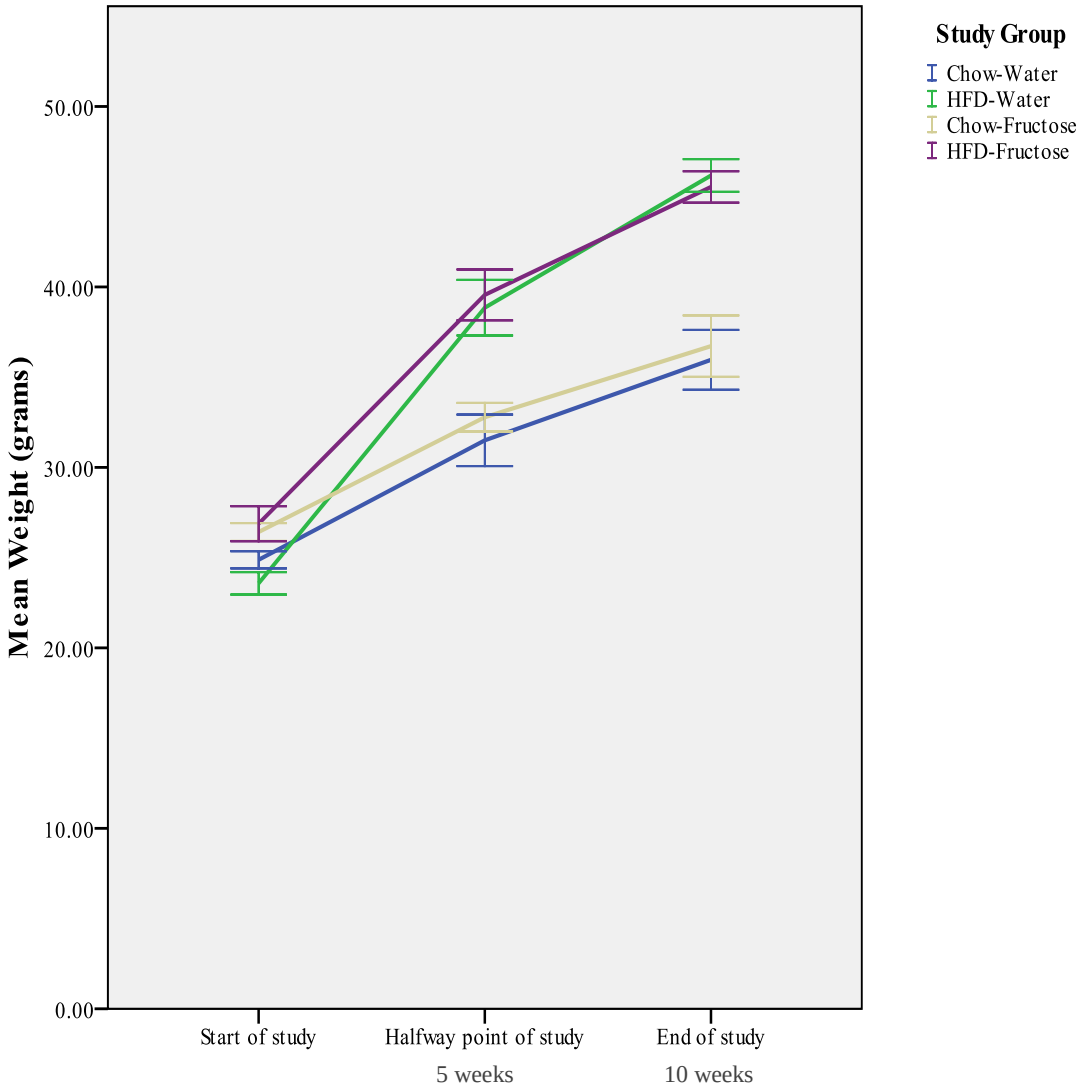


Figure 4. Graph showing mean body weights of the mice in each study group over the course of the HFD/Fructose experiment ± 1 standard error of the mean.

2.4.1.2. Biochemical analysis of hepatic triglyceride content

Mean triglyceride concentrations for each study group are shown in **Table 5**. It can be seen that mice fed a high fat diet with fructose have significantly higher triglyceride concentrations within the liver than those fed chow/water or chow/fructose (p=0.004 and

p=0.006 respectively). The mice fed a high fat diet with water had higher triglyceride concentration within the liver than those with chow/water or fructose. However, this did not reach statistical significance (p=0.197 and p=0.253 respectively), possibly due to the small sample size and one of the mice in the high fat diet/water group becoming unwell during the study and therefore being excluded from subsequent analysis.

2.4.1.3. Comparison of steatosis quantification methods with hepatic triglyceride content

The mean percentage steatosis identified within the liver by pathologists on H&E, H&E DIA and ORO DIA are shown in **Table 5** and **Figure 5**. ORO DIA correlated well with the total liver triglyceride concentration and is, therefore, a reasonable reflection of liver steatosis (Pearson correlation R=0.706, p=0.001), whereas, visual assessment of H&E by liver pathologists showed poor correlation (R=-0.422). H&E DIA also showed poor correlation with the total liver triglyceride concentration (Pearson correlation R=0.447, p=0.055).

	Chow & Water	High Fat Diet & Water	Chow & Fructose	High Fat Diet & Fructose
Mean Percentage Steatosis on H&E by Pathologists	0	71.63±5.34	0	71.90±4.15
Mean Percentage Steatosis on H&E by DIA	26.67±4.18	55.66±4.89	19.83±4.68	41.97±7.10
Mean Percentage Steatosis on ORO by DIA	11.36±2.49	46.20±4.46	18.55±0.97	47.04±4.24
Mean Concentration of Triglyceride (nmol per mg of liver)	192.17±50.71	383.01±101.70	202.61±29.21	516.59±36.84

Table 5. Mean percentage steatosis by various methods and mean triglyceride concentration within the liver ±1 standard error of the mean in each study group.

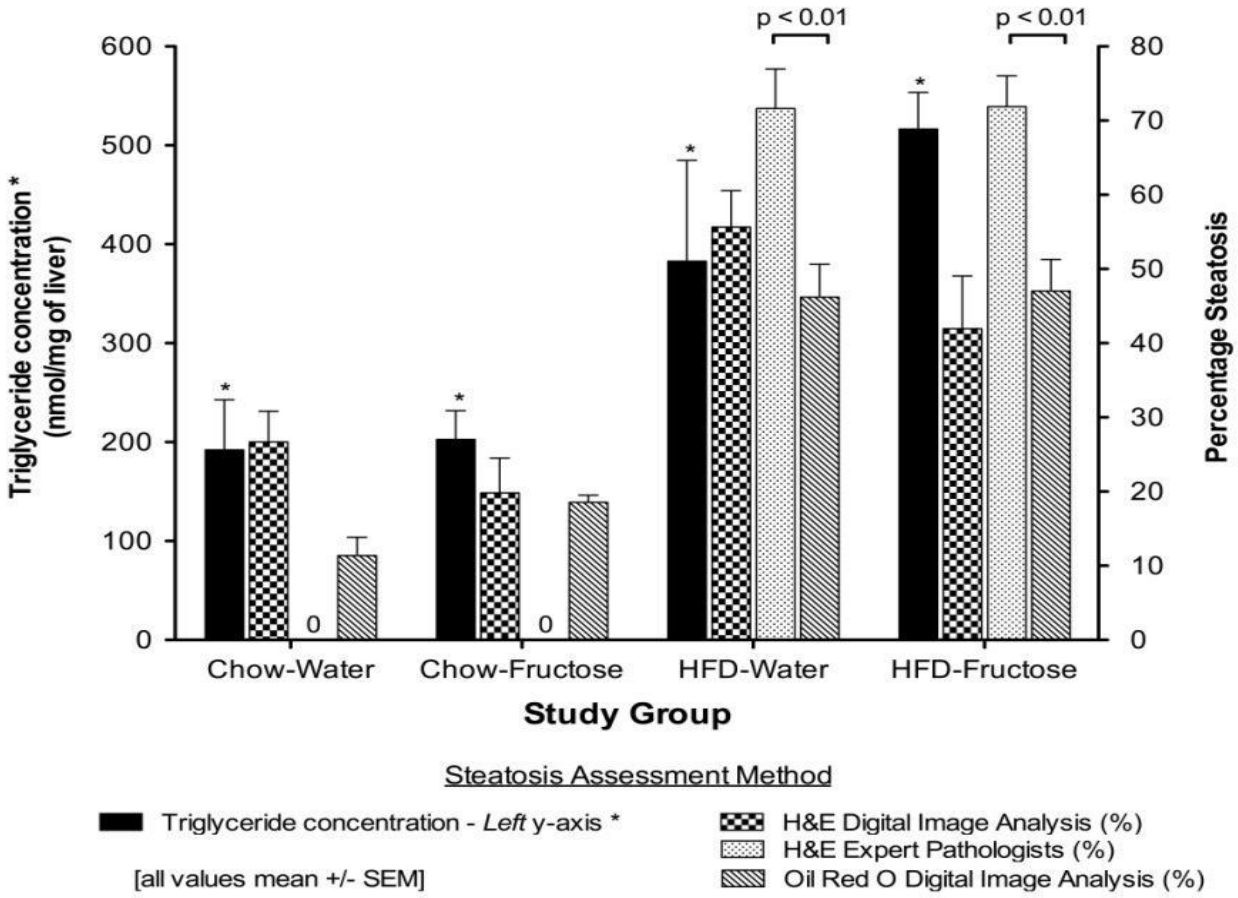


Figure 5. The mean triglyceride concentration for each mouse study group and the mean percentage steatosis for each mouse study group using H&E DIA, H&E expert pathologists and ORO DIA ± 1 standard error of the mean.

2.4.1.3.1. H&E histopathologist steatosis assessment

Visual assessment of H&E by liver pathologists identified large amounts of steatosis in the high fat/water and high fat/fructose groups which contained much macrovesicular steatosis, with a mean percentage of hepatocytes involved by steatosis of 71.63%±3.54 and 71.90%±3.17 respectively. However, steatosis was not identified in the chow fed study groups which contained mainly microvesicular steatosis. There was good inter-observer agreement between the two pathologists when assessing mean percentage of hepatocytes with steatosis using H&E stained slides, Pearson correlation R=0.991, $p<0.0001$ **(Table 6)**.

The NAS steatosis score for both histopathologist's was between 2 and 3 in the high fat diet groups with or without fructose and 0 for the chow groups as no steatosis was identified **(Table 6)**. There was strong inter-observer agreement between the histopathologist's NAS steatosis scores, intraclass correlation coefficient 0.976, $p<0.0001$**.**

	Expert Pathologist 1		Expert Pathologist 2	
Experimental Group	Percentage of hepatocytes involved by steatosis (%)	NAS steatosis score	Percentage of hepatocytes involved by steatosis (%)	NAS steatosis score
Chow & Water 1	0	0	0	0
Chow & Water 2	0	0	0	0
Chow & Water 3	0	0	0	0
Chow & Water 4	0	0	0	0
Chow & Water 5	0	0	0	0
High Fat Diet & Water 1	85	3	82	3
High Fat Diet & Water 2	77	3	75	3
High Fat Diet & Water 4	57	2	60	2
High Fat Diet & Water 5	67	3	70	3
Chow & Fructose 1	0	0	0	0
Chow & Fructose 2	0	0	0	0
Chow & Fructose 3	0	0	0	0
Chow & Fructose 4	0	0	0	0
Chow & Fructose 5	0	0	0	0
High Fat Diet & Fructose 1	77	3	81	3
High Fat Diet & Fructose 2	80	3	76	3
High Fat Diet & Fructose 3	82	3	76	3
High Fat Diet & Fructose 4	55	2	68	3
High Fat Diet & Fructose 5	55	2	69	3

Table 6. The percentage of hepatocytes involved by steatosis and NAS for each mouse as assessed by the two expert pathologists on H&E

2.4.1.3.2. ORO histopathologist steatosis assessment

The pathologists calculating the percentage of hepatocytes involved by steatosis with ORO staining found approximately 90-100% of hepatocytes in all the study groups contained steatosis, so this method could not be used in conjunction with the NAS to discriminate between groups.

2.4.1.3.3. H&E DIA steatosis assessment

H&E DIA identified fat in all four experimental groups (**Table 5**) with the high fat/water and high fat/fructose groups having a mean percentage area steatosis of 55.66%±4.89 and 41.97%±7.10 respectively. The chow/water and chow/fructose groups showed less steatosis with mean values of 26.67%±4.18 and 19.83%±4.68.

2.4.1.3.4. ORO DIA steatosis assessment

ORO DIA identified fat in the chow/water (8.20%±1.09 microvesicular, 3.16%±1.09 macrovesicular) and chow/fructose (9.60%±1.01 microvesicular, 8.95%±1.01 macrovesicular) groups where no fat was identified by visual assessment of H&E by liver pathologists **(Figure 6)**. This demonstrates that visual assessment of H&E by liver pathologists will not identify microvesicular or small macrovesicular fat droplets.

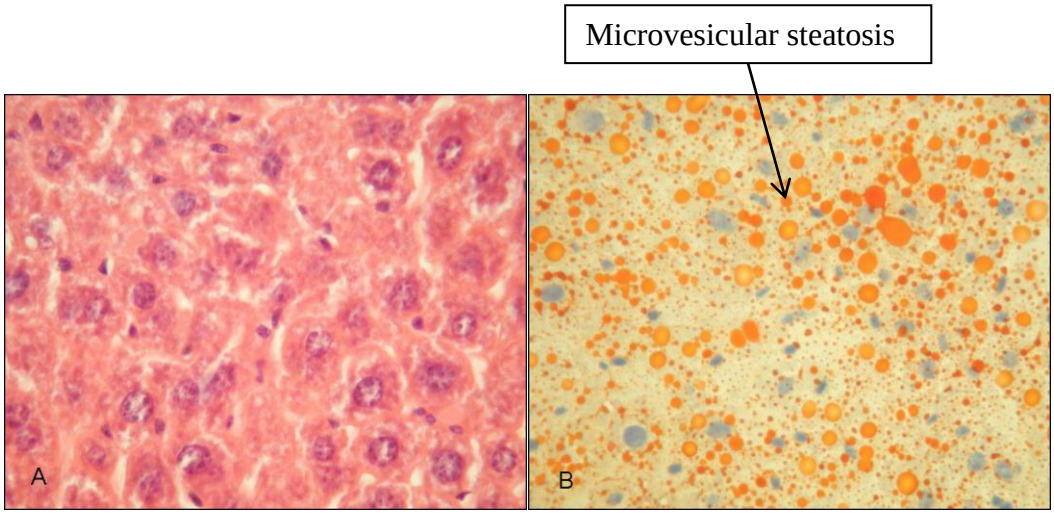


Figure 6a) H&E stained slide from mouse liver with no steatosis. **Figure 6b)** ORO stained slide of the same mouse liver showing mainly microvesicular steatosis. x400 original magnification.

In samples with mainly macrovesicular steatosis (**Figure 7**) visual assessment of H&E by liver pathologists overestimated the amount of steatosis as compared with ORO DIA (71.63%±3.54 vs. 46.20%±4.46 and 71.90%±3.17 vs. 47.04%±4.24, both p=<0.01, **Figure 5**).

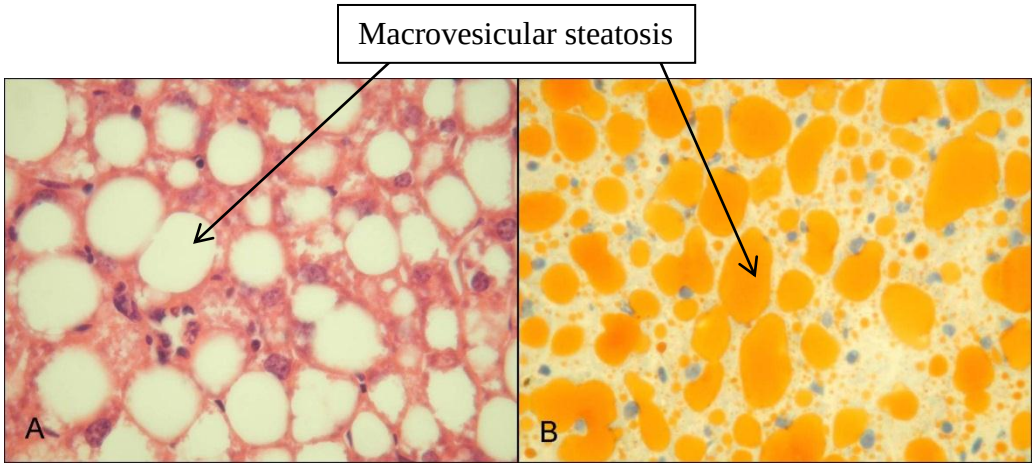


Figure 7a) H&E stained slide from mouse liver with marked mainly macrovesicular steatosis. **Figure 7b)** ORO stained slide of the same mouse liver showing mainly macrovesicular steatosis. x400 original magnification.

The NAS steatosis score for ORO DIA (**Table 7**) was 2 in all cases in the high fat diet groups with or without fructose and 1 for all the samples in the chow groups. Therefore, in 67% of the high fat diet cases the NAS steatosis score decreased from 3 to 2 when using ORO DIA compared to visual assessment of H&E by liver pathologists. In 100% of the chow samples the NAS steatosis score increased from 0 to 1 when using ORO DIA compared to histopathologists with H&E.

	Mean Expert Pathologists		ORO DIA	
Experimental Group	Percentage of hepatocytes involved by steatosis (%)	NAS steatosis score	Percentage area of steatosis (%)	NAS steatosis score
Chow & Water 1	0	0	7.20	1
Chow & Water 2	0	0	15.59	1
Chow & Water 3	0	0	6.62	1
Chow & Water 4	0	0	18.94	1
Chow & Water 5	0	0	8.44	1
High Fat Diet & Water 1	83.5	3	48.47	2
High Fat Diet & Water 2	76	3	34.48	2
High Fat Diet & Water 4	58.5	2	55.98	2
High Fat Diet & Water 5	68.5	3	45.85	2
Chow & Fructose 1	0	0	17.39	0
Chow & Fructose 2	0	0	22.15	0
Chow & Fructose 3	0	0	17.96	0
Chow & Fructose 4	0	0	16.49	0
Chow & Fructose 5	0	0	18.78	0
High Fat Diet & Fructose 1	79	3	35.70	2
High Fat Diet & Fructose 2	78	3	54.39	2
High Fat Diet & Fructose 3	79	3	49.12	2
High Fat Diet & Fructose 4	61.5	2	57.25	2
High Fat Diet & Fructose 5	62	2	38.74	2

Table 7. The percentage steatosis and NAS for each mouse using the mean expert pathologists on H&E and ORO DIA.

2.4.1.4. The size of steatosis as assessed by ORO DIA

Computer assisted measurement of the distribution of droplet size was performed to characterise the profile of lipid deposition within hepatocytes. The median diameter of fat droplets across all four study groups was <2µm, consistent with a predominance by number of microvesicular (≤15µm) fat droplets (**Table 8**). However, the fat droplets were significantly larger in the high fat diet groups than in the non-high fat diet groups with a mean fat droplet size of 7.31µm±0.23 and 7.77µm±0.23 compared to 2.70µm±0.04 and

3.67µm±0.04 ($p<0.001$). When using ORO DIA it should be noted that the smallest size fat droplet that can be seen by the microscope and imaging software used for this experiment is 0.22µm. This is why the minimum droplet size is the same for all experimental groups. The largest fat droplet in the two high fat diet groups was 1739.54µm and 1706.71µm which is much larger than fat droplets usually seen in biopsies from humans with NAFLD.

	Chow & Water	**High Fat Diet & Water**	**Chow & Fructose**	**High Fat Diet & Fructose**
Minimum Fat Droplet Size (µm)	0.22	0.22	0.22	0.22
Mean Fat Droplet Size (µm)	2.70±0.04#^	7.31±0.23#*	3.67±0.04~*	7.77±0.23~^
Median Fat Droplet Size (µm)	0.83	1.53	0.92	1.96
Maximum Fat Droplet Size (µm)	332.34	1739.54	159.79	1706.71

Table 8. Fat size distribution in the experimental groups using ORO DIA (#,~,^,* $p<0.001$)

Although the high fat diet study groups had a majority of microvesicular fat droplets by number (14175 vs. 1485 and 15181 vs. 1655, **Table 9**), when assessed by area the vast majority of steatosis was macrovesicular (40.86%±1.10 vs. 5.34%±1.10 and 40.89±1.44 vs. 6.15%±1.44, **Table 10**).

	Chow & Water	High Fat Diet & Water	Chow & Fructose	High Fat Diet & Fructose
Number of microvesicular droplets	24887	14175	31797	15181
Number of macrovesicular droplets	618	1485	1497	1655
Total number of fat droplets	25505	15660	33294	16836

Table 9. Fat droplet numbers in the experimental groups using ORO DIA

The steatosis identified in the chow/water (8.20%±1.09 microvesicular, 3.16%±1.09 macrovesicular) and chow/fructose (9.60%±1.01 microvesicular, 8.95%±1.01 macrovesicular) groups by ORO DIA was mainly microvesicular, **Table 10**. In these groups no steatosis was identified on visual assessment of H&E by expert pathologists **(Figure 6)**. This demonstrates that on visual assessment of H&E pathologists can not identify microvesicular or small macrovesicular fat droplets.

Experimental Group	Mean percentage microvesicular steatosis (%)	Mean percentage macrovesicular steatosis (%)
Chow & Water	8.20±1.09	3.16±1.09
High Fat Diet & Water	5.34±1.10	40.86±1.10
Chow & Fructose	9.60±1.01	8.95±1.01
High Fat Diet & Fructose	6.15±1.44	40.89±1.44

Table 10. The mean percentage of microvesicular and macrovesicular steatosis present in each study group identified by ORO DIA.

The steatosis identified and overestimated on visual assessment of H&E by the expert pathologists in the High Fat Diet/Water (40.86%±1.10 macrovesicular, 5.34%±1.10 microvesicular) and High Fat Diet/Fructose (40.89%±1.44 macrovesicular, 6.16%±1.44 microvesicular) groups was identified as being mainly macrovesicular on ORO DIA (**Figure 7)**. This suggests that on visual assessment of H&E pathologists overestimate macrovesicular steatosis when they identify it.

2.4.1.5. The zonation of steatosis as assessed by ORO DIA

The percentage of microvesicular and macrovesicular steatosis for each zone within the liver was calculated using ORO DIA **(Figure 8)**. This showed that there was less steatosis in zone 1 in each experimental group than in zones 2 and zone 3. Zones 2 and 3 both had similar percentages of steatosis. Within all zones, even in the experimental groups with far larger percentages of overall steatosis, the amount of microvesicular steatosis within the tissue was similar with a range of 2.4% – 6.2%. The main difference was in macrovesicular steatosis with there being a much larger percentage of macrovesicular steatosis in zones 2 and 3, especially in the high fat diet study groups with increased overall steatosis.

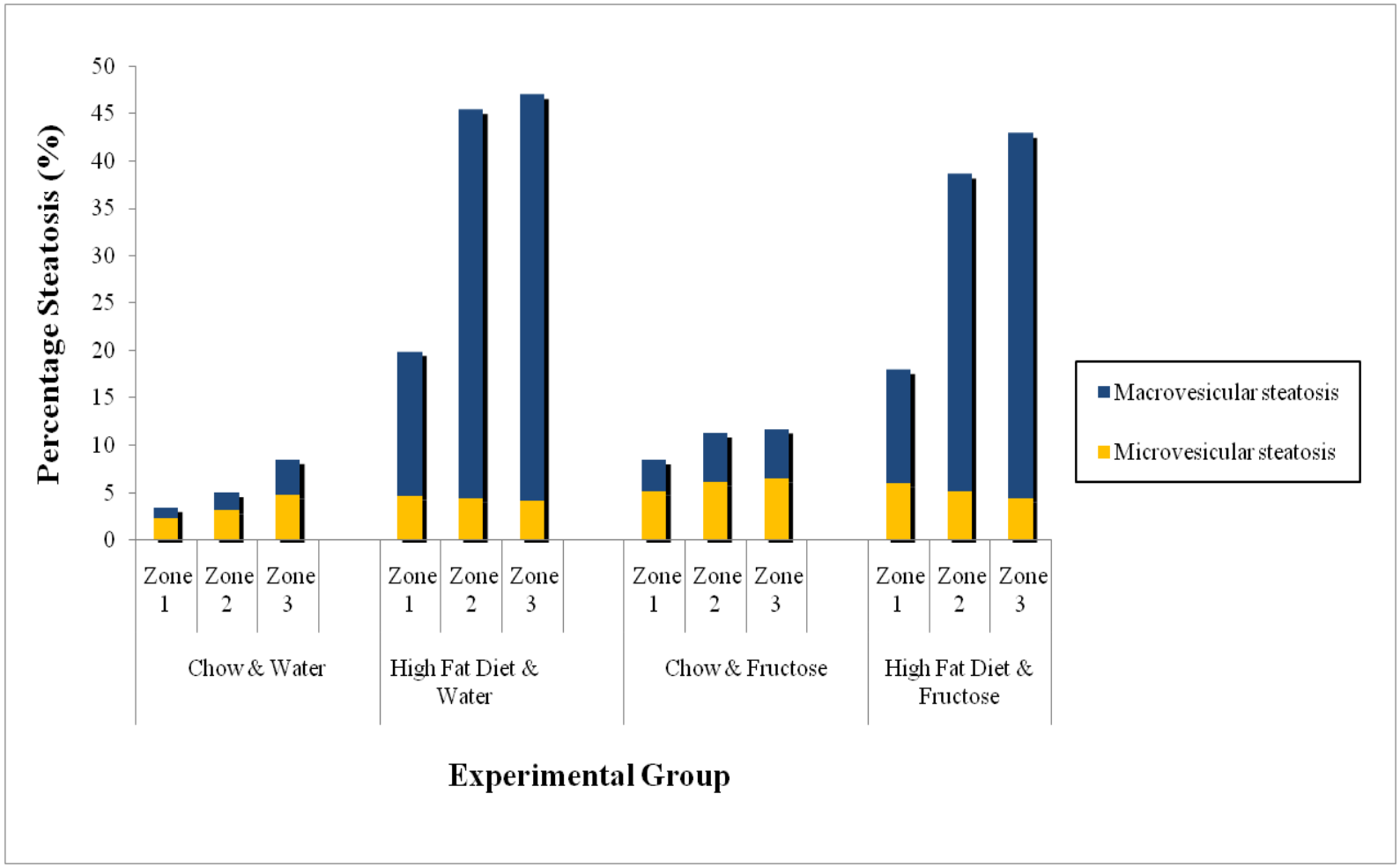


Figure 8. The mean percentage of microvesicular and macrovesicular steatosis present in each zone of the liver for each experimental group

2.4.2. Human liver biopsy study

ORO DIA had good correlation with hepatic triglyceride content in the mouse experiment, so the aim was to validate these results with human liver biopsies, **Table 11**.

2.4.2.1. Comparison of steatosis quantification methods with hepatic triglyceride content

The triglyceride concentrations for the liver biopsies ranged from 260.21nmol/mg liver±6.95 to 1550.75nmol/mg liver±22.46. **(Table 11)**

ORO DIA showed a strong correlation with the triglyceride content in the human liver biopsies, confirming that ORO DIA is an accurate reflection of liver steatosis, **Figure 9** (Pearson correlation R=0.894, p=0.041). The visual assessment of H&E by a liver pathologist and H&E DIA showed poor correlation with triglyceride content in the human liver biopsies, replicating the results from the mouse experiment, **Figure 9** (R=-0.071, p=0.909 and R=-0.319, p=0.600 respectively). MRI steatosis calculation also correlated poorly with triglyceride content in the human liver biopsies, **Figure 9** (Pearson correlation R=-0.521, p=0.368)

The mean percentage steatosis and corresponding NAS steatosis scores identified within the liver biopsies by pathologist on H&E, H&E DIA, ORO DIA and triglyceride assay are shown in **Table 11**. The mean percentage steatosis within the right lobe of the liver by MRI is also shown.

	Patient 1	Patient 2	Patient 3	Patient 4	Patient 5
Percentage Steatosis on H&E by Pathologist	72.10	24.97	4.96	15.22	11.49
H&E Pathologist NAS Steatosis Score	3	1	0	1	1
Mean Percentage Steatosis on H&E DIA	67.28±1.45	37.58±3.31	35.33±2.71	28.09±5.28	23.57±2.69
H&E DIA NAS Steatosis Score	3	2	2	1	1
Mean Percentage Steatosis on ORO DIA	37.00±1.22	30.20±0.99	16.25±0.94	52.18±2.36	25.02±1.66
ORO NAS Steatosis Score	2	1	1	2	1
Mean Percentage Steatosis on MRI	29.35±0.28	12.38±0.72	44.38±6.03	23.70±1.59	12.10±1.35
MRI NAS Steatosis Score	1	1	2	1	1
Mean Triglyceride Concentration (nmol/mg liver)	644.82±4.58	917.29±7.88	260.21±6.95	1550.75±22.46	775.96±23.86

Table 11. Mean percentage steatosis by various methods within the liver ±1 standard error of the mean in each NAFLD patient.

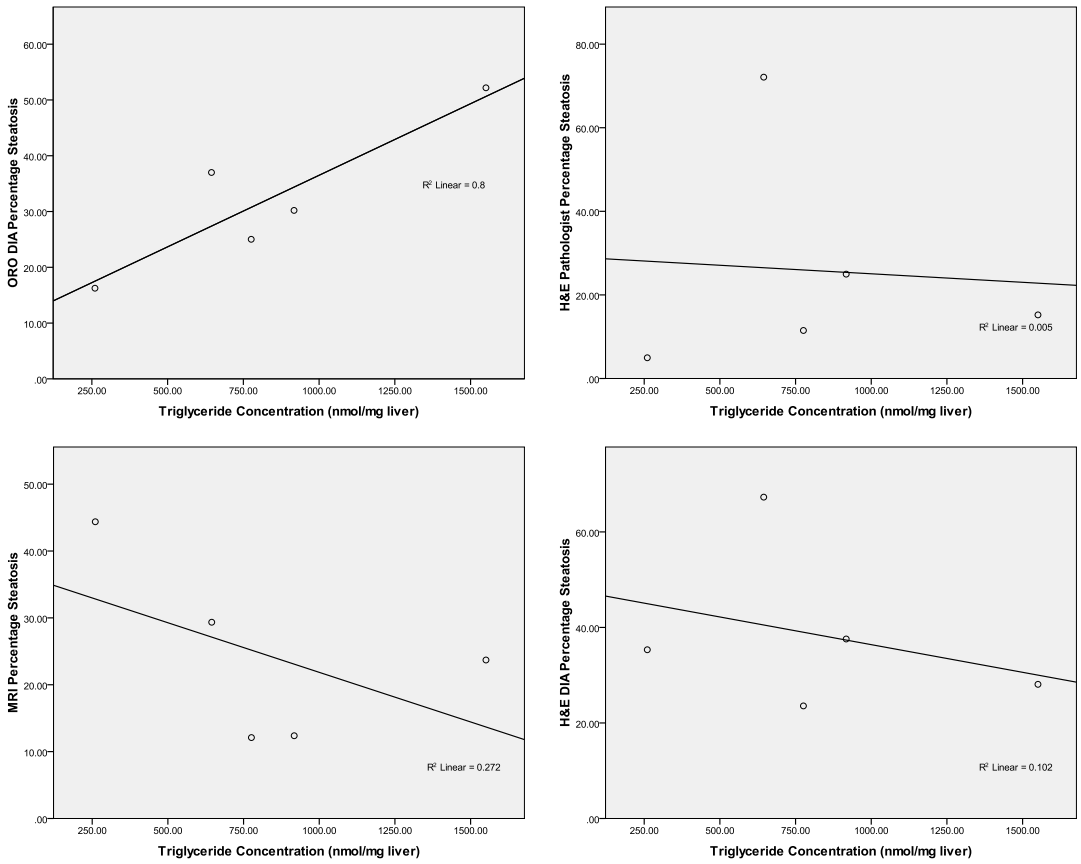


Figure 9. Scatter graphs showing percentage steatosis by a)ORO DIA, b)H&E pathologist, c)H&E DIA and d)MRI compared to triglyceride concentration in the five human patients including the best fit line and R^2 value.

2.4.2.1.1. H&E histopathologist steatosis assessment

Visual assessment of H&E by a liver pathologist identified steatosis in all five liver biopsies, with a range of values from 4.96% to 72.10%. There was poor correlation between H&E and the percentage steatosis on ORO DIA. (Pearson correlation R=0.307, p=0.615) The NAS steatosis score ranged from 0-3 and changed in three of the five patients when using ORO DIA compared to visual assessment of H&E by a liver pathologist.

2.4.2.1.2. H&E DIA steatosis assessment

H&E DIA identified steatosis in all five liver biopsies, with a range from 23.57%±2.69 to 67.28%±1.45. There was poor correlation between H&E DIA and the percentage steatosis on ORO DIA. (Pearson correlation R=0.097, p=0.877) The NAS steatosis score ranged from 1-3 and changed in four of the five patients when using ORO DIA compared to H&E DIA.

2.4.2.1.3. ORO DIA steatosis assessment

ORO DIA identified steatosis in all five liver biopsies, with a range of values from 16.25%±0.94 to 52.18%±2.36. The NAS steatosis score for the patients was either 1 or 2.

2.4.2.1.4. MRI Steatosis Assessment

MRI demonstrated different steatosis percentages within the right lobe of the liver to ORO DIA on the biopsies with four out of the five patients showing at least 10% variability with a maximum of 46% in one patient. There was poor correlation between MRI and ORO DIA results (Pearson correlation R= -0.271, p=0.660). The NAS steatosis score changed in three of the five patients when using MRI steatosis percentages compared to ORO DIA steatosis percentages.

2.5. Discussion

Accurate quantification of hepatic fat content histologically is a key requirement both for the diagnosis of NAFLD and for the assessment of treatment response. The existing NAS uses a semi-quantitative scale based on visual assessment of the number of hepatocytes with steatosis using a single H&E stained section. Fat droplets on H&E are triglyceride stores, therefore assessment of fat by light microscopy is an indirect assessment of liver triglyceride burden. Measuring triglycerides within a liver biopsy is, in itself a surrogate measure for free fatty acid flux which is currently thought to be critical in the pathogenesis of NAFLD.[30]

2.5.1. The merits of the various techniques for steatosis assessment

This study has shown that whilst visual H&E assessment of steatosis shows good correlation between histopathologists it is inaccurate when compared to the true hepatic triglyceride content. H&E DIA was assessed as an alternative method as it has the obvious advantage of being performed on previously fixed and processed slides, does not need any further preparation and can therefore be used retrospectively, I have used this method in previous research studies.[59] However, it also showed poor correlation with hepatic triglyceride content and was therefore not reliable as an alternative method of steatosis quantification. A recent study looking at the correlation of steatosis assessment on H&E by expert pathologists and computer analysis also found that there was poor correlation between the two methods and also in the assessment of microvesicular and macrovesicular steaosis.[63] ORO DIA technique is the optimum method for assessing steatosis, it correlated well with hepatic triglyceride content in mouse and human liver

and provides a more accurate quantification of steatosis than H&E DIA, visual assessment of H&E by expert pathologists or MRI.

There are inherent flaws with H&E DIA, it identifies steatosis by its white colour, and therefore, it also identifies sinusoids, blood vessel lumens and processing artefacts as steatosis as they are also white spaces. For these reasons, although H&E DIA results are closer to ORO DIA than visual assessment of H&E by a liver pathologist this is likely to be due to the imprecise way H&E DIA identifies steatosis rather than picking up all the true steatosis. This problem is largely resolved using ORO DIA as steatosis is identified by its red colour and nothing else in the slide stains red.

The study has shown that ORO staining without DIA is too sensitive for fat to be used by pathologists with the NAS in its current format. In all study groups 90-100% of hepatocytes contained small amounts of steatosis, as described in previous work.[64] Therefore ORO needs to be used in conjunction with DIA to accurately quantify the percentage area of steatosis, number and size of fat droplets and subsequently the type (microvesicular or macrovesicular) of steatosis.

2.5.1.1. ORO use in human liver biopsies

ORO staining was successfully performed on frozen human liver biopsies and ORO DIA showed excellent correlation with triglyceride content in the liver biopsies. There was poor correlation between triglyceride content or ORO DIA and visual assessment of steatosis on H&E by a liver pathologist/H&E DIA. This replicated the findings in the

mouse study that the percentage steatosis cannot be accurately assessed using H&E stained sections and this error leads to changes in NAS steatosis score.

MRI steatosis quantification also showed poor correlation with triglyceride content/ORO DIA in the human liver biopsies. When compared with ORO DIA this caused alterations in NAS steatosis score for three of the five patients. This strongly suggests that MRI is not as accurate as ORO DIA for steatosis quantification. Although sampling error may be present all readings were taken from the right lobe of the liver, the same area as the biopsy, to minimise this. Another possibility for the difference in steatosis quantification could be that MRI is quantifying free fatty acids as well as triglycerides within the liver, but, this does not appear to be the case as the MRI values were both above and below those of ORO DIA with no consistent pattern one would expect if this was the case. The results here contrast with those from a recent study in mice which suggest that MRI can accurately measure intrahepatic fat and correlate better with a chemical lipid analysis than pathologist's assessment or automated software.[65] The reasons for this lack of correlation with the pathologist and automated software in this study is likely to be because they did not use ORO and relied on H&E assessment of steatosis, which we have shown in this study is not accurate. However, the difference in correlation between the MRI and their chemical lipid analysis and our MRI and triglyceride quantification suggests further work in the area is needed.

2.5.2. The reasoning for triglyceride quantification

Visible fat within the liver in NAFLD consists mainly of triglycerides in the form of lipid droplets with a smaller amount present as cholesterol.[66] In an animal model of NAFLD the relative ratio of triglycerides to cholesterol in the liver is approximately 15:1, although we cannot be certain in our model.[67] Increased serum triglyceride levels are a major component of the metabolic syndrome and NAFLD.[68] ORO the "gold standard" histochemical stain for identifying fat in tissue identifies mainly triglycerides, and is less effective at staining phospholipids and cholesterol. The assay used in liver tissue from this study measured triglyceride levels; this assay was used because triglycerides are the main type of visible fat present in NAFLD.

2.5.3. Steatosis size assessment and comparison with previous studies

Using ORO DIA and robust criteria for microvesicular and macrovesicular fat, ≤15μm for microvesicular fat, it was apparent that visual assessment of droplet size on H&E by liver pathologists was inaccurate.[61] Virtually all fat identified on H&E by liver pathologists was actually macrovesicular fat, even the small droplets initially thought to be microvesicular fat. The work in this thesis shows that with a definition of ≤15μm, microvesicular fat is almost impossible to detect by the naked eye on H&E stained sections. Therefore when conditions associated with large amounts of microvesicular fat are suspected such as acute fatty liver of pregnancy, Reye's syndrome, drugs, aflatoxins and mitochondrial cytopathies, an ORO stain is essential.[69-71]

The cut off size of 15μm for the microvesicular and macrovesicular fat comes from a study in Hepatitis C patients.[61] This figure is not evidence based and it would be interesting to look at liver from patients with conditions associated with microvesicular fat such as acute fatty liver of pregnancy using ORO DIA to see what size the fat droplets are.

Many studies have assessed the percentage of macrovesicular and microvesicular steatosis, especially in the transplant and NAFLD settings.[72-76] All of the studies used H&E stained slides with occasional studies also performing ORO staining, although ORO was not used for any formal assessment of fat droplet size in these studies or in conjunction with DIA. No study has accurately defined the difference between macrovesicular and microvesicular steatosis with some using imprecise definitions and others not defining macrovesicular and microvesicular. Even in a study comparing H&E DIA to pathologists, microvesicular steatosis was defined as fat vacuoles smaller than the nuclear diameter and macrovesicular as fat droplets larger than the nuclear diameter.[74] Considering the variability in the size of nuclei and their relatively large size this would seem to be a flawed definition. In another study macrovesicular steatosis was defined as hepatocytes containing a single vacuole of fat which displaced the nucleus to the periphery of the cell and microvesicular steatosis as hepatocytes containing many small fatty inclusions in the cytoplasm without displacement of the nucleus.[72] According to these definitions, microvesicular steatosis would be much larger than 15μm and visible with the naked eye on H&E which is not the case in conditions with definite microvesicular steatosis such as acute fatty liver of pregnancy and Reye's syndrome.

Considering, microvesicular and macrovesicular steatosis are such widely used terms in liver pathology it is surprising that within the literature there seems to be such ambiguity. This does not allow routine comparison of results between different studies and increases interobserver error. The use of ORO DIA allows the accurate assessment of fat droplet size and differentiation into microvesicular and macrovesicular steatosis based on a size of $\leq$15μm.

2.5.4. Steatosis zonation assessment

There was an increased amount of macrovesicular steatosis in zones 2 and 3 when assessed by ORO DIA, especially in the mice on a high fat diet. This was apparent on H&E sections examined by expert pathologists but could not be quantified and again shows the advantage of using ORO DIA. This technique will allow comparison of the zonation of steatosis present in experimental models to see which most closely replicates the human pattern. The reason for the increase in macrovesicular steatosis in zones 2 and 3 is outside the scope of this thesis but is presumably related to fat processing within the liver.

2.5.5. The future use of ORO DIA and NAS

In this study we have used the NAS, which is a useful and proven tool in clinical practice and for patient selection for trial entry, indeed we have shown again in this study that the NAS shows strong interobserver correlation. However, when used as an outcome measure in a clinical trial setting, its performance is less robust. When changes in steatosis are the major study outcome, it is therefore difficult to know whether inaccurate

visual assessment of H&E stained sections by expert pathologists confounds these observations.[57] I propose a modification for steatosis calculation for use in research settings which can be used to give a quantitative steatosis score. Rather than using the percentage of hepatocytes involved by steatosis on an H&E stained section, the percentage area of steatosis on an ORO stained section calculated by ORO DIA should be used as a better reflection of steatosis.

2.5.6. Conclusions

This study has shown that ORO DIA is more accurate in quantifying steatosis than the current visual assessment on H&E by pathologists, H&E DIA or MRI quantification. Given this advantage and the ability of ORO DIA to correctly measure the size and zonation of steatosis I suggest that all NAFLD work in experimental models should use this technique in future to accurately assess steatosis. In experimental models there is the advantage over human biopsy work of having relatively larger amounts of liver tissue, including fresh frozen tissue available. Therefore, there should be no reason for not adopting ORO DIA.

This technique would accurately assess the zonation of steatosis and steatosis size in mouse models which currently has not been routinely performed. This would allow further comparison of different mouse models to see which is closest to the human NAFLD phenotype.

ORO staining is not practical for everyday use as it is optimally performed on frozen tissue because processing removes the lipids, hence I am not suggesting the stain be routinely performed on liver biopsies. However, this technique does give more accurate information regarding steatosis quantification and size than is currently available from a liver biopsy. During this study ORO staining has been successfully performed on frozen sections of human liver biopsies, making wider adoption of this technique viable. This study shows that ORO staining in conjunction with DIA should definitely be used in future NAFLD experimental model work and its use may be of merit in clinical trials where changes in steatosis are anticipated.

Chapter 3.

Exploring the use of Multi-Excitation Fluorescence Spectroscopy in the Diagnosis of Non-Alcoholic Fatty Liver Disease.

3.1. Introduction

NAFLD as described earlier encompasses a broad spectrum of disease ranging from isolated steatosis to NASH to cirrhosis. Because of the implications of a diagnosis of NASH with the future risk of progressive fibrosis, cirrhosis, liver failure and hepatocellular carcinoma it is important to distinguish patients with NASH from those with isolated steatosis.[77]

Multi-excitation fluorescence spectroscopy is a novel potential approach for real-time, minimally invasive characterisation of steatosis and NASH within liver tissue based on tissue oxidative stress and the levels of endogenous fluorophores within the liver. Fluorescence spectroscopy has been used for cancer diagnosis in various organs because it provides a fast and objective alternative to histopathology.[78]

3.1.1. Diagnosis of NASH

Currently the gold standard technique for the diagnosis of NASH is histological assessment of a liver biopsy. It is far more sensitive and specific than biochemical and imaging methods and is the only investigation able to accurately distinguish between simple steatosis, NASH and cirrhosis.[7] Radiological techniques are improving for the

detection of steatosis but they and laboratory test abnormalities are currently still unable to distinguish between the different degrees of NAFLD.[55, 56] Some of these limitations were discussed in the previous chapter.

A liver biopsy in suspected NASH patients may be performed for many reasons, for example, when there is diagnostic uncertainty or in patients with increasing liver function tests and risk factors for NAFLD (diabetes, obesity, hypertension, hypertriglyceridemia). A liver biopsy as with most procedures has possible risks, the commonest adverse effect is pain, other potential complications include bleeding (approximately 0.2% of biopsies); bleeding that requires hospitalisation or transfusion (approximately 0.05% of biopsies); puncture of a surrounding organ (approximately 0.03% of biopsies) and extremely rarely death (approximately 0.01% of biopsies).[79]

An accurate, less invasive method to distinguish between NASH and isolated steatosis that is sensitive, specific and readily available would offer benefits for determining treatment strategies, response to therapies, and prognosis. There are also potential implications within the transplant setting.

3.1.2. Autofluorescence spectroscopy

Autofluorescence spectroscopy is based on the principle that emission of light in the form of fluorescence may occur when an electronically excited molecular species deactivate. Fluorescence analysis is generally classified on the characteristics of the fluorophores present: endogenous fluorophores are naturally occurring in most biological samples

whereas exogenous fluorophores are externally administered to the tissues. Some fluorescence emission spectra for the commonest endogenous fluorophores in living tissues are shown in **Figure 10.** Exogenous fluorophores are widely used as labelling agents and were previously used as first generation photosensitisers in photodynamic therapy.[80] Because endogenous fluorophores are present in tissue, pathological conditions can result in alteration of the autofluorescence emission properties.[81]

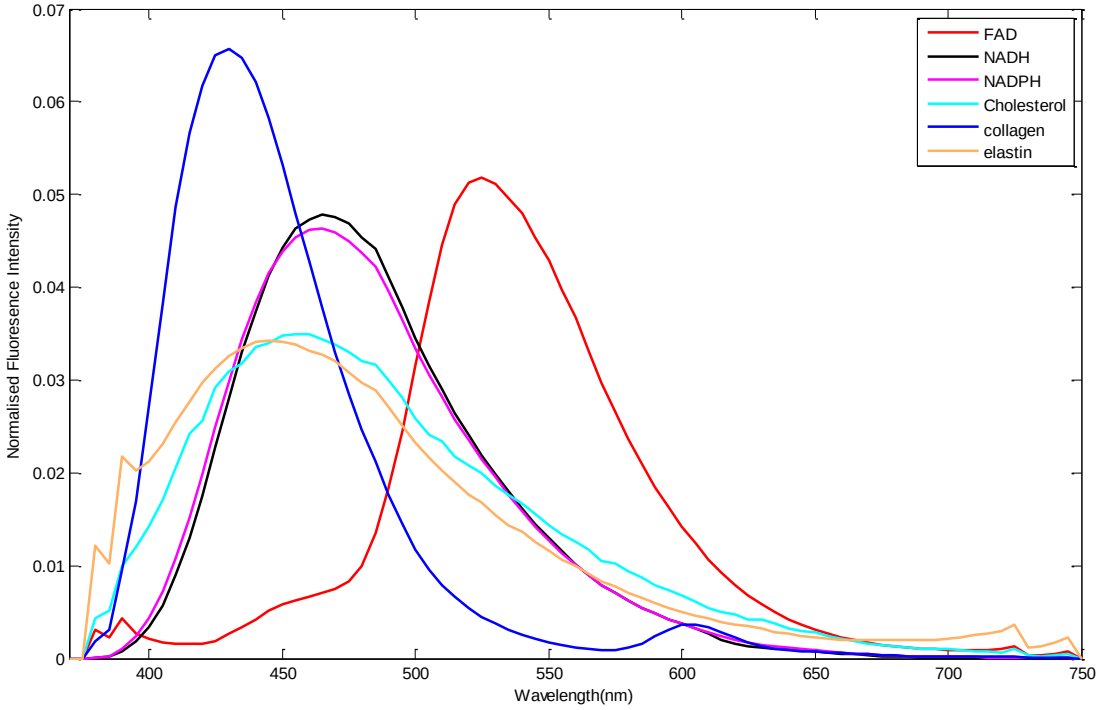


Figure 10. Emission spectra of endogenous fluorophores at 375nm excitation.[82]

FAD = flavin adenine dinucleotide, NADH = nicotinamide adenine dinucleotide and NADPH = nicotinamide adenine dinucleotide phosphate

As described earlier, liver biopsy is currently the only accurate method to diagnose and stage NAFLD. However, autofluorescence spectroscopy could be a powerful approach

for real time, minimally invasive liver characterisation which could potentially reduce complications and health care costs and allow for repeated testing. Because of the livers multiple metabolic functions it contains numerous endogenous fluorophores. These include the reduced forms of nicotinamide adenine dinucleotide (NADH) and nicotinamide adenine dinucleotide phosphate (NAD(P)H), vitamin A, flavin adenine dinucleotide (FAD), lipofuscin, collagen and elastin. Many of these fluorophores have previously been demonstrated to provide significant information about differences in tissues.[82] NAD(P)H and Vitamin A in particular have been shown to be major contributors to liver autofluorescence.[83]

A brief summary of these fluorophores is provided below:

- NADH & NAD(P)H: In the reduced protonated form, nicotinamide adenine dinucleotide (NADH) and nicotinamide adenine dinucleotide phosphate (NADPH) are important fluorescent substances in most types of living cells, especially hepatocytes. They are both coenzymes with key roles in cell energy metabolism and have previously been used to study oxidative stress in yeast cells.[84] A study in rats has shown increased NAD(P)H fluorescence associated with steatosis within the liver.[85] The excitation maximum of free NAD(P)H occurs at 360nm with emission at 460 nm, while the protein-bound coenzyme emits around 440nm.
- Vitamin A: This fluorophore is largely stored within stellate cells in the liver. Nutritional disorders have been reported to induce alterations of liver metabolism, therefore, affecting the autofluorescence emission properties of the liver. A study using fluorescence showed that accumulation of lipid within the liver is associated

with increased Vitamin A levels.[82] Decreased Vitamin A levels are associated with the conversion of stellate cells to a myofibroblastic phenotype, which is seen in fibrosis.[86] Vitamin A has an anti-oxidant activity and therefore it may have a role in dealing with enhanced cell oxidative stress in NAFLD caused by lipid accumulation within hepatocytes. Vitamin A has a maximum excitation at 366nm with an autofluorescence emission maximum of 488nm.

- Flavin: Flavins are derivatives of riboflavin (vitamin B_2), the commonest is flavin adenine dinucleotide (FAD). FAD is the oxidised form of the co-enzyme and has a key role in cell energy metabolism and is fluorescent, while the reduced form, $FADH_2$, is not. Several investigators have shown that FAD has an excitation maximum around 450nm and emission maximum around 515nm.[87]
- Lipofuscin is a pigment present within all livers which is associated with cell damage and normally increases with age. Lipofuscin is often present at the end stage of autophagocytosis. Lipofuscin has a maximum fluorescence emission around 575 nm.[88]
- Elastin and collagen: Fluorescence has been noted in structural proteins such as collagen and elastin. Collagen and elastin autofluorescence is associated with cross-links. In elastin, two major types of cross-links are formed by desmosine and isodesmosine. The excitation and emission maximum of this elastin cross-link are 325nm and 400nm respectively. In collagen, the cross-link formation is considered to have two pathways: one is enzymatically controlled cross-links that occurs during development and maturation, the other is an age-related, non enzymatic mechanism.

Excitation and emission maxima for collagen powder were reported, respectively, at 280 and 310nm, 265 and 385nm, 330 and 390nm, 450 and 520nm.[81]

3.1.2.1. Photobleaching phenomenon

Autofluorescence signal intensity decays as a result of light exposure due to photobleaching. Photobleaching refers to the permanent loss of fluorescence ability of fluorophores following their photon-induced chemical modification.[89] This can be a problem with measuring organic fluorophores as they disappear over time but can also be used as a benefit to ascertain which fluorophore one has been measuring as each fluorophore has an intrinsic photobleaching rate modulated by its environment and the intensity of irradiation.[90] Vitamin A and NAD(P)H by far the largest fluorophores within the liver both have short photobleaching rates at 375nm excitation with an emission wavelength between 450 and 550nm.[83] Photobleaching measurements whilst performing autofluorescence spectroscopy in NAFLD would therefore help to confirm which fluorophores have been measured during studies.

3.1.3. Mouse models of NAFLD

There are numerous mouse models of NAFLD that exhibit evidence of histological steatosis, some of which also show evidence of steatohepatitis. Three of the commoner models are the leptin resistant Db/Db mice, mice fed a diet deficient in both choline and the essential amino acid methionine (MCD) and mice fed a HFD.[58, 91]

The db/db mice have mutations in the diabetes gene on mouse chromosome 4, leading to an autosomal recessive, diabetic, obese phenotype.[92] The db/db mice have normal or elevated levels of leptin but are resistant to its effects. The Db/m mice have no resistance to leptin and are phenotypically normal.

Mice fed an MCD diet develop steatohepatitis and in time hepatic fibrosis. The MCD diet impairs mitochondrial β-oxidation and leads to induction of alcohol-inducible CYP2E1 expression, a finding later confirmed in a cohort of NASH patients.[93, 94] These findings support the hypothesis that alcoholic and non-alcoholic steatohepatitis may share pathogenic mechanisms. Reactive oxygen species (ROS) produced by CYP2E1 ω-oxidation, coupled with depletion of hepatic antioxidants (*e.g.* reduced glutathione and *s*-adenosylmethionine), promote oxidative stress and induce a histological steatohepatitis. The MCD diet induces significantly greater ROS production, mitochondrial DNA damage and apoptotic cell death than many of the other mouse models of NAFLD.[95]

Feeding steatotic db/db mice the MCD diet is shown to produce an accelerated fibrosing steatohepatitis.[96] The db/MCD combined model is thought to represent an obese, diabetic experimental model of progressive steatohepatitis. However, the aetiology in this model is not representative of the true pathological mechanism encountered in clinical practice.

C57BL/6 mice are genetically prone with ageing to develop obesity, hyperinsulinaemia and glucose intolerance irrespective of their diet. This phenotype can be exacerbated leading to florid hepatic steatosis by feeding a HFD. HFD fed C57BL/6 mice are

therefore considered a good model for investigating NAFLD and the metabolic syndrome.[97] Studies based on gastrostomy HFD overfeeding of C57BL/6 mice also demonstrate inducible steatohepatitis.[98]

Diets with increased carbohydrates such as 65% sucrose in C57BL/6 mice for 8 weeks have also been used to induce obesity and hepatic steatosis.[99]

Despite the proven use of mouse models, there is a difference between human NAFLD and that seen in most mouse models. There are very few mouse models of advanced steatohepatitis, especially when combined with insulin resistance.[58] Mice such as C57BL/6 fed a high fat diet can provide an accepted model of the metabolic syndrome with histological features of a mild-moderate steatohepatitis. They also show steatosis which begins predominantly in zone 3, the same zone as in humans, which many other mouse models do not. However, there is a lack of progression to fibrosing steatohepatitis which has limited the use of such models in testing potential medications.

A more severe fibrosing steatohepatitis can be induced by feeding the MCD diet and this is commonly used when a study needs to induce fibrosis. It must be noted though that the steatohepatitis induced in this model is via a non-physiological process, there is no insulin resistance and the mice lose weight which can limit the length of time this disease can progress in these models.[100] One of the most promising and more commonly used models for studying steatohepatitis with fibrosis is the Db/Db mice fed an MCD diet. This combines genetic and dietary manipulation to produce the metabolic syndrome

background with the liver showing histological features of severe fibrosing steatohepatitis which are similar to those present in humans.

3.2. Aims

The aim was to determine whether it was possible to differentiate steatosis and NASH from histologically normal liver using autofluorescence spectroscopy in animal models and human liver biopsies with varying degrees of NAFLD.

3.3. Methodology

3.3.1. Animal husbandry

The research was approved by the local ethics committee and was carried out under Home Office supervision in accordance with the Animal (Scientific Procedures) Act 1986 taking care to minimise any distress caused to the animal. Procedures were performed under the authority of licence 30/2505 'Mouse Models of Steatohepatitis for Basic Science & Therapeutics Investigation'. Animals were housed under standard conditions (12 hour light/dark cycle, temperature 21 ± 2°C, humidity 55 ± 10%).

3.3.2. Liver tissue and blood for MCD model of NAFLD

Ten male Db/Db mice and five male Db/m mice were housed under standard conditions. From 8 weeks of age the ten Db/Db mice were randomly divided into two groups and fed a standard pelleted commercial chow containing 11.5 kcal% fat (#801722, SDS, UK), or a methionine and choline deficient (MCD) diet for the remaining 8 weeks of the study.

The five Db/m mice were fed a standard pelleted commercial chow containing 11.5 kcal% fat (#801722, SDS, UK) until being culled. Two of the mice in the Db/Db standard chow group became unwell, and were culled early and subsequently excluded from the study. (**Table 12)**

N=	Strain	Diet	Drink	Duration (Weeks)	Model
5	Db/Db	MCD	Water	8	Fibrosing Steatohepatitis
5*	Db/Db	Standard Chow	Water	8	Steatosis
5	Db/m	Standard Chow	Water	8	Control

Table 12. MCD study groups

*Two of the mice in the Db/Db standard chow group became unwell during the study and were culled early and subsequently excluded from the study.

Mice were culled by overdose of anaesthetic administered by intraperitoneal injection (0.2ml Sagatal, Pentobarbitone sodium 60mg/ml, Merial Ltd., UK). Cardiac puncture and exsanguination were then performed to collect blood for biochemical analysis. The liver was explanted and divided into two, half was probed and then placed in 10% formalin and half was snap frozen in liquid nitrogen and stored at -80°C.

3.3.3. Liver tissue and blood for HFD/Fructose model of NAFLD

Twenty male C57BL/6J and ten male C3H mice (Charles River, UK) were housed under standard conditions. From 8 weeks of age the C57BL/6J mice were randomly divided into four groups and fed a standard pelleted commercial chow containing 11.5 kcal% fat (#801722, SDS, UK), or a nutritionally replete pelleted high fat diet (45%kcal fat derived

from lard; D12451, Research Diets Inc, USA) with or without 30% fructose w/v (Sigma-Aldrich, UK) in drinking water for the remaining 15 weeks of the study **(Table 13**). One of the mice in the high fat diet and water group became unwell, and was subsequently excluded from the study. The C3H mice were also randomly divided into two groups from 8 weeks of age and fed either standard pelleted commercial chow containing 11.5 kcal% fat (#801722, SDS, UK), or a nutritionally replete pelleted high fat diet (45%kcal fat derived from lard; D12451, Research Diets Inc, USA) with drinking water for the remaining 15 weeks of the study (**Table 13**).

N=	Strain	Diet	Drink	Duration (Weeks)	Model
5	C3H	Standard Chow	Water	15	Control
5[#]	C3H	HFD	Water	15	Steatosis
5	C57BL/6J	Standard Chow	Water	15	Control
5*	C57BL/6J	HFD	Water	15	Steatosis
5	C57BL/6J	Standard Chow	Fructose	15	Control
5	C57BL/6J	HFD	Fructose	15	Steatohepatitis

Table 13. HFD/Fructose study groups

[#] Two of the mice in the high fat diet became unwell during the study and had to be culled early.
* One of the mice in the high fat diet and water group became unwell during the study and was excluded from the analysis.

Mice were culled by overdose of anaesthetic administered by intraperitoneal injection (0.2ml Sagatal, Pentobarbitone sodium 60mg/ml, Merial Ltd., UK). Cardiac puncture and exsanguination were then performed to collect blood for biochemical analysis. The liver was explanted and divided into two, half was probed and then placed in 10% formalin and half was snap frozen in liquid nitrogen and stored at -80°C.

3.3.4. Human liver tissue

Consent for research was obtained from seven patients with suspected NAFLD who were having a liver biopsy. At the time of biopsy the liver tissue was probed and then placed in 10% formalin and processed as normal.

3.3.5. Histopathology and special stains

Formalin fixed liver tissue was processed into paraffin wax and sections were stained with H&E and Sirius Red, a collagen stain. H&E and Sirius Red stained sections were assessed using the validated NASH CRN histological classification to give a NAS and fibrosis stage, as described earlier.[41] See **Tables 1 and 2**.

3.3.6. Malondialdehyde immunohistochemistry

3.3.6.1. Rationale

The MCD mouse model of NASH is characterised by increased ROS production.[95] Lipid peroxidation of polyunsaturated fatty acids generates toxic aldehyde by-products including malondialdehyde (MDA) and 4-hydroxynonenal (HNE) that can be used as markers of oxidative stress within tissue.[101] To compare tissue oxidative stress within the livers of the MCD model MDA immunohistochemistry was performed.

3.3.6.2. Deparaffinisation

Sections were heated in an oven for 10 minutes and then immersed in 100% Xylene (Genta Enviromental Ltd, York, UK) solution for 10 minutes twice and rehydrated by

immersing in 100 % Ethanol (Biotech Solutions Ltd, York, UK) for 5 minutes, 90% Ethanol for 5 minutes and 75% Ethanol for 5 minutes. Sections were then washed with distilled water.

3.3.6.3. Blocking of endogenous peroxidise activity

Sections were treated with 0.3% hydrogen peroxide (H3410; Sigma, St. Louis, MO, USA) in methanol (Fischer Scientific, Leicestershire, UK) for 30 minutes and then washed once with Tris buffered saline.

3.3.6.4. Antigen retrieval

Sections were immersed in 0.01M of sodium citrate buffer (HDS05; HD Supplies, Bucks, UK), pH 6.0 and placed in a boiling pressure cooker for 3 minutes. They were then microwaved (1500 W) twice for 5 minutes each. The sections were then washed once in Tris buffered saline.

3.3.6.5. Incubation with the primary antibody

Sections were incubated with the primary antibody, a rabbit polyclonal to malondialdehyde (Ab 6463, Abcam, Cambridge, UK). The primary antibody was diluted to the optimised dilution (1:200) with buffer (Dako REAL substrate buffer), 100µl was placed on each section and left for 60 minutes. The sections were then washed three times with Tris buffered saline**.** For one set of tissue sections, which were to act as negative controls, the primary antibody was omitted, and the sections were incubated only in the antibody diluent buffer (Dako REAL substrate buffer).

3.3.6.6. Incubation with the secondary antibody

Sections were incubated with 100µl of the secondary antibody (Dako REAL Envision, anti-Rabbit/Mouse Detection System) for 10 minutes at room temperature. The sections were then washed three times in Tris buffered saline.

3.3.6.7. Application of the DAB/Chromogen detection system

Sections were incubated with the DAB/Chromogen detection system (Dako REAL DAB and Chromogen) for 5 minutes at room temperature. The DAB/Chromogen solution was diluted (1:50) with buffer (DAKO REAL substrate buffer). Sections were then washed with distilled water.

3.3.6.8. Counterstaining and mounting

Sections were counterstained in haematoxylin for 1 minute and then rinsed in running water for 5 minutes**.** Sections were then mounted in the aqueous mounting medium. (Dako permanent aqueous mount; Dako).

3.3.7. Thiobarbituric Acid Reactive Substances as a Marker of Oxidative Stress

The MCD mouse model of NASH is characterised by increased ROS production as described earlier. To quantify this thiobarbituric acid reactive substances (TBARS) assay was performed.

Approximately 100 mg of frozen liver was placed into a ceramic beads tube. Then 300µl of RIPA buffer was added and the tubes placed into a Precellys rotor at 6500rpm, 1 cycle for 50 seconds to homogenise the samples. The supernatant was then kept on ice and used in the assay. 100µl of the lysate was placed into a 1.5ml eppendorf and 200µl of ice cold 10% Trichloracetic acid was added. The sample was then incubated for 15 minutes on ice. The samples were then centrifuged at 3000g for 10 minutes. Standards were prepared using distilled water and 500µM MDA to give known MDA concentrations from 0µM to 50µM. 300µl of the samples and standards were then mixed with 300µl of 0.67% thiobarbituric acid and incubated at 95°C for 10 minutes. The samples were then allowed to chill.

Using a 96 well plate 150µl of each standard and sample was placed into a well, this was performed in duplicate. Spectrophotometry at O.D. 532nm was measured using a plate reader. Using the absorbance values and standard curve the MDA concentration in µM per 100mg of liver for each sample was calculated.

3.3.8. Plasma Alanine Aminotransferase levels as a biochemical marker of hepatitis

The blood obtained when the mice were culled was placed in a plasma capillary tube with lithium heparin (Microvette CB300, Sarstedt) which when centrifuged at 3000rpm for 10 minutes separated the plasma from the erythrocytes. The supernatant plasma was removed from the blood and stored at -80°C until analysed in an automated biochemical analyser to give ALT measurements in IU/L.

3.3.9. Autofluorescence spectroscopy system

This system was developed by Dr D Elson & Dr V Sauvage at Imperial College in the Institute of Biomedical Engineering. The data processing and acquisition was performed in conjunction with Dr Sauvage. A violet laser induced fluorescence system **(Figure 11)** was used combining two laser diodes emitting at 375 nm and 405 nm and a fibre optic probe. These two excitation wavelengths were chosen as NAD(P)H, NADH, Vitamin A, flavins and lipofuscin are excited at these wavelengths. The custom made fibre optic probe (Romack Inc, USA) consists of six hexagonally distributed excitation fibres which collect the fluorescence emission light, surrounding a central emission fibre which delivers the excitation light to the tissue. The diameter and numerical aperture of the fibres are 200 μm and 0.22 respectively. The excitation light was provided by two laser diodes, one for 375nm excitation wavelength and the other for 405nm. The diameter of the distal end of the probe touching the tissue was 2mm.

Two beam shutters (one for each laser diode) enable selective blocking of one of the beams and two 4.6 mm focal length lenses, collimate the beams. Two mirrors, located after the 405 nm laser diode, allow the alignment of both beams. A dichroic mirror reflects the light from the 375 nm laser diode and transmits the 405 nm beam.

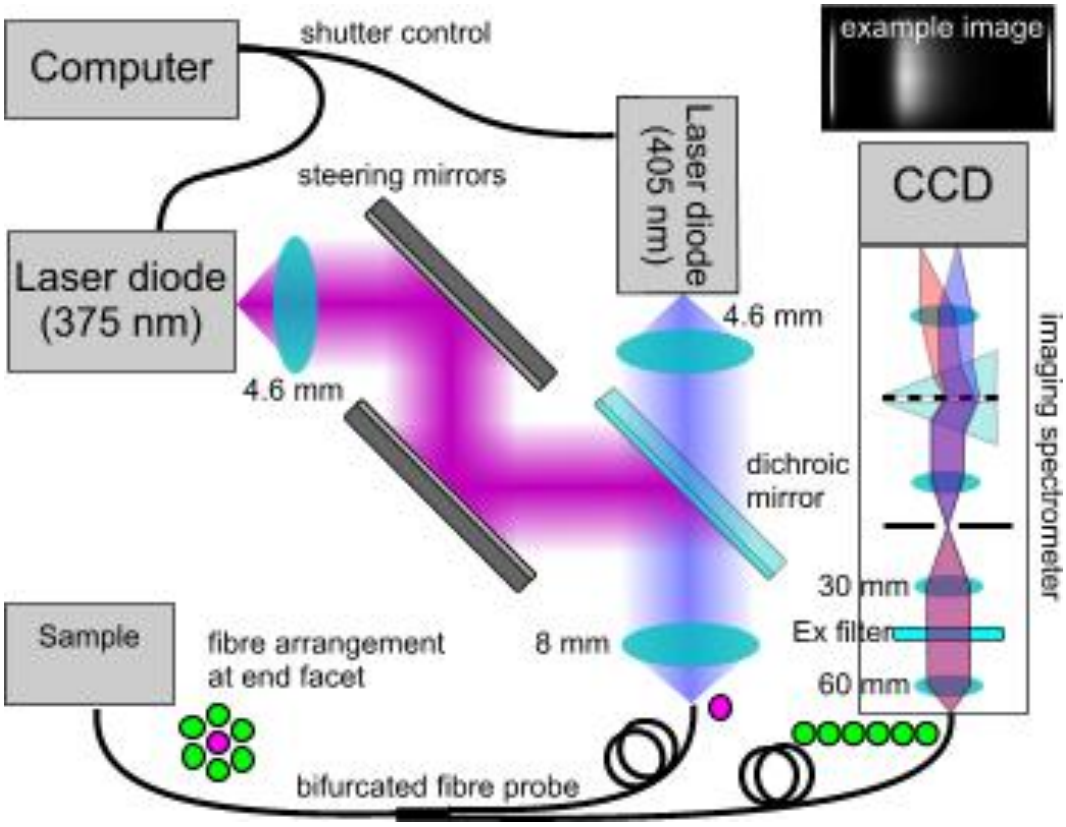


Figure 11. Experimental set-up of multi excitation wavelength fluorescence spectroscopy probe.

An 8 mm focusing lens situated after the dichroic mirror enables coupling of the laser beam in the excitation fibre. A lens doublet (60 mm and 30 mm) was used to collimate and focus the light from the emission fibre into the 80 µm wide slit of the spectrograph (Specim Ltd). A 405 nm long-pass filter was inserted between these two lenses to block the light of the laser diodes reflected by the sample. The light dispersed by the prism-grating prism element of the spectrograph was then acquired with a cooled CCD camera (Retiga EXI, Qimaging, 1392 x 1040 pixels). The optical power at the distal end of the probe was 3.5 mW for both lasers. A Labview program controlled the exposure time, the

region of interest, the beam shutters and enabled acquisition of fluorescent signals from the laser diodes sequentially with an adjustable number of measurements.

3.3.9.1. Autofluorescence data acquisition

In both the MCD study and HFD/Fructose study between three and four measurements were performed on each liver at each excitation wavelength, with each measurement producing six spectra (one from each of the six emission fibres). See **Tables 14 and 15.**

Model	Number of spectra at each excitation wavelength
Fibrosing steatohepatitis	114
Steatosis	72
Control	114

Table 14. The number of emission spectra for each disease model in the MCD study.

Model	Number of spectra at each excitation wavelength
Steatohepatitis	102
Steatosis	258
Control	252

Table 15. The number of emission spectra for each disease model in the HFD/Fructose study.

In the human liver biopsies between two and five measurements were performed on each liver depending on the size of the biopsy at 375nm excitation wavelength, with each measurement producing six spectra (one from each of the six emission fibres). See **Table 16.**

Diagnosis	Number of spectra
NASH	36
Steatosis	24
Normal	60

Table 16. The number of emission spectra for each diagnosis in the human liver biopsies.

The spectrum of a tungsten-halogen calibrated light source (Ocean optics Inc.) was recorded at the start of each experiment to calibrate the system spectral response. The ratio of this spectrum over the real spectrum was used to correct the raw spectra. Then, spectra were normalised by their area under the curve and truncated between 450 and 750nm.

3.3.9.2. Autofluorescence data processing and analysis

Sparse multinomial logistic regression (SMLR), was used to attempt to separate the spectral features into the disease categories in both experiments.[102] SMLR belongs to the family of supervised learning algorithm; it proposes a true multiclass classification of the spectra thanks to classifiers built as a linear combination of the input features, for example, the 106 fluorescence intensities at the 106 wavelengths sampled between 450nm and 750 nm for each spectrum. The probability that a spectrum belongs to a certain class was assumed to follow the multinomial logistic regression model where the regression coefficients are the classifier weight vectors of the corresponding class. The spectrum was assumed to belong to the class whose weight vector maximised this probability. The estimation of the weight matrix (106 lines, 3 columns) for the 3 different

classes, in other words the learning of the classifier, is calculated from a maximum a posterior estimate, with the spectra as input training data.

This approach differs from the traditional maximum likelihood estimation in that, it was not only the log-likelihood function which was maximised to estimate the weight vectors but the sum of the log-likelihood function and the logarithm of a prior on the weights distribution. A laplacian prior, a formula used in supervised learning models, was chosen because the logarithm of this distribution was proportional to the l1-norm of the weights. Consequently, this maximisation problem was similar to an l1-penalised regression which presents the major advantage to promote sparse coefficient vectors, i.e. vectors with coefficients either large or null. The benefits of sparse estimates are numerous: as many coefficients are set to zero, their variance is low which produce stable models with high prediction accuracy, inherent feature selection and handling of large datasets as the weights of the spectral features inconsequential for the classification are set to zero.[102, 103]

3.3.9.3. Photobleaching data acquisition

In the follow up study only photobleaching was evaluated by measuring the emission intensity spectra on the same area of each liver exposed to continuous irradiation at 375nm excitation. Each sample had 20 sequential emission intensity spectral measurements taken at 300 millisecond intervals (total 6 seconds). The light dose at the point of measurement was 3.5 $mWcm^2$ for excitation at 375nm.

3.3.9.4. Photobleaching data processing and analysis

Photobleaching rates like fluorescence lifetimes are likely to follow a continuous distribution in tissue rather than a discrete distribution of measurements at certain time points.[104] For this reason, a stretched exponential model was used to describe the temporal evolution of the fluorescence with photobleaching rather than a multi-exponential model which does not reveal the complexity of the photobleaching time distribution.[105]

The stretched exponential model uses the fluorescence intensity at the start of the measurement and at any given time in conjunction with the characteristic rate of fluorescence decay by photobleaching and a heterogeneity coefficient which is linked to the width of the photobleaching time distribution.[104]

Within each study group, the spectra were averaged and the changes in fluorescence intensity measurements were fitted into the stretched exponential function model at each emission wavelength between 450 nm and 650 nm to extract the photobleaching fluorescence intensity, and the heterogeneity coefficient.

3.3.10. Statistical analysis

The non-fluorescence data were collated in Microsoft Excel (Microsoft Inc, USA) and statistical analysis performed using SPSS version 17 (SPSS, USA). Quantitative data are expressed as the mean unless otherwise stated. Normally distributed continuous variables were compared by Student's t-test or ANOVA. Two-tailed p-values are shown unless otherwise stated. Statistical significance was accepted at $p<0.05$.

3.4. Results

3.4.1. MCD study results

3.4.1.1. Phenotypic differences in experimental groups

After 8 weeks on different diets, phenotypic differences were apparent between groups (**Figure 12**). The Db/Db mice fed a MCD diet showed significant weight loss over the course of the experiment (42.54±0.83g vs. 32.90±0.79g, $p<0.001$). At the end of the experiment the Db/Db mice fed a MCD diet weighed significantly less than the Db/Db mice fed a standard Chow diet (32.90±0.79g vs. 44.23±1.22g, $p <0.001$). This effect was attributed to the diet consumed as the body weights at the start of the experiment were not significantly different (42.54±0.83g vs. 46.60±1.62g respectively). The Db/m mice were lighter than the obese Db/Db mice at the start of the experiment and unlike the mice on a MCD diet their body weight increased during the experiment.

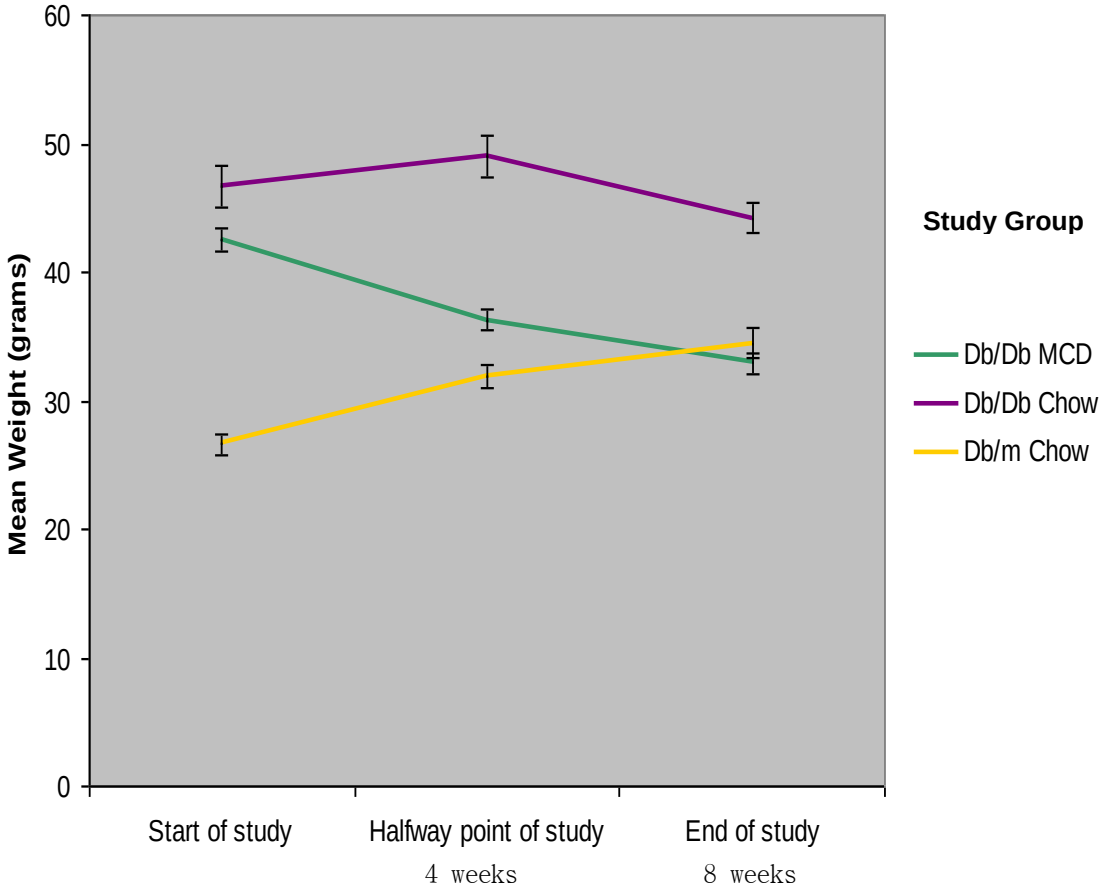


Figure 12. Graph showing mean body weights of the mice in each experimental group over the course of the study ± 1 standard error of the mean.

3.4.1.2. H&E and Sirius Red stains

H&E and Sirius Red stained sections showed that the three study groups could be clearly distinguished. The Db/Db mice fed a MCD diet had NASH & early fibrosis, there was marked steatosis, moderate lobular inflammation and many ballooned hepatocytes. The Db/Db mice fed Chow exhibited features of isolated steatosis without lobular

inflammation and non-obese Db/m mice fed Chow had normal liver histology. **(Table 17 and Figures 13 and 14)**

Study Group	Model	Steatosis	Lobular Inflammation	Hepatocyte Ballooning	NAFLD Activity Score	Fibrosis Stage
Db/Db MCD	Fibrosing Steatohepatitis	3 (3)	2 (2)	2 (2)	7 (7)	1A (1A)
Db/Db Chow	Steatosis	2 (1-2)	0 (0)	0 (0)	2 (1-2)	0 (0)
Db/m Chow	Control	0 (0)	0 (0)	0 (0)	0 (0)	0 (0)

Table 17. Median NAFLD activity score and fibrosis stage for the MCD study mice with the range in brackets.

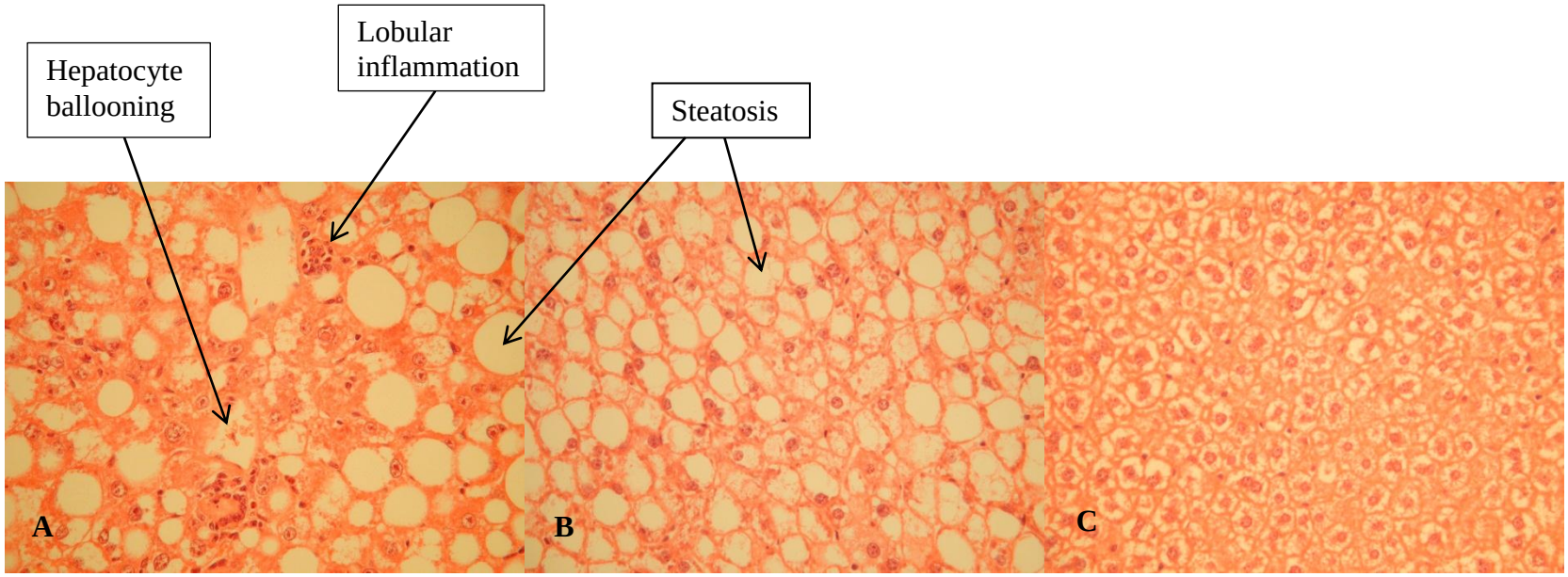


Figure 13. H&E stained sections of mouse livers. **A)** Db/Db mouse fed MCD showing steatosis, lobular inflammation and hepatocyte ballooning, **B)** Db/Db mouse fed standard Chow showing steatosis only, **C)** Db/m mouse fed standard Chow. x400 original magnification.

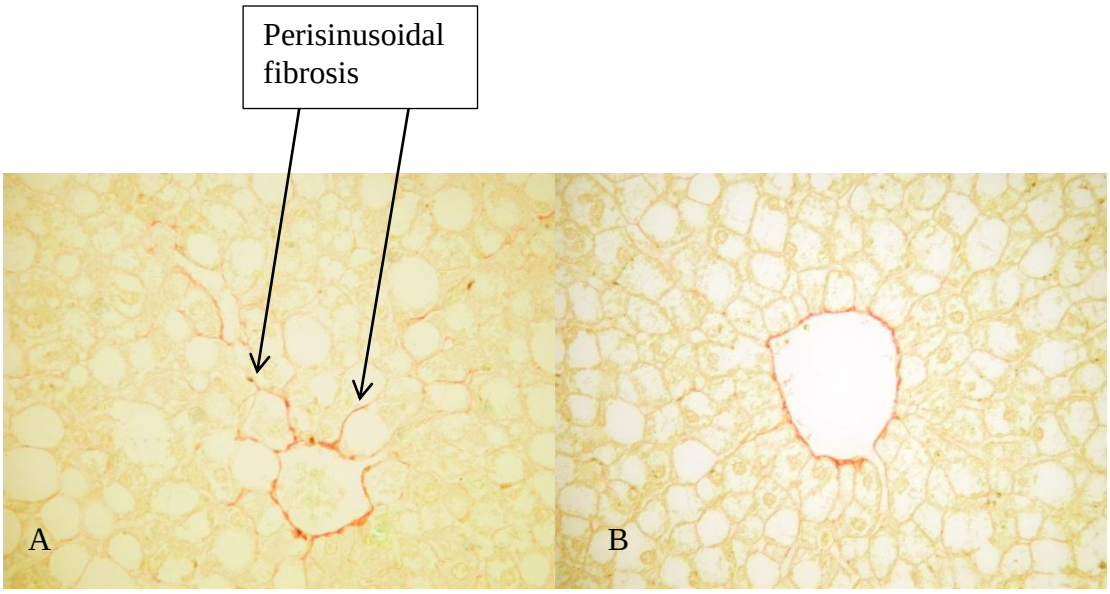


Figure 14. Sirius Red stained sections of mouse livers. **A)** Db/Db mouse fed MCD showing mild, zone 3, perisinusoidal fibrosis, stage 1A. **B)** Db/Db mouse fed standard Chow showing a normal architecture with no fibrosis. x400 original magnification.

3.4.1.3. MDA immunohistochemistry

Staining for MDA was graded as either positive or negative. There was positive staining in 5% of hepatocytes from Db/Db mice fed an MCD diet (**Figures 15A & B**). The staining had a granular pattern and was present within the cytoplasm of hepatocytes which appeared ballooned. There was no staining within the Db/Db mice on control diet (**Figure 15C**) or the Db/m mice on control diet (**Figure 15D**).

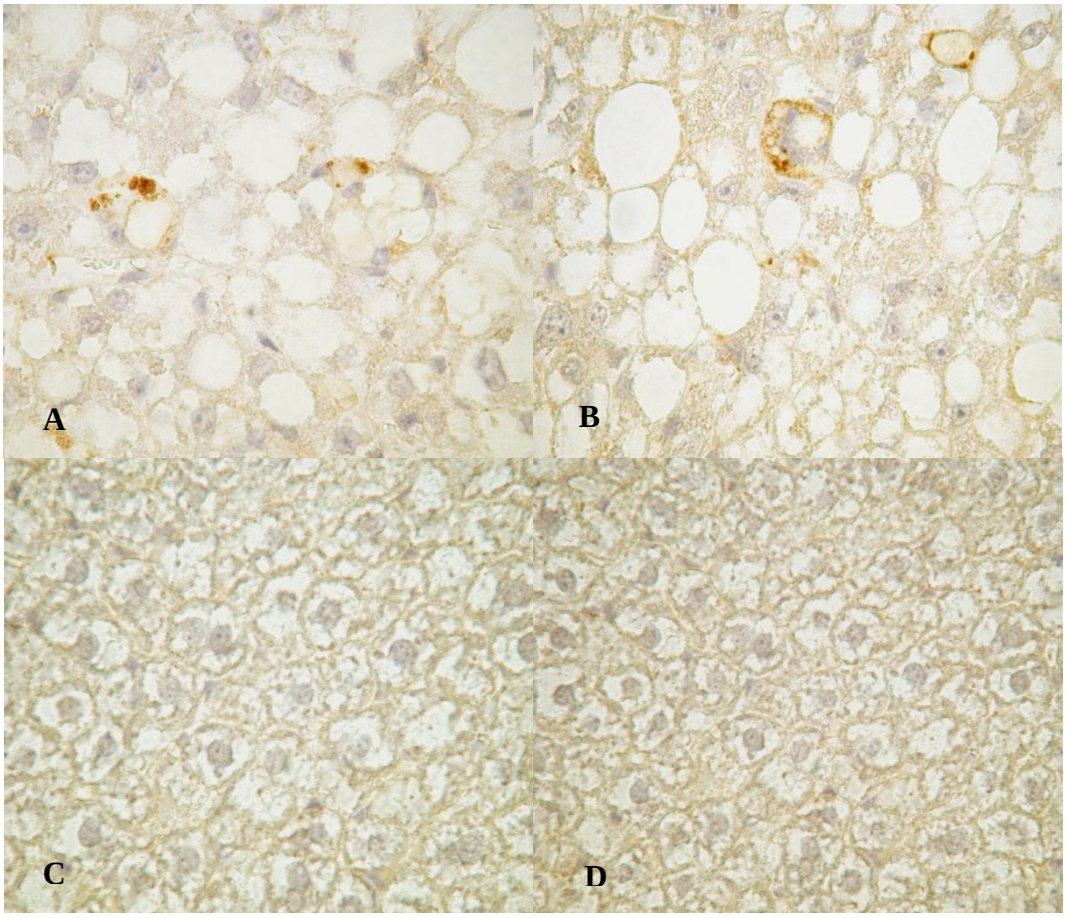


Figure 15. MDA immunohistochemistry on mouse livers. **A & B)** Db/Db mice fed an MCD diet, showing positive brown granular staining in the cytoplasm of hepatocytes. **C)** Db/Db mice fed a standard Chow diet showing no staining. **D)** Db/m mice fed a standard Chow diet showing no staining, x400 original magnification.

3.4.1.4. TBARS assay

There were significantly raised MDA concentrations in the liver of Db/Db mice on MCD diet compared to the two other study groups as expected (p=0.028 with Db/Db mice on standard chow and p=0.011 with Db/m mice on standard chow, **Figure 16**). The mean MDA concentrations (µM per 100mg of liver) were 1.79±0.46 for the Db/Db mice on MCD diet, 0.28±0.02 for the Db/Db mice on standard chow and 0.26±0.02 for the Db/m

mice on standard chow (**Table 18**). These results confirm that there was increased oxidative stress within the liver of the Db/Db mice on the MCD diet and is in keeping with the positive MDA immunohistochemistry staining seen in the livers of these mice. No significant difference was detected between the chow fed Db/Db mice with isolated steatosis or the phenotypically normal Db/m mice fed chow.

MCD Study Group	Malondialdehyde Concentration (µM per 100mg of liver) ± SEM
Db/Db mice on MCD diet	1.79±0.46
Db/Db mice on standard chow	0.28±0.02
Db/m mice on standard chow	0.26±0.02

Table 18. Mean malondialdehyde concentration in the livers of the MCD study group mice ±SEM.

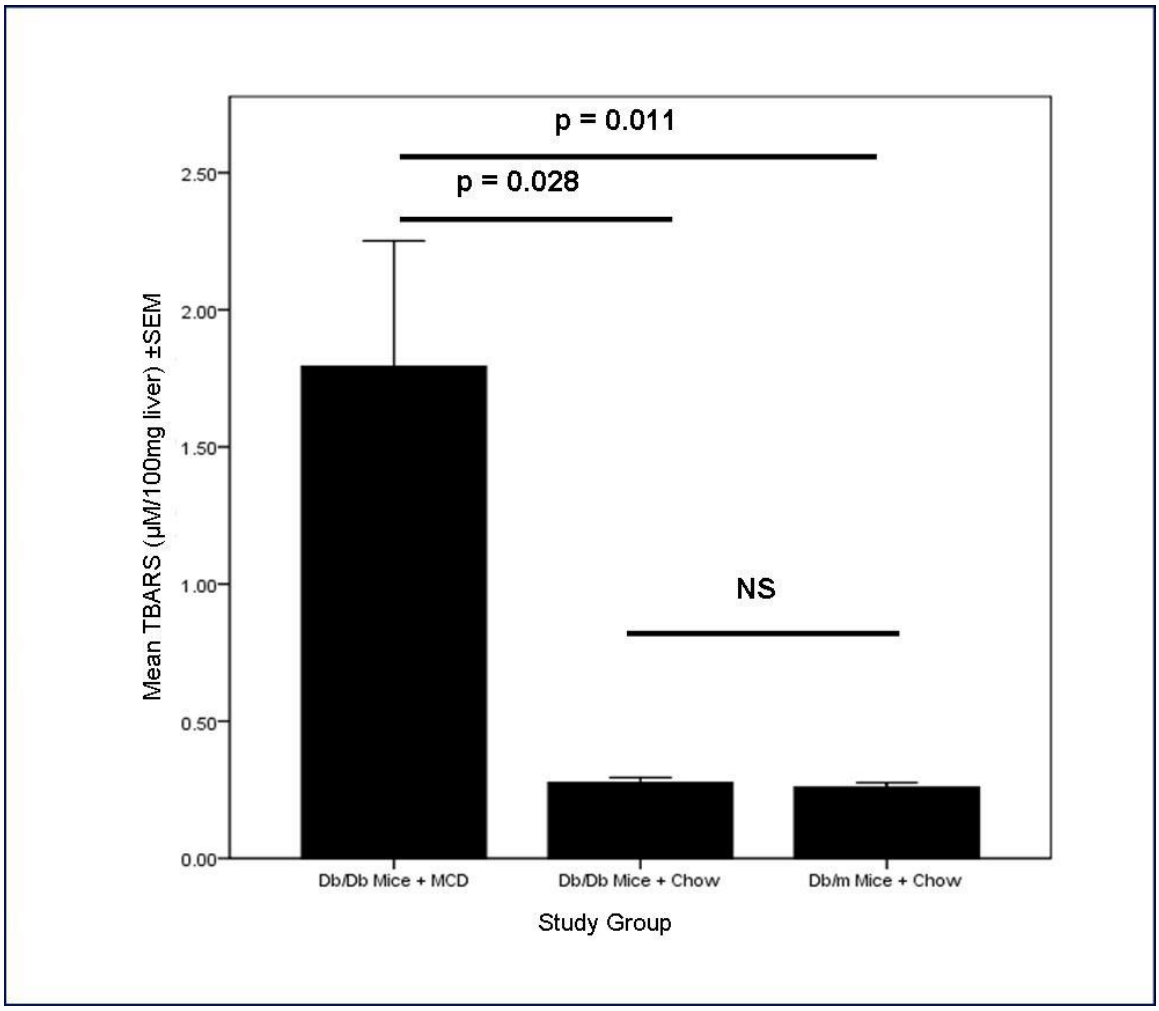


Figure 16. Mean malondialdehyde concentration in the livers of the MCD study group mice ±SEM.

3.4.1.5. ALT biochemistry

There was significantly increased ALT levels in the plasma of the Db/Db mice fed MCD diet compared to the two other study groups as expected (p=<0.001 for Db/Db mice on standard chow and Db/m mice on standard chow, **Figure 17**). The mean ALT levels in the plasma (IU/L) were 307.34±33.38 for the Db/Db mice on MCD diet, 91.77±4.78 for the Db/Db mice on standard chow and 26.40±4.07 for the Db/m mice on standard chow

(**Table 19**). These results confirm that there was a biochemical hepatitis within the liver of the Db/Db mice on the MCD diet which is in keeping with the lobular inflammation and ballooning identified on H&E stain histologically. No significant difference was detected between the chow fed Db/Db mice with isolated steatosis or the phenotypically normal Db/m mice fed chow although there does appear to be a trend towards increased ALT in the steatotic Db/Db mice.

MCD Study Group	ALT Biochemistry (IU/L) ± SEM
Db/Db mice on MCD diet	307.34±33.38
Db/Db mice on standard chow	91.77±4.78
Db/m mice on standard chow	26.40±4.07

Table 19. Mean ALT levels in the plasma of the MCD study group mice ±SEM.

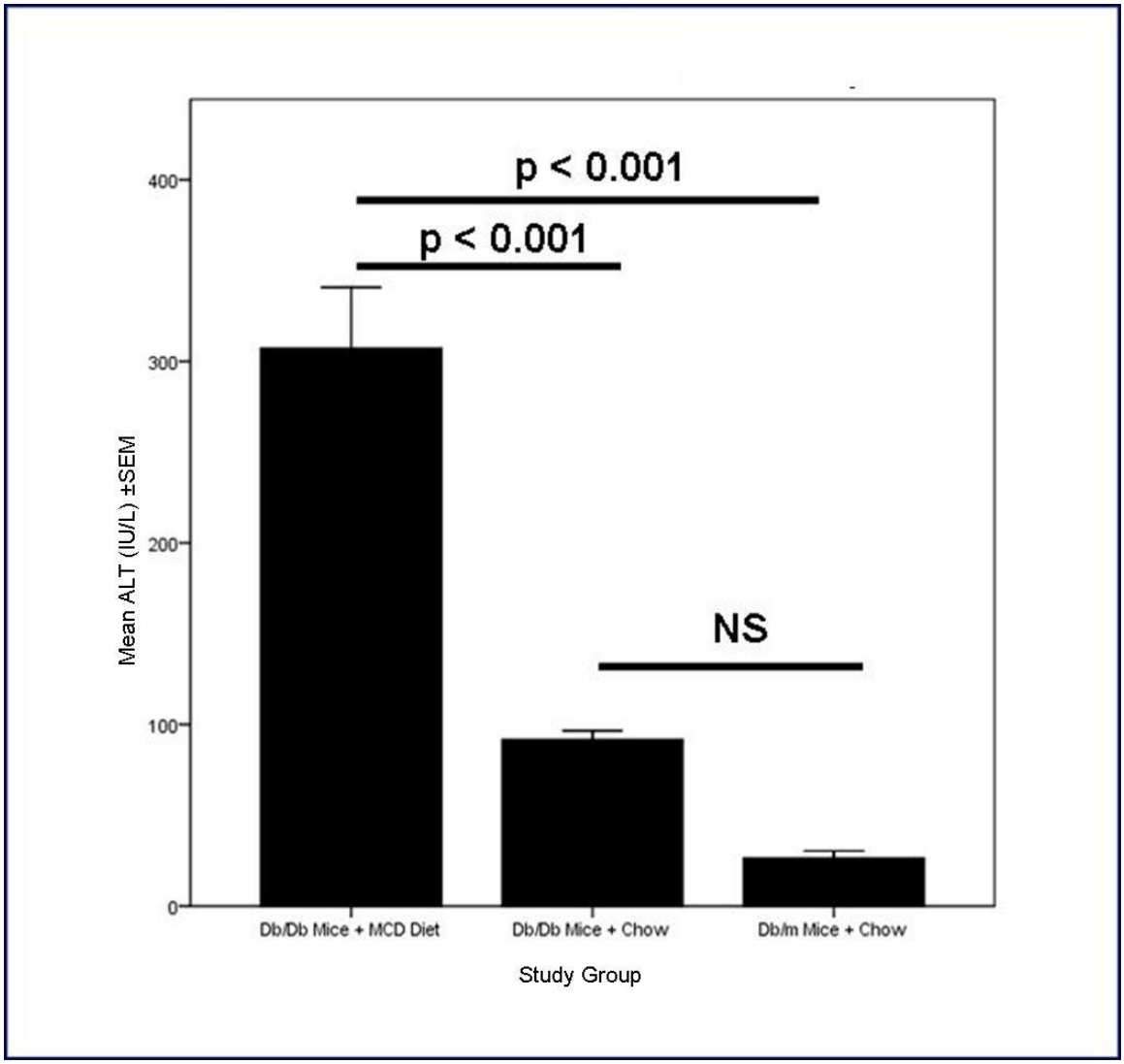


Figure 17. Mean ALT levels in the plasma of the MCD study group mice ±SEM

3.4.1.6. Autofluorescence spectroscopy

Mean spectra data from 375 nm and 405 nm excitation ± SEM, are shown in **Figures 18 and 19.** At 375 nm excitation the liver autofluorescence peaks at around 475 nm. The liver with steatosis shows higher 475 nm intensity than the control liver tissue. In the liver with steatohepatitis the tissue exhibits lower peak fluorescence than control or steatotic liver. The 405 nm excitation spectra reveal peak intensity at 500 nm and a

secondary peak at 610 nm. The spectral differences between disease groups at 405nm excitation are not as apparent as at 375nm excitation. At both excitation wavelengths the fluorescence spectra also show a 575 nm peak.

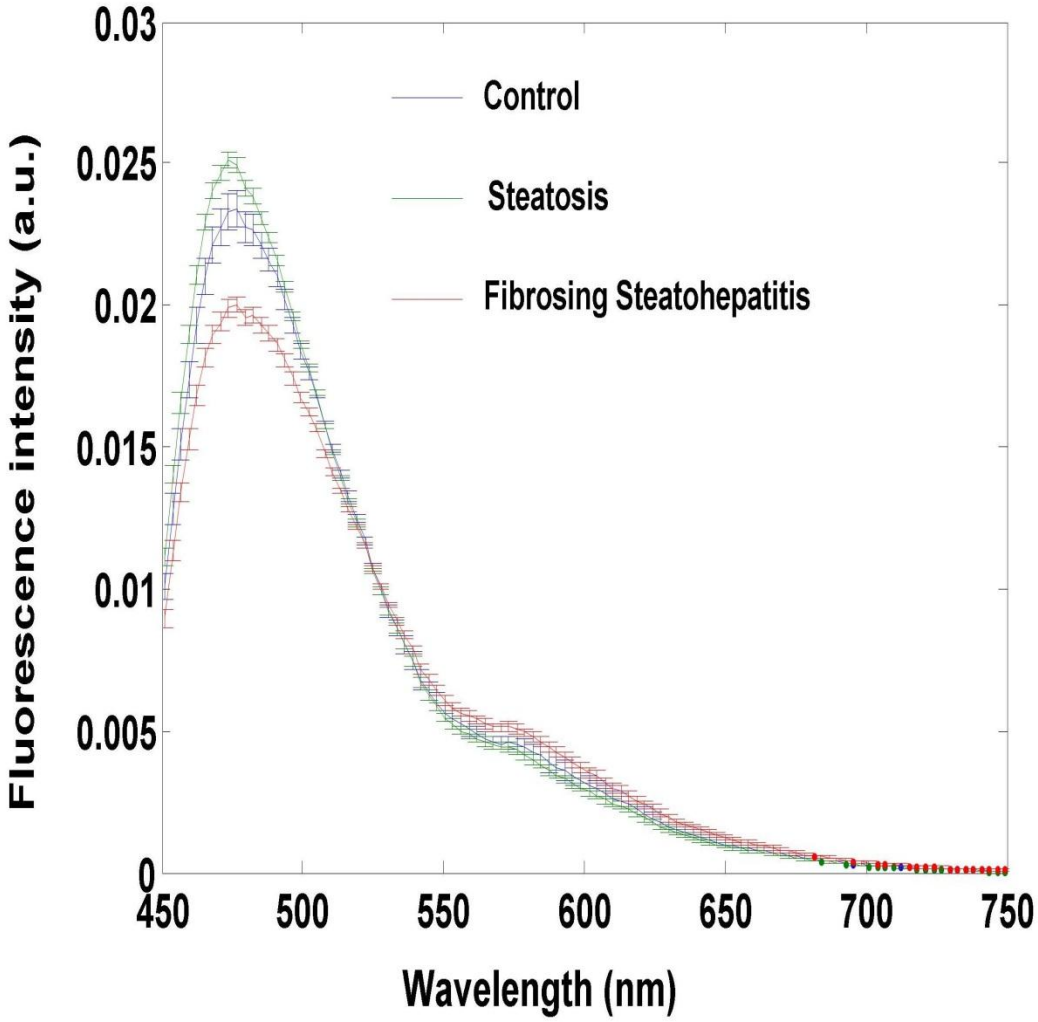


Figure 18. Mean spectra at 375 nm excitation ± SEM for the MCD study.

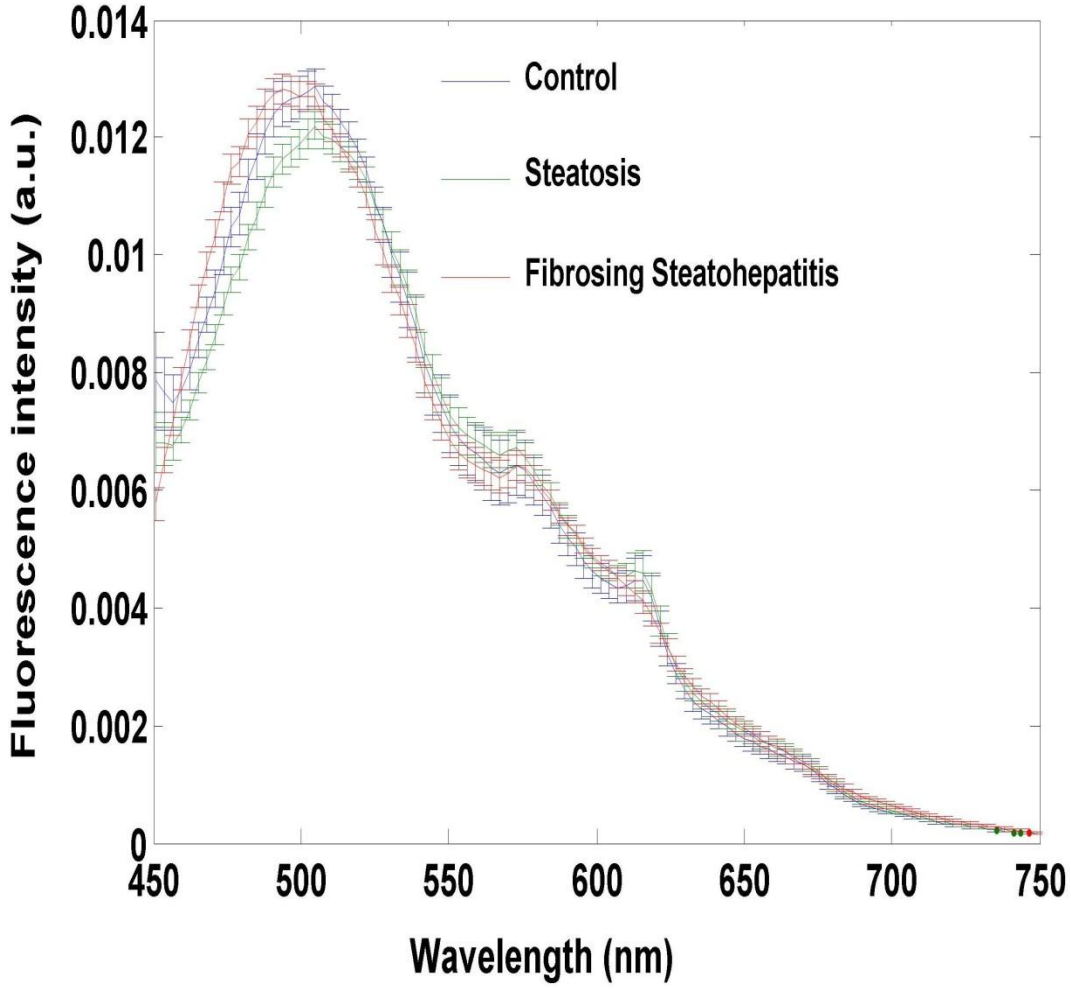


Figure 19. Mean spectra at 405 nm excitation ± SEM for the MCD study.

The results of the SMLR classification performed with a leave-one-out cross validation are presented in the confusion matrix below, **Table 20**. The overall classification accuracy reached 99.6%.

		Fluorescence Spectroscopy Classification		
	Disease Group	Control	Steatosis	Fibrosing Steatohepatitis
Histopathology Classification	Control	114	0	0
	Steatosis	0	72	0
	Fibrosing Steatohepatitis	0	1	113

Table 20. Confusion matrix demonstrating the ability of fluorescence spectroscopy to distinguish between control, steatosis and fibrosing steatohepatitis disease groups in the MCD study.

This table can be reinterpreted in terms of diagnostically more meaningful parameters by considering the sensitivity, specificity, positive and negative predictive values (PPV and NPV) of one group against the two others. The control liver tissue could be differentiated from the tissue with steatosis and fibrosing steatohepatitis with 100% sensitivity, specificity, PPV and NPV. The liver tissue with steatosis was discriminated from the control tissue and tissue with fibrosing steatohepatitis with 100% sensitivity, 99% specificity, 98.6% PPV, and 100% NPV. Tissue with fibrosing steatohepatitis was separated from the control and steatotic tissue with 99% sensitivity, 100% specificity, 100% PPV and 99.5% NPV.

The posterior probabilities of fluorescence spectra of tissue probe sites, calculated by SMLR, to belong to the correct disease group as classified by histopathology are demonstrated in **Figure 20**. Probe sites, are classed as being spectrally misclassified if they demonstrate a probability below 50%. All except one site were spectrally classified with probabilities above 70%, with the vast majority over 90%, indicating a strong confidence in the classification of the tissues sites.

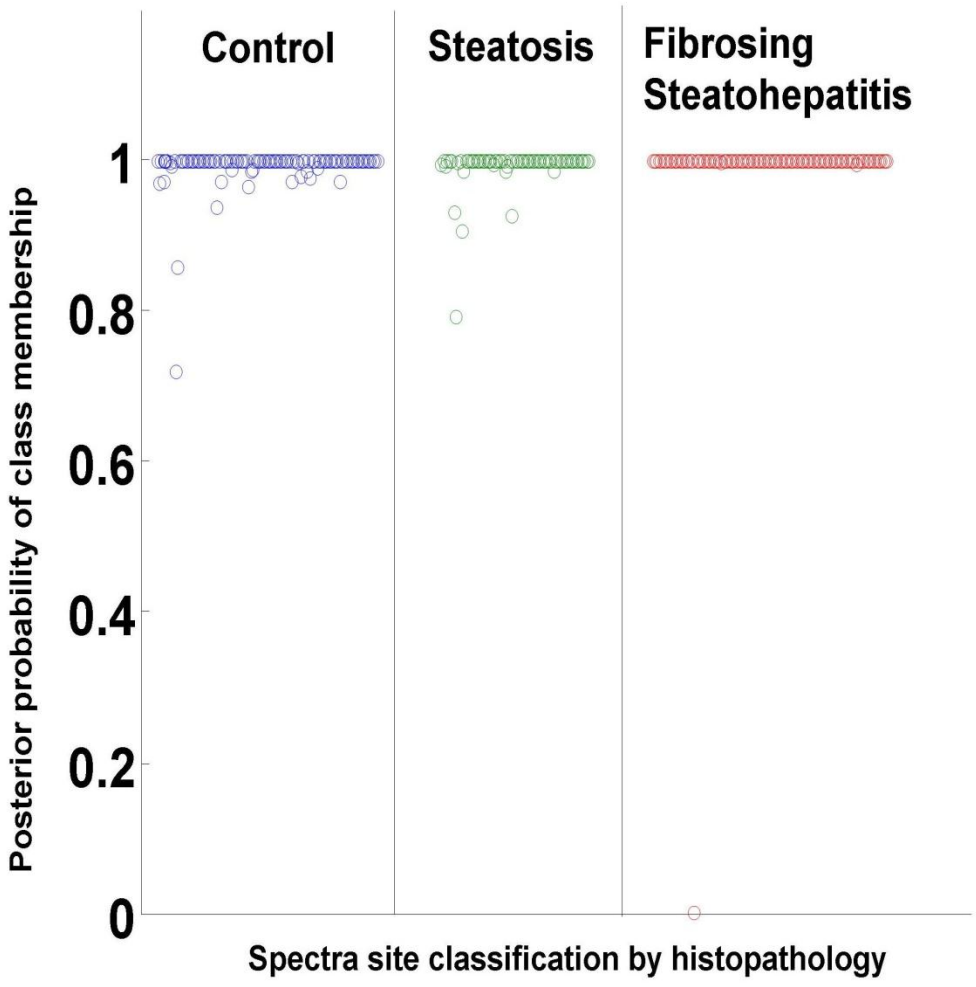


Figure 20. Posterior probability of fluorescence spectra from the sites of probe readings to belong to their correct (as classified by histopathology) disease group in the MCD study.

3.4.2. HFD/Fructose study results

3.4.2.1. Phenotypic differences in experimental groups

After 15 weeks on different diets, phenotypic differences were apparent between groups (**Table 4 and Figure 4**). Whilst fructose consumption made only minor contributions to body weight, mice fed a high fat diet (with or without fructose) were significantly heavier than those fed a standard chow diet (45.82±0.60g vs. 36.34±1.13g, $p<0.001$). This effect was attributed to the diet consumed as the body weights at the start of the experiment were not significantly different (25.41±0.81g vs. 25.65±0.41g respectively). The mice receiving a high fat diet, with or without fructose, also had a heavier mean liver weight (2.31±0.18g) compared to those receiving a standard chow diet, with or without fructose (1.54±0.08g). The liver to body weight ratio did not show any significant difference between groups.

3.4.2.2. H&E & Sirius Red stains

H&E and Sirius Red stained sections showed that the HFD study groups could be clearly distinguished from the non high fat diet study groups. Within the HFD study groups the group with fructose could be distinguished from those with water whereas in the chow fed study groups those with water could not be distinguished from those with fructose. The C57BL/6J mice fed a HFD and fructose had NASH with marked steatosis, moderate lobular inflammation and scattered ballooned hepatocytes. The C57BL/6J and C3H mice fed a HFD and water had moderate to marked steatosis with occasional ballooned hepatocytes but no lobular inflammation. The chow fed C57BL/6J mice with or without

fructose and the chow fed C3H mice showed normal liver histology on H&E stain. There was no fibrosis in any of the study groups. (**Table 21 and Figure 21**)

H&E stained sections in the HFD/Fructose study therefore showed as expected that the mice could be divided into three groups (**Table 21**): control (C3H mice fed chow/water, C57BL/6J mice fed chow/water and C57BL/6J mice fed chow/fructose), NAFLD with steatosis only (C3H mice fed HFD/water, C57BL/6J mice fed HFD/water) and NASH (C57BL/6J mice fed HFD/fructose)

Study Group	Model	Steatosis	Lobular Inflammation	Hepatocyte Ballooning	NAFLD Activity Score
Chow & Water	Control	0 (0)	0 (0)	0 (0)	0 (0)
Chow & Fructose	Control	0 (0)	0 (0-1)	0 (0)	0 (0-1)
High Fat Diet & Water	Steatosis	2 (1-3)	0 (0-1)	1 (0-1)	3 (2-5)
High Fat Diet & Fructose	Steatohepatitis	3 (3)	2 (1-2)	1 (1)	6 (5-6)

Table 21. Median NAFLD activity score for the HFD/Fructose study mice with the range in brackets.

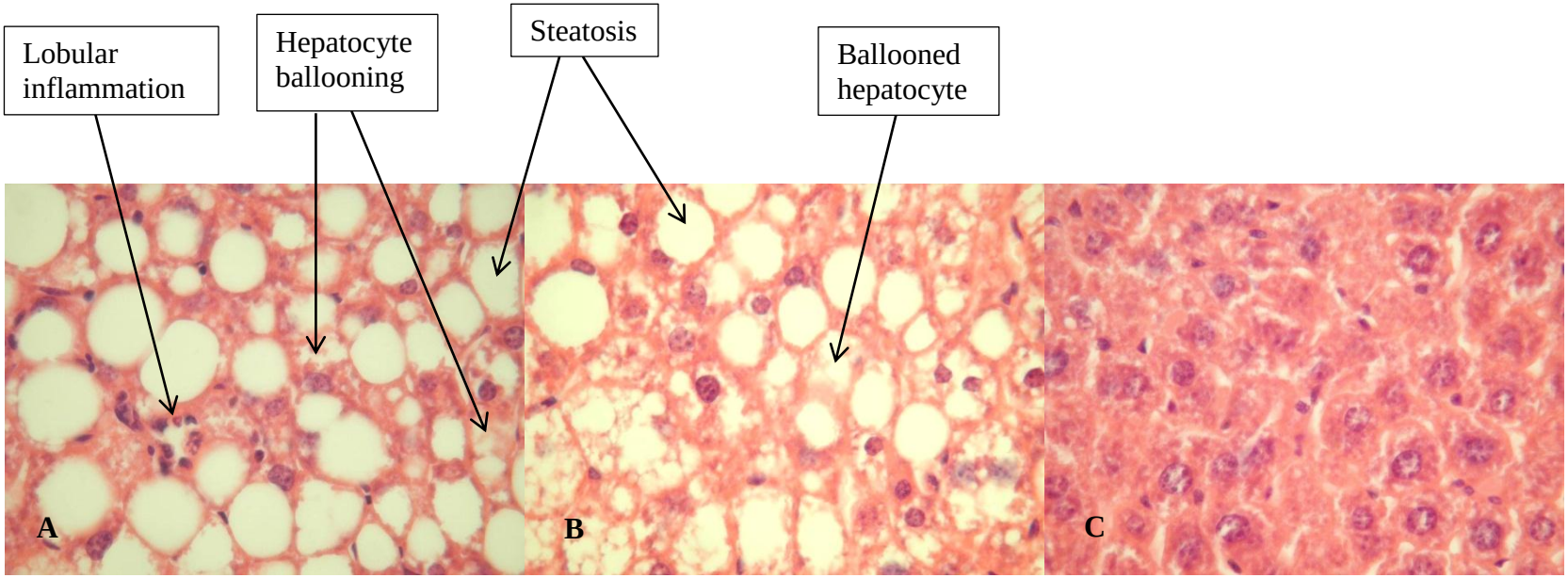


Figure 21. H&E stained sections of mouse liver. **A)** Mice fed HFD and fructose showing steatosis, lobular inflammation and ballooned hepatocytes. **B)** Mice fed HFD and water showing steatosis and an occasional ballooned hepatocyte. **C)** Mice fed chow and water (the H&E appearance is the same for mice fed chow and fructose) showing normal liver histology. x400 original magnification.

3.4.2.3. ALT biochemistry

The mean ALT levels in the plasma (IU/L) were 144.96±25.35 for the steatohepatitis study group, 95.10±17.06 for the steatosis group and 31.18±1.85 for the control group (**Table 22)**. The ALT levels were significantly increased in the plasma of the steatohepatitis and steatosis study groups compared to the control group (p=<0.001 and p=0.002 respectively). Although the ALT levels were increased in the steatohepatitis group compared to the steatosis group, this did not quite reach statistical significance (p=0.062), this may have been because three of the animals in the steatosis group became unwell during the study and had to be culled early so decreasing the statistical power of the experiment. (**Figure 22**).

HFD/Fructose Study Groups	ALT Biochemistry (IU/L) ± SEM
Control	31.18±1.85
Steatosis	95.10±17.06
Steatohepatitis	144.96±25.35

Table 22. Mean ALT levels in the plasma of the HFD/Fructose study mice ±SEM.

These results confirm that there was a biochemical hepatitis within the liver of the steatohepatitis group which is in keeping with the lobular inflammation and ballooning identified on H&E stain histologically. The steatosis group did not have as marked a biochemical hepatitis as the steatohepatitis group, which is in keeping with the milder steatosis and ballooning identified on H&E stain histologically. The control group had no biochemical hepatitis in keeping with the normal histology.

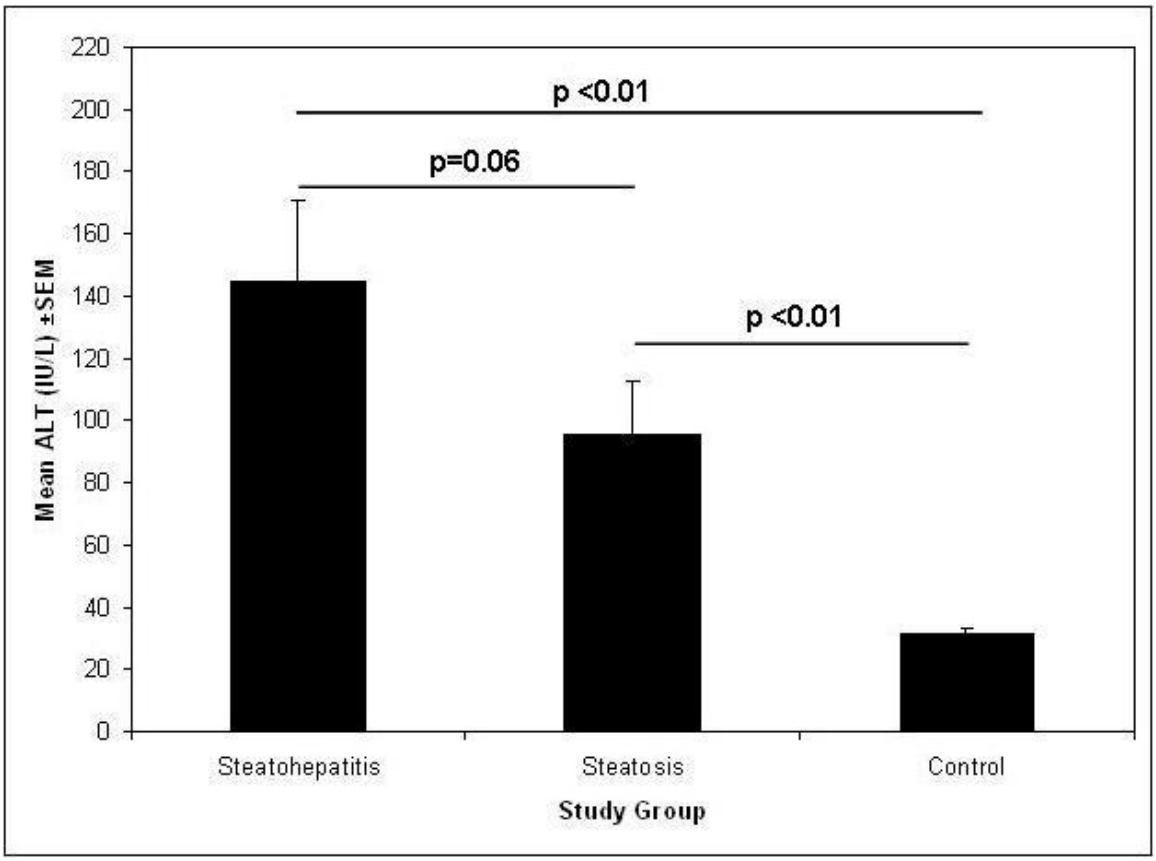


Figure 22. Mean ALT levels in the plasma of the HFD/Fructose study mice ±SEM

3.4.2.4. Autofluorescence spectroscopy results

Mean spectra data from 375 nm and 405 nm excitation ± SEM, are shown in **Figures 23 and 24**. The spectra demonstrate a peak at 475nm with 375nm excitation similar to the pilot study. The liver with steatohepatitis demonstrates higher 475 nm intensity than the liver with steatosis or control liver tissue. The 405 nm excitation spectra reveal peak intensity at 500 nm and a smaller secondary peak at 610 nm. The spectral differences between disease groups at 405nm excitation are not as apparent as at 375nm excitation.

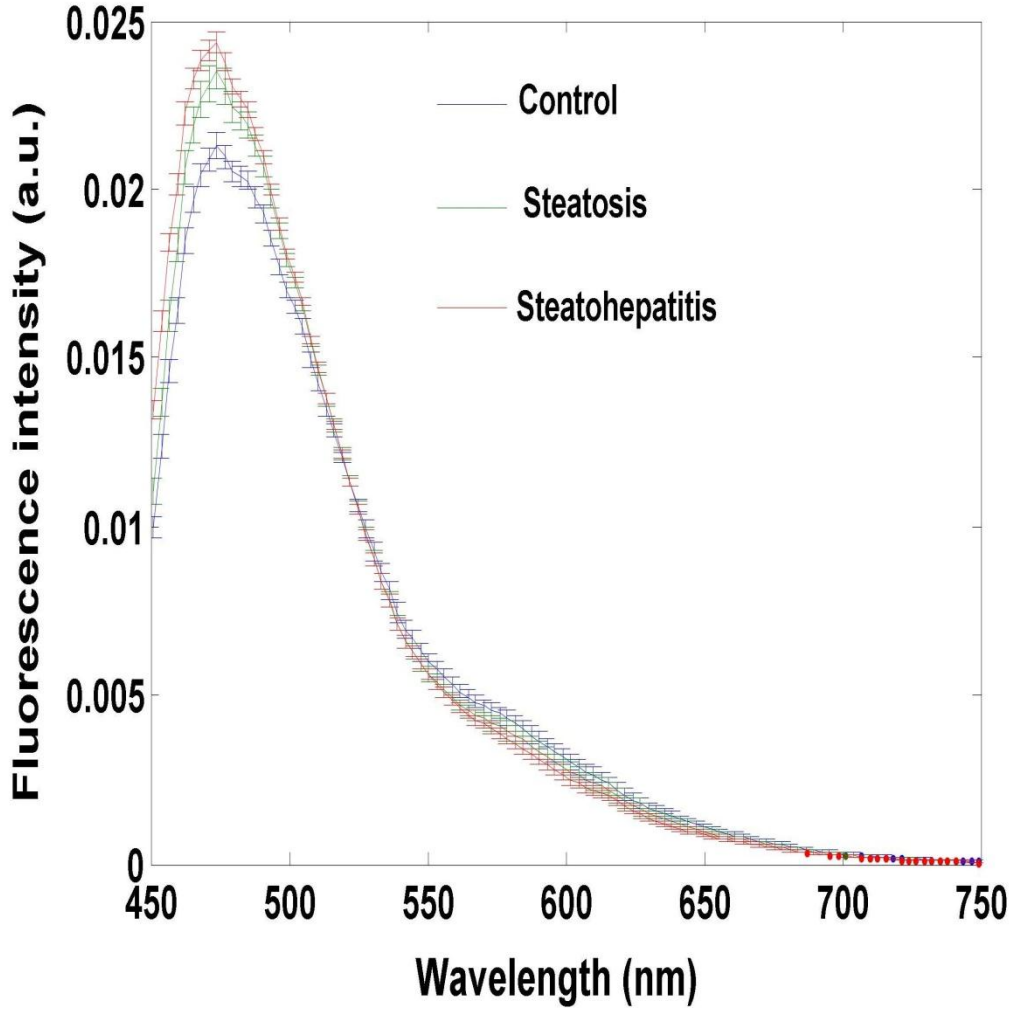


Figure 23. Mean spectra at 375 nm excitation ± SEM in the HFD/Fructose study.

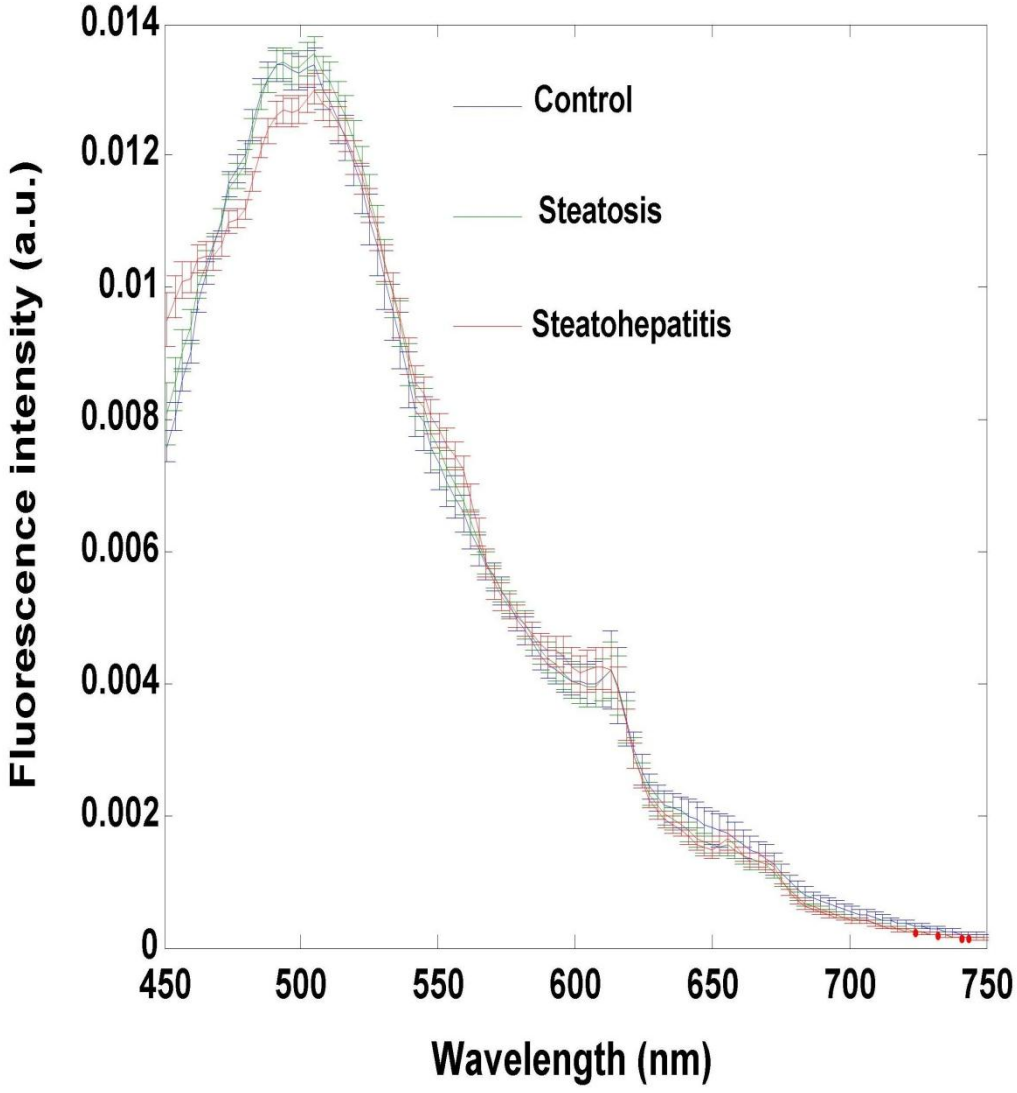


Figure 24. Mean spectra at 405 nm excitation ± SEM in the HFD/Fructose study.

The results of the SMLR classification performed with a leave-one-out cross validation are presented in the confusion matrix below, **Table 23**. The overall classification accuracy reached 95.2%.

		Fluorescence Spectroscopy Classification		
	Disease Group	Control	Steatosis	Steatohepatitis
Histopathology Classification	Control	239	7	6
	Steatosis	9	249	2
	Steatohepatitis	7	0	95

Table 23. Confusion matrix demonstrating the ability of fluorescence spectroscopy to distinguish between control, steatosis and steatohepatitis disease groups in the HFD/Fructose study.

The control liver tissue could be discriminated from the tissue with steatosis and steatohepatitis with 94.8% sensitivity, 96.3% specificity, 93.7% PPV and, 96.4% NPV. The liver tissue with steatosis was differentiated from the normal and steatohepatitis tissue with 95.7% sensitivity, 98% specificity, 97.2% PPV, 96.9% NPV. Finally, the liver tissue with steatohepatitis was distinguished from the control and steatosis tissue with 93.1% sensitivity, 98.4% specificity, 92.2% PPV, and 98.6% NPV.

The posterior probabilities of fluorescence spectra of tissue probe sites, calculated by SMLR, to belong to the correct disease group as classified by histopathology are demonstrated in **Figure 25**. Probe sites, are classed as being spectrally misclassified if they demonstrate a probability below 50%. The vast majority of probe sites had a probability over 90%, indicating a strong confidence in the classification of the tissues sites.

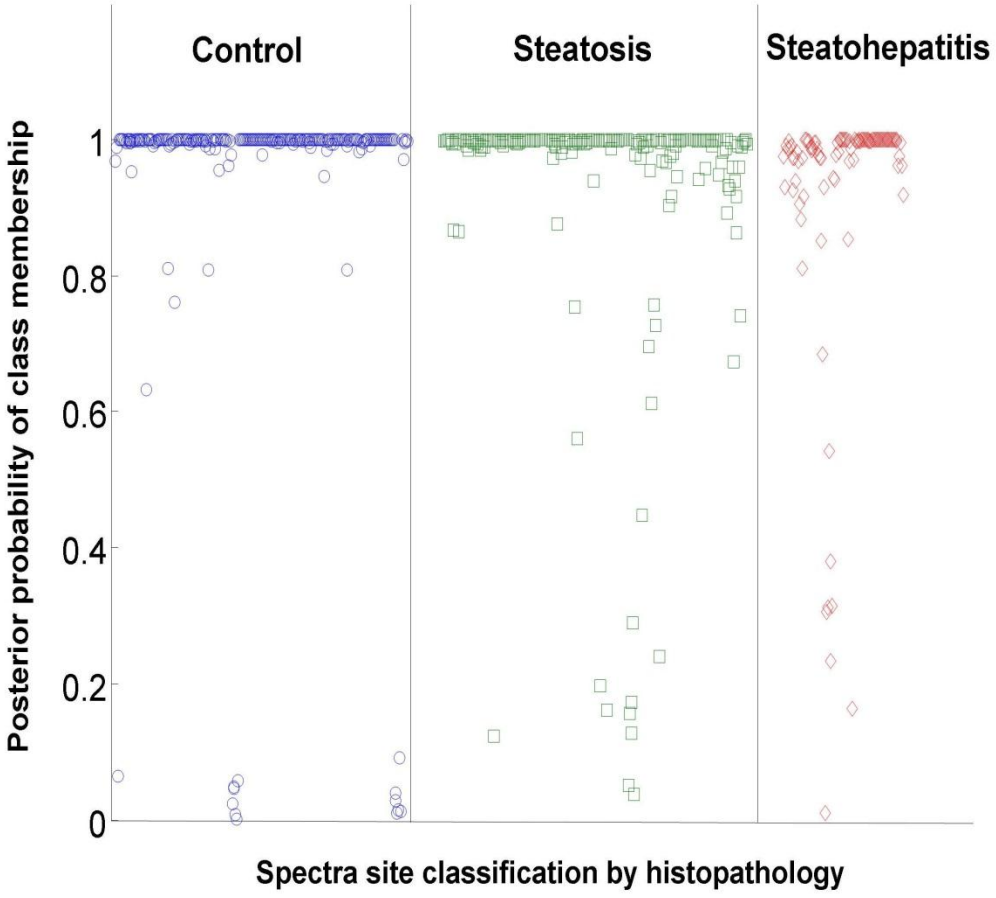


Figure 25. Posterior probability of fluorescence spectra from the sites of probe readings to belong to their correct (as classified by histopathology) disease group in the HFD/Fructose study.

3.4.2.5. Photobleaching results

The mean photobleaching rate between 450 nm and 530 nm emission, averaged for each study group is demonstrated in **Figure 26.** The photobleaching rate (measured by the fluorescence intensity) curve of the control group is higher than that of the steatosis group, which is itself above the steatohepatitis group until 530 nm where the readings from the three study groups reach the same level.

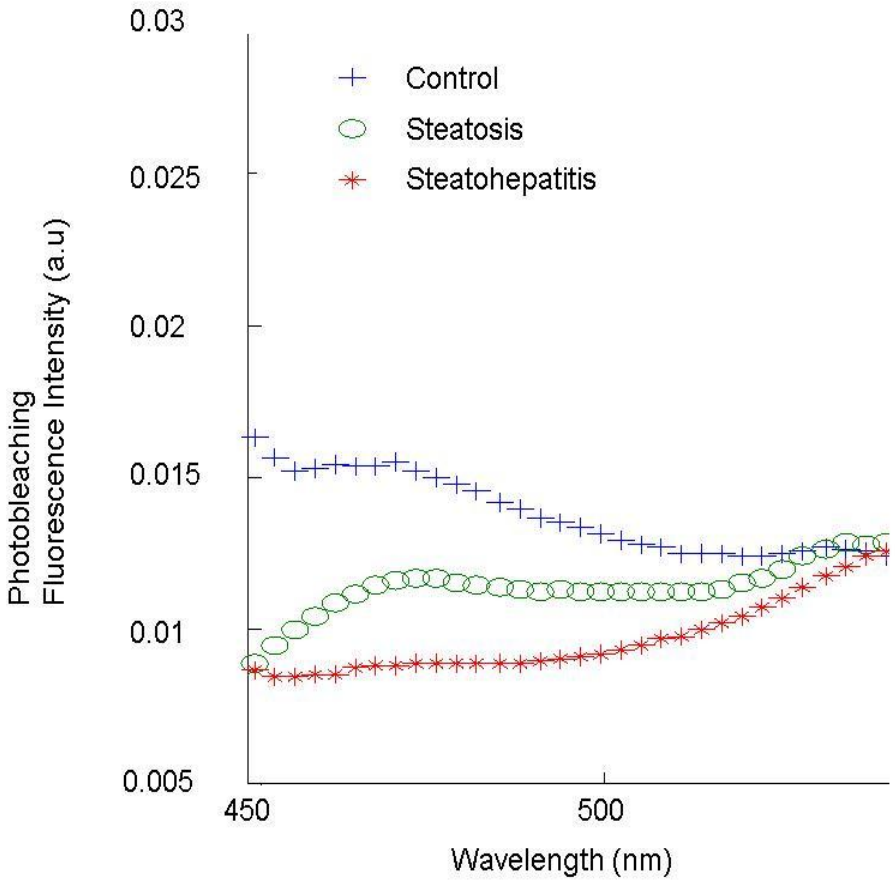


Figure 26. Mean photobleaching rates at 375nm excitation in the HFD/Fructose study.

3.4.3. Human liver biopsies

There were five male and two female patients with ages ranging from 25 to 61 and body mass indexes ranging from 28.1 to 31.9kg/m^2.

3.4.3.1. H&E & Sirius Red stains

H&E and Sirius Red stained sections showed that the seven liver biopsies could be divided into three groups. Four patients had NASH (3 with fibrosis) one had steatosis and minimal inflammation only and the final two patients had normal liver biopsies. **(Table 24 and Figure 27)**

Diagnosis	Steatosis	Lobular Inflammation	Hepatocyte Ballooning	NAFLD Activity Score
NASH	2 (1-2)	1 (1)	2 (1-2)	5 (4-5)
Steatosis	1 (1)	1 (1)	0 (0)	2 (2)
Normal	0 (0)	0 (0)	0 (0)	0 (0)

Table 24. Median NAFLD activity score for the suspected NAFLD patients undergoing liver biopsy with the range in brackets.

.

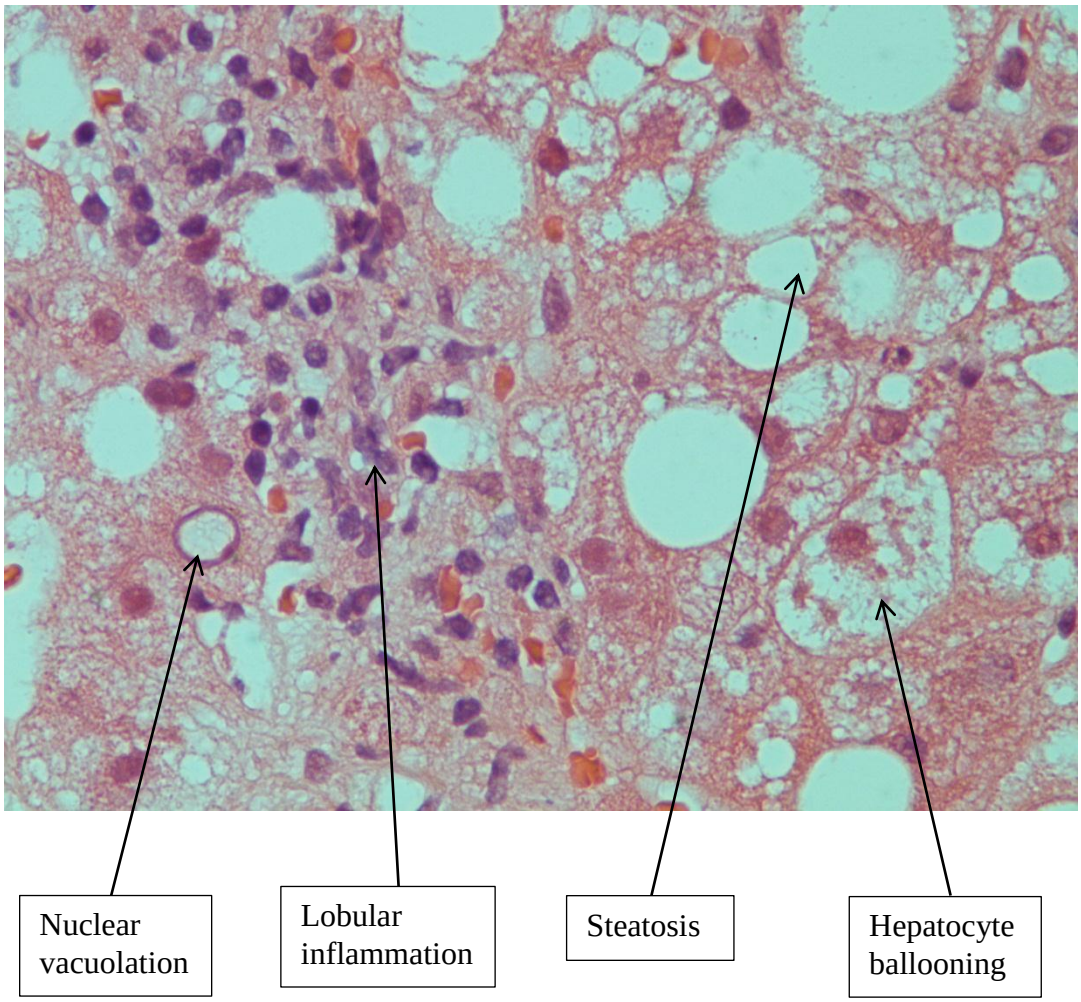


Figure 27. Photomicrograph showing steatosis, hepatocyte ballooning, lobular inflammation and nuclear vacuolation in a patient with NASH. Original magnification x400.

3.4.3.2. ALT biochemistry

The mean ALT levels in the plasma (IU/L) were 92.25±12.75 for the NASH patients, 83.00 for the steatosis patient and 31.00±4.00 for the normal patients (**Table 25)**. The ALT levels were increased in the plasma of the NASH and steatosis patients compared to the normal patients and there was little difference between the NASH and steatosis

patients. However, the numbers are very small so care needs to be taken when interpreting them and for this reason statistical analysis has not been performed.

Patients Diagnosis	ALT Biochemistry (IU/L) ± SEM
Normal	31.00±4.00
Steatosis	83.00
NASH	92.25±12.75

Table 25. Mean ALT levels in the plasma of the suspected NAFLD patients undergoing liver biopsy ±SEM.

These results confirm that there was a biochemical hepatitis within the liver of the NASH and steatosis patients which is in keeping with the lobular inflammation identified on H&E stain histologically. The normal patients had no biochemical hepatitis in keeping with the normal histology.

3.4.3.3. Autofluorescence spectroscopy results

Mean spectra data from 375 nm excitation ± SEM, are shown in **Figure 28**. The spectra demonstrate a peak at 475nm similar to the mouse studies but also have a second smaller peak at 640nm. The steatosis liver biopsy has higher 475nm intensity than the NASH biopsies with the normal biopsies having the lowest 475nm intensity.

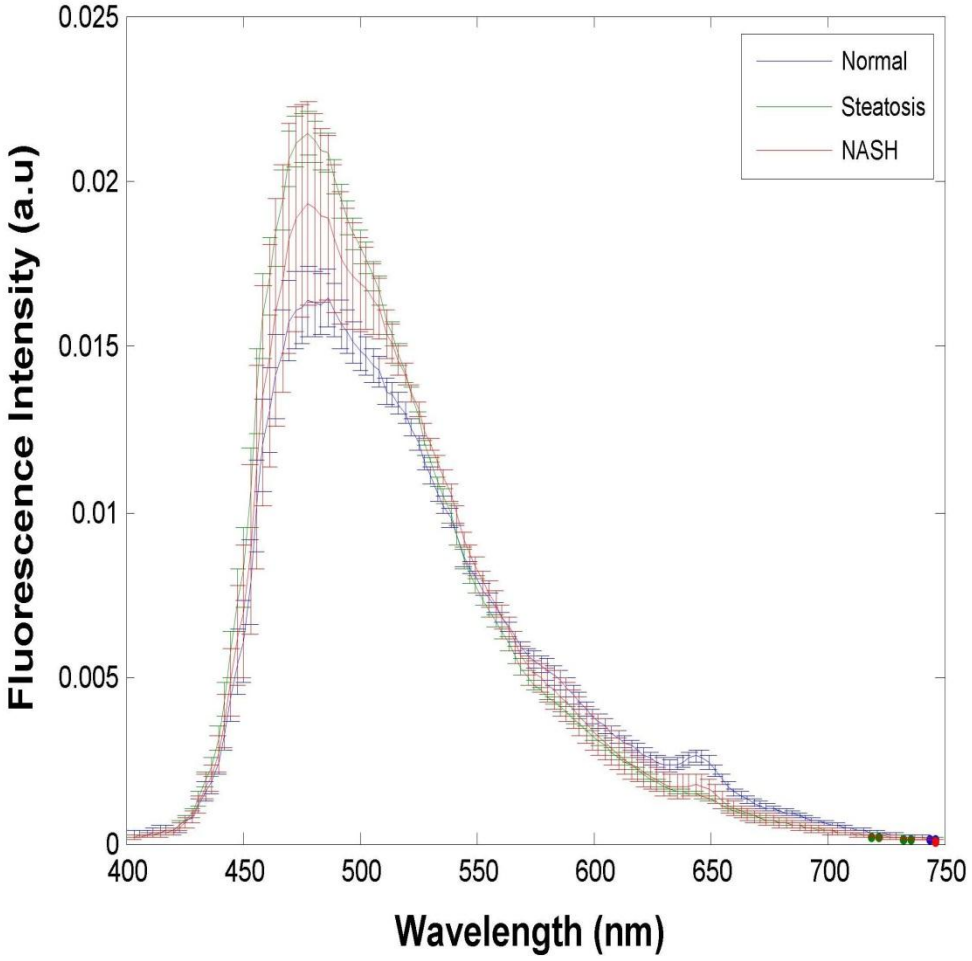


Figure 28. Mean spectra at 375 nm excitation ± SEM in the human NAFLD patients.

The results of the SMLR classification performed with a leave-one-out cross validation are presented in the confusion matrix below, **Table 26**. The overall classification accuracy was 100%. However, the number of biopsies examined was small.

		Fluorescence Spectroscopy Classification		
	Disease Group	Control	Steatosis	NASH
Histopathology Classification	Control	60	0	0
	Steatosis	0	24	0
	NASH	0	0	36

Table 26. Confusion matrix demonstrating the ability of fluorescence spectroscopy to distinguish between control, steatosis and NASH in human liver biopsies.

3.5. Discussion

Using autofluorescence spectra from excitation at 375nm and 405nm the different study groups could be distinguished in both mouse studies and in the human study with high degrees of accuracy. The 375nm excitation spectra were especially useful in classifying all the study groups, most likely because at this excitation wavelength there was maximal excitation of NAD(P)H/NADH and Vitamin A, two of the largest fluorophores within the liver. Excitation at 405nm wavelength produced a spectra with less marked changes between the mouse study groups, this is likely to be due to less excitation of NAD(P)H/NADH and Vitamin A at this wavelength as compared to excitation at 375nm.

Vitamin A and NAD(P)H have been shown to increase with steatosis accumulation and would therefore be expected to increase corresponding to the amount of steatosis in the study groups.[85] In this study there was most steatosis in the steatohepatitis study groups, then the

steatosis groups and least in the control groups. The increase in vitamin A would lead to increased fluorescence intensity at approximately 490nm emission.[82]

The fibrosing steatohepatitis study group in the MCD study had increased lobular inflammation compared to the steatosis and control groups (NAS score 2 compared to 0 for the other two groups), increased TBARS ($p=0.011$, $p=0.028$ respectively) and increased ALT levels (both $p<0.001$). These measures along with positive immunohistochemistry staining for malondialdehyde in hepatocytes strongly suggest that there are increased ROS in the fibrosing steatohepatitis study group compared to the steatosis and control groups in the MCD study. This would be expected to lead to an increase in tissue oxidative stress in the fibrosing steatohepatitis study group and therefore an increase in NAD(P)H and fluorescence intensity at 475nm emission.

In the MCD study the steatosis group had increased levels of fluorescence intensity compared to the control group, especially at 375nm excitation with a large emission peak at 475-490nm, this would be in keeping with increased levels of steatosis (Vitamin A and NAD(P)H) and tissue oxidative stress (NAD(P)H) as outlined above. The fibrosing steatohepatitis group however did not have increased levels of fluorescence intensity as predicted by increased levels of steatosis (NAD(P)H and Vitamin A) and tissue oxidative stress (NAD(P)H) but actually had decreased levels of fluorescence intensity compared to the control and steatosis groups. The reason for this is likely to be due to the fibrosis within the livers as collagen scatters light in all directions, this disperses the light returning to the probe so that less fluorescence is measured by the probe and therefore a lower fluorescence intensity is

measured. Another contributing factor could be the loss of Vitamin A caused by the conversion of stellate cells to a myofibroblastic phenotype and subsequent fibrosis.[86]

The steatohepatitis study group in the HFD/Fructose study had increased lobular inflammation compared to the steatosis and control group (NAS score 2 compared to 0 for the other two groups) and increased ALT levels ($p=0.06$ and $p<0.01$ respectively). Although the increase in ALT levels compared to the steatosis group did not quite reach statistical significance ($p=0.06$), they did show a trend. The lack of statistical significance is likely to be due to three animals in the steatosis group becoming unwell during the study and having to be culled early so decreasing the statistical power of the experiment. The steatosis study group did not have increased lobular inflammation compared to the control group (both NAS score of 0) but did have significantly increased levels of ALT compared to the control group ($p<0.01$). These measures strongly suggest that there are increased ROS in the steatohepatitis study group compared to the steatosis and control groups and the steatosis group compared to the control group in the HFD/Fructose study. This would be expected to lead to an increase in tissue oxidative stress in the steatohepatitis study group and therefore an increase in NAD(P)H and fluorescence intensity at 475nm emission.

In the HFD/Fructose study unlike the MCD study there was no fibrosis in the steatohepatitis study group so increased levels of fluorescence intensity as predicted above by increased levels of steatosis (NAD(P)H and vitamin A) and tissue oxidative stress (NAD(P)H) were expected. This was indeed the case with increased levels of fluorescence intensity compared to the steatosis and control groups, especially at 375nm excitation with a large emission peak at 475-

490nm in keeping with increased levels of Vitamin A and NAD(P)H. The steatosis group had increased fluorescence intensity compared to the control group, especially at 375nm excitation with a large emission peak at 475-490nm in keeping with increased levels of Vitamin A and NAD(P)H. This was expected with the increased levels of steatosis and tissue oxidative stress as outlined above.

In the human liver biopsies the NASH patients had most steatosis with the steatosis patients next and the normal patients the least. The increased steatosis was expected to increase the Vitamin A and NAD(P)H levels and fluorescence intensity at 490nm emission. The ALT levels and lobular inflammation in the NASH patients were not increased compared to the steatosis patient but both the NASH and steatosis patient's ALT levels and lobular inflammation were increased compared to the normal patient (92.25±12.75 and 83.00 vs. 31.00±4.00 and NAS scores 1 vs. NAS score 0 respectively). These measures strongly suggest that there are increased ROS in the NASH and steatosis patients compared to the normal patients. This would be expected to lead to an increase in tissue oxidative stress in the NASH and steatosis patients and therefore an increase in NAD(P)H and fluorescence intensity at 475nm emission. However, three of the four NASH patients had fibrosis in their liver biopsy and based on the earlier findings in the mouse pilot study this could decrease the fluorescence intensity expected.

In the human liver biopsies increased levels of fluorescence intensity as predicted above by increased levels of steatosis (NAD(P)H and vitamin A) and tissue oxidative stress (NAD(P)H) were expected in the steatosis patient compared to the normal patients. This was indeed the

case with increased levels of fluorescence intensity in the steatosis patient compared to the normal patients, especially at 375nm excitation with a large emission peak at 475-490nm in keeping with increased levels of Vitamin A and NAD(P)H. The NASH group had fluorescence intensity above the normal patients but below the steatosis patients. This fits with the increased levels of steatosis (NAD(P)H and vitamin A) and tissue oxidative stress (NAD(P)H) increasing fluorescence intensity in all the patients but also the fibrosis in three of the four patients lowering the fluorescence intensity due to less light reaching the probe as outlined earlier. The reason that the NASH patients fluorescence intensity spectra was not below the normal patients as in the mouse pilot study earlier can be explained by one of the NASH patients not having any fibrosis so the average of the four NASH patients fluorescence intensity readings was above the normal patients.

In all the study groups with excitation at 375nm wavelength there was a fluorescence emission peak at 475-490nm which is likely to be due to the combined fluorescence of NAD(P)H (emission at around 475 nm) and vitamin A (emission at around 490 nm) as outlined above. The spectra shape also results from the contributions of other fluorophores present in the liver. Lipofuscin could account for the small emission peak at 575 nm, seen at 375nm excitation in the mouse pilot study. This pigment within the liver is associated with cell damage, and is likely to be increased in the MCD mouse model used in this experiment. Lipofuscin has a maximum fluorescence emission around 575 nm and in normal hepatocytes its concentration increases with age.[88, 106] Other fluorophores include flavins which have an emission band between 500 nm and 600nm.[1]

At 405nm excitation in both the MCD and HFD/Fructose mouse studies there is a peak at 610nm emission, this could be attributed to porphyrins, these are synthesised in the liver and have an excitation peak near 405nm, and emit fluorescence between 600 and 700nm with a maximum near 610 nm.[26]

Photobleaching with Vitamin A and NAD(P)H/NADH are particularly fast, leading to short photobleaching times. Photobleaching at 375nm excitation with an emission wavelength between 450 and 530nm, particularly examined Vitamin A and NAD(P)H/NADH within the liver as they are by far the largest contributors between these wavelengths. This helped determine whether these compounds were what the probe had measured with the fluorescence intensity.

The photobleaching rate in the HFD/Fructose study between 450 and 530nm would be expected to be smallest in the steatohepatitis study group with the most steatosis (NAD(P)H and Vitamin A) and tissue oxidative stress (NAD(P)H), and then slightly larger in the steatosis group and largest in the control group with least steatosis (NAD(P)H and Vitamin A) and tissue oxidative stress (NAD(P)H). This is exactly what happened in the HFD/Fructose study and shows a good inverse correlation between increasing severity of NAFLD and decreasing photobleaching rate. This helps confirm that there is increased Vitamin A and NAD(P)H in the steatohepatitis and steatosis groups compared to the control.

These results demonstrate that autofluorescence spectroscopy has potential as a diagnostic tool in NAFLD and importantly suggest that the fluorescence readings correlate with biological principles and compounds. Further work is needed to confirm the preliminary human results and further experiments to measure NAD(P)H and Vitamin A would help validate the biological principles of the probe.

There are several possible applications in liver tissue, *ex vivo*, it could be an alternative or complementary method to histopathology to assess liver biopsies and/or it could enable the immediate detection of NAFLD without the need for liver biopsy in liver transplant grafts which are more prone to primary non-function. *In vivo*, it could replace liver biopsy in patients who are at high risk of bleeding, however, although there would be no need for biopsy the probe would still have to be introduced via a needle or laparoscope or some other invasive means to touch the liver and obtain a measurement. Of possible greater interest it could be used as an adjunct in the transplant setting or in patients already undergoing a surgical procedure (such as bariatric surgery). In the current climate of increased bariatric surgery, and with the increased prevalence of NAFLD in the obese population this novel method of NAFLD diagnosis at the time of surgery could offer widespread economic and health benefits.[2] These patients are at high risk of having NAFLD and would not normally have a liver biopsy at the time of surgery but with this new, fast, non-destructive method of diagnosis every patient could have a probe measurement at the time of surgery to see if they had NAFLD. This would enable earlier diagnosis and therefore treatment of NAFLD in these patients thus reducing morbidity and future healthcare costs. A pilot study in bariatric surgery patients is currently being planned.

In conclusion, autofluorescence spectroscopy is able to rapidly differentiate the different forms of NAFLD in mouse models and in preliminary studies on human liver biopsies. This technique has the potential in the future to allow the assessment of NAFLD in the liver without the need for biopsy to determine the relative severity of the disease.

Chapter 4.

The Role of Autophagocytosis in Non-Alcoholic Fatty Liver Disease

4.1. Introduction

Autophagy is the degradation of intracellular components by the lysosome system.[107] There are three types of autophagy that differ in how the cytoplasmic materials are delivered to the lysosome: macroautophagy, microautophagy and chaperone mediated autophagy. Macroautophagy is the most important in NAFLD and has recently been discovered to have a major role in regulating lipid metabolism.[30] Microautophagy is not thought to have a role in fat metabolism and chaperone mediated autophagy is only involved in Mallory Denk body formation and turnover with no direct role in lipid metabolism.[108, 109]

Macroautophagy is involved in many physiological and pathological processes.[110-112] In adults, it extends the life span of cells and protects them from the stress response in times of starvation by providing an alternative energy source with the breakdown of cellular components by autophagy.[113, 114]

One of the cellular components utilised by macroautophagy to provide energy are lipid droplets. Macroautophagy in lipid metabolism (sometimes called macroautolipophagy) is a process where fat is sequestered in a double membrane structure called an autophagosome (autolipophagosome once it contains fat) which then fuses with the

lysosome to form a single membrane autophagolysosome, the contents of which are degraded by lysosomal hydrolases to form free fatty acids which can then undergo oxidation to provide energy.[107] **See Figure 29.**

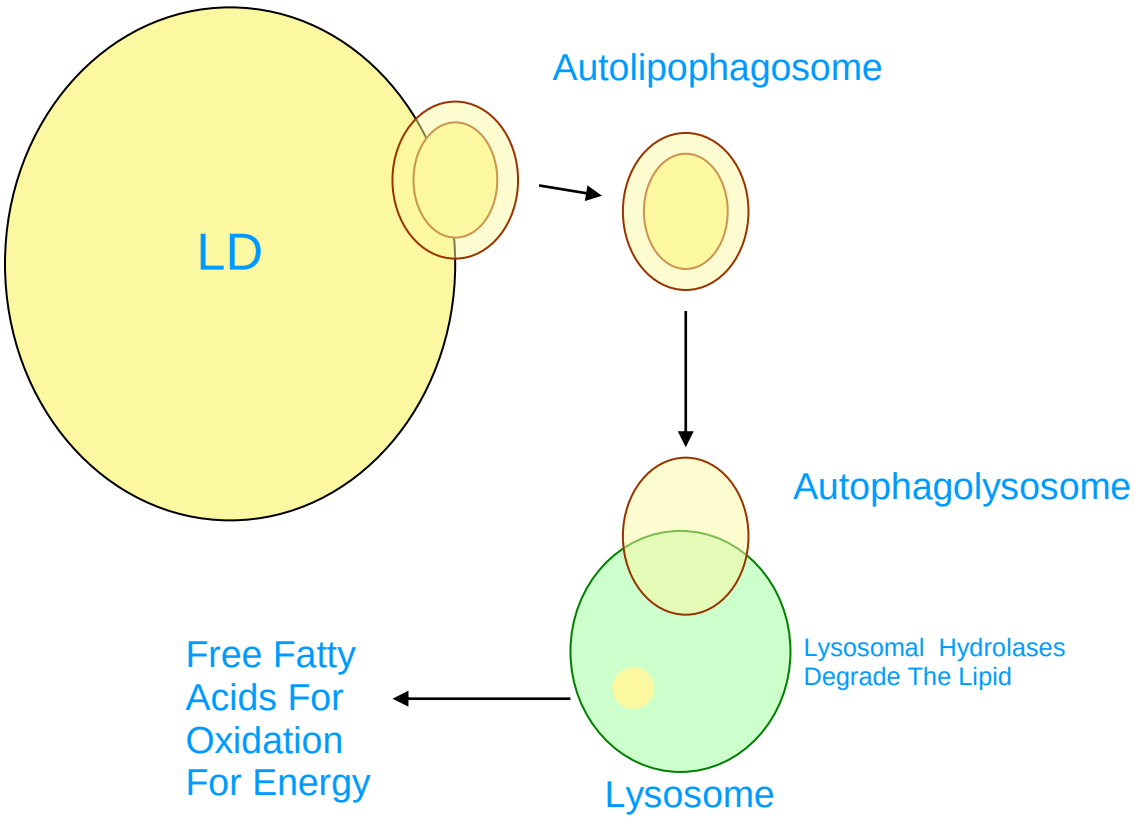


Figure 29. Schematic diagram of autophagocytosis in lipid metabolism.

There are many stains and markers in use for analysing macroautophagy, for example, neutral lipids and lipid droplets can be stained by BODIPY 493/503 or ORO and markers for lysosomes include the lysosomal associated membrane protein type 1 (LAMP1). Using these and other markers it has been shown that in cells with nutrient deprivation, and subsequent increased macroautophagy, lipid droplets and autophagosomes have

shown increased association. The inhibition of autophagy in cultured hepatocytes and mouse liver has also been shown to increase triglyceride storage in lipid droplets.[30]

One of the major pathways that regulates macroautophagy is the inhibitory mammalian target of rapamycin (mTOR) pathway. In direct response to nutrients (particularly amino acids), or through nutrient induced insulin, class I phosphatidylinositol 3-kinase activates mTOR. This signalling pathway blocks macroautophagy through the ability of mTOR to inhibit autophagy related gene 1 (Atg1) from recruiting its partners Atg13 and Atg17.[115] The Atg1–Atg13–Atg17 complex recruits and organises other proteins for the developing autophagosome.[116] There are many inhibitors and activators of autophagy, one of the best known is Rapamycin which suppresses mTOR and increases autophagy even in nutrient rich conditions.[117]

In NAFLD, there are increased circulating free fatty acids, once inside hepatocytes the majority are converted to triglycerides and stored as lipid droplets.[66] Increased triglycerides and fat droplets within hepatocytes are one component of increased lipid peroxidation and ROS which subsequently cause increased DNA oxidative damage and apoptosis.[118] Additionally, an increased delivery of fatty acids to the liver results in induction of CYP2E1, leading to increased formation of ROS, which may directly contribute to the development of NASH and the activation of stellate cells, the main effectors of fibrosis in the liver.[43] The effect of autophagocytosis on cell death and ROS generation in the setting of NAFLD is currently unclear.[119-121] Autophagy may have a

role in regulating hepatocyte steatosis and cell death, particularly death caused by oxidative stress indicating that autophagy might modulate the development of NASH.[122]

5-(and-6)-carboxy-2′,7′-difluorodihydrofluorescein diacetate (carboxy-H2DFFDA) is a ROS sensitive membrane permeant probe which can be used to measure intracellular ROS. Chemically reduced and acetylated forms of carboxy-H2DFFDA are non-fluorescent until the acetate groups are removed by intracellular esterases and oxidation occurs within the cell. The oxidation of the probe can be detected by monitoring the increase in fluorescence with a flow cytometer.

Annexin V (AV) and propidium iodide (PI) can be used to assess apoptosis and necrosis in cells. In normal viable cells phosphatidyl serine (PS) is located on the cytoplasmic surface of the cell membrane. Upon induction of apoptosis, rapid alterations in the organisation of phospholipids occurs leading to exposure of PS on the cell surface. AV binds to PS and is a marker of early stage apoptosis which when combined with a fluorescein isothiocyanate (FITC) conjugate allows detection of apoptosis by flow cytometry. PI is a fluorescent DNA stain that cannot enter cells with an intact cell membrane.[123] PI and AV-FITC can be used in conjunction to distinguish between viable (AV-FITC and PI negative), early apoptotic (AV-FITC positive, PI negative), late apoptotic (AV-FITC positive, PI positive) and necrotic (AV-FITC negative, PI positive) cells.[124]

4.2. Aims

The first aim was to determine whether activating autophagocytosis using Rapamycin in HUH7 liver differentiated cells in a normal or high fat environment will increase co-localisation of lipid droplets and lysosomes and lead to decreased lipid droplets. This was investigated using ORO DIA, confocal immunofluorescence, a triglyceride assay and electron microscopy. The second aim was to look at the effect activating autophagocytosis using Rapamycin had on cell death and ROS generation. This was investigated using fluorescent activated cell sorting.

4.3. Methodology

4.3.1. Overall cell culture methods

HUH7 cells, an adherent liver differentiated cell line were cultured in a $25cm^3$ flask with high glucose serum free Dulbecco's Modification of Eagle's Medium (DMEM) supplemented with 10% fetal calf serum and penicillin/streptomycin. The cells were cultured at 37°C in an atmosphere with 5% CO_2 and a relative humidity of 95%. Rapamycin (R8781, Sigma) was used at a concentration of 0.2µg/ml and Oleate DMEM was used in experiments at a concentration of 35.3µg/ml (Oleic Acid: O3008, Sigma) for all cell culture experiments.

4.3.2. Confocal immunofluorescence experiment

4.3.2.1. Cell culture methods for confocal immunofluorescence experiment

HUH7 cells were grown in an 8 well chamber slide with four chambers containing HUH7 cells grown in DMEM with Rapamycin (0.2µg/ml) added for 24 hours and then the immunofluorescent probes added. The remaining four chambers were controls with HUH7 cells grown in DMEM with no Rapamycin added and then the immunofluorescent probes added. This was repeated for HUH7 cells grown in an Oleate DMEM (35.3µg/ml), see the schematic chamber slides below, **Figure 30.**

Therefore in total 4 experimental groups were examined

1) DMEM only
2) DMEM and Rapamycin
3) Oleate DMEM
4) Oleate and Rapamycin

The experiments were performed in duplicate.

DMEM only	No immunofluorescent probes added	LAMP1 probe only	BODIPY 493/503 only	LAMP1 probe and then BODIPY probe
DMEM & Rapamycin	No immunofluorescent probes added	LAMP1 probe only	BODIPY 493/503 only	LAMP1 probe and then BODIPY probe

Oleate DMEM	No immunofluorescent probes added	LAMP1 probe only	BODIPY 493/503 only	LAMP1 probe and then BODIPY probe
Oleate & Rapamycin	No immunofluorescent probes added	LAMP1 probe only	BODIPY 493/503 only	LAMP1 probe and then BODIPY probe

Figure 30. Schematic chamber slides for the confocal immunofluorescence experiment.

4.3.2.1.1. Cell preparation for confocal immunofluorescence DMEM ± Rapamycin experiment

The DMEM from the 25cm^3 flask containing HUH7 cells was discarded into the waste reservoir. The HUH7 cells were washed twice with 3mls Phosphate Buffered Saline (PBS) at room temperature and the PBS then discarded into the waste reservoir. 1ml of trypsin at room temperature was placed into the flask and mixed well. The flask was then placed in the incubator for 2 minutes at 37°C in an atmosphere with 5% CO_2 and a relative humidity of 95%. Then the flask was assessed under the microscope and once all the cells were detached 10mls of room temperature DMEM was added to the flask and mixed well. The DMEM containing the cells was then pipetted from the flask and placed into a 20ml tube. The cell mixture was centrifuged at 700rpm for 5 minutes at room temperature. The supernatant medium was pipetted out from the tube and placed into the waste reservoir. The cell pellet was resuspended in 8mls of DMEM and then using a haemocytometer and further DMEM the cell concentration was diluted to 50,000 cells per ml of DMEM. 370µl of the diluted cell suspension was placed into each of the 8 wells in an 8 chamber slide. In four of the wells 3µl of Rapamycin was added to give a final Rapamycin concentration of 0.2µg/ml. The cells were then incubated for 24 hours at 37°C in an atmosphere with 5% CO_2 and a relative humidity of 95%.

4.3.2.1.2. Cell preparation for confocal immunofluorescence Oleate DMEM ± Rapamycin experiment

The cells were prepared as detailed for the DMEM experiment above in sections 4.3.2.1.1. with the exception of Oleate DMEM being used instead of DMEM for the experiment.

4.3.2.1.3. Protocol for the addition of BODIPY and LAMP1 immunofluorescent markers

1.375mls of the LAMP1 transduction solution was prepared by combining 0.5ml of Organelle Lights lysosome reagent (Organelle Lights Lysosomes ,O10100, Invitrogen) with 0.875ml of PBS without Ca^{2+} or Mg^{2+}. The cell culture medium was then aspirated from the 4 chambers receiving LAMP1 probe and 0.34mls of the LAMP1 transduction solution was added to these 4 chambers. The cells were then incubated at room temperature in the dark for 4 hours with gentle shaking. The LAMP1 transduction solution was then aspirated from the 4 chambers and 0.4mls of enhancer solution was added to the 4 chambers. The cells were then incubated for 2 hours in the dark at 37°C in an atmosphere with 5% CO_2 and a relative humidity of 95%. The enhancer solution was then aspirated from the well and replaced with DMEM (or Oleate DMEM in the oleate experiment) and the cells incubated for >16 hours in the dark at 37°C in an atmosphere with 5% CO_2 and a relative humidity of 95% to allow for the expression of the LAMP1 fluorescent protein

The next day the DMEM or Oleate DMEM was aspirated from all eight chambers and the cells were fixed using 0.3mls, 4% paraformaldehyde in PBS, pH 7.4 for 15 minutes at room temperature. This was then aspirated and the cells washed with PBS at room temperature for 5 minutes. The PBS was aspirated and 0.3mls of 0.1% Triton-X in PBS was added to all the chambers for 5 minutes to allow cell permeabilisation, this was then aspirated and the cells washed again with PBS at room temperature for 5 minutes. The 4 chambers receiving BODIPY 493/503 (D-3922, Invitrogen) then had the PBS aspirated and 0.4mls of 10µg/ml BODIPY 493/503 added for 30 minutes at room temperature. The BODIPY solution was aspirated and the chambers washed three times for 5 minutes with PBS at room temperature. The PBS was then aspirated and 0.3ml 4-6-Diamidino-2-phenylindole (DAPI) was added to each chamber for 10 minutes as a fluorescent nuclear stain. The DAPI was then aspirated and each chamber washed three times for 5 minutes with PBS at room temperature and then finally with distilled water for 5 minutes. The chambers were then removed and the slide was mounted in PBS with a coverslip placed on top and sealed. The slide was then stored in the dark at 4 degrees until it was ready to be examined using a confocal immunofluorescence microscope.

4.3.2.2. Confocal immunofluorescence microscopy

The slides with BODIPY and LAMP1 immunofluorescent probes and DAPI were examined under fluorescent light using a Zeiss LSM confocal scanning microscope. The excitation/emission wavelength of LAMP1 was 554nm/584nm which appeared red under the microscope and 493nm/503nm for BODIPY which appeared green under the microscope. DAPI is excited at 358nm with a peak emission at 461nm and appears blue

under the microscope. Photomicrograph images taken for each experiment were stored and could be examined and exported for further analysis using LSM Image Browser from Zeiss.

4.3.2.3. Confocal immunofluorescence digital image analysis

To examine the number and area of lipid droplets per cell (BODIPY staining) quantification and thresholding of the green BODIPY staining was performed in individual frames using Image J software (National Institute of Health) in a minimum of 10 cells per experiment. Thresholding of the images with BODIPY staining was performed so that only the green coloured areas indicating neutral lipids were present in the image. The numerical values used in Image J for the three colour differentiation were: Red 0, 60. Green 56, 255. Blue 0, 114. The total number of lipid droplets per cell and the lipid droplet area in pixels^2 per cell were then calculated.

To examine the co-localisation of LAMP1 (lysosomal marker) and BODIPY (neutral lipids) quantification and thresholding was performed in individual frames from the confocal microscope using Image J software (National Institute of Health) in a minimum of 10 cells per experiment. When the two fluorescent probes, LAMP1-red and BODIPY-green co-localised the colour appeared yellow. Thresholding of the images with both LAMP1 and BODIPY staining was performed so that only the yellow coloured areas indicating co-localisation of the stains were present in the image. The numerical values used in Image J for the three colour differentiation were: Red 187, 255. Green 103, 255 and Blue 0, 94. Co-localisation was quantified by dividing the yellow thresholded area of

combined LAMP1/BODIPY staining by the area of LAMP1 only staining. This identified the percentage area of lysosomes stained by LAMP1 which showed co-localisation with neutral lipids stained by BODIPY.

4.3.3. Electron microscopy experiment

4.3.3.1. Cell culture methods for electron microscopy experiment

HUH7 cells were grown on cell culture treated Thermanox coverslips (Agar Scientific Ltd, L4354) in an 8 well chamber slide with three chambers containing HUH7 cells in DMEM with Rapamycin (0.2µg/ml) added for 24 hours. Three chambers were controls with HUH7 cells grown in DMEM with no Rapamycin added and two chambers were left empty. This was repeated for HUH7 cells grown in an Oleate DMEM (35.3µg/ml), see the schematic chamber slides below, **Figure 31.**

Therefore in total 4 experimental groups were examined

1) DMEM only
2) DMEM and Rapamycin
3) Oleate DMEM
4) Oleate and Rapamycin

DMEM only	HUH7 Cells	HUH7 Cells	HUH7 Cells	Empty
DMEM & Rapamycin	HUH7 Cells	HUH7 Cells	HUH7 Cells	Empty

Oleate DMEM	HUH7 Cells	HUH7 Cells	HUH7 Cells	Empty
Oleate & Rapamycin	HUH7 Cells	HUH7 Cells	HUH7 Cells	Empty

Figure 31. Schematic chamber slides for the electron microscopy experiment.

4.3.3.1.1. Cell preparation for electron microscopy DMEM ± Rapamycin experiment

The DMEM from the 25cm^3 flask containing HUH7 cells was discarded into the waste reservoir. The HUH7 cells were washed twice with 3mls PBS at room temperature and the PBS then discarded into the waste reservoir. 1ml of trypsin at room temperature was placed into the flask and mixed well. The flask was then placed in the incubator for 2 minutes at 37°C in an atmosphere with 5% CO_2 and a relative humidity of 95%. Then the flask was assessed under the microscope and once all the cells were detached 10mls of room temperature DMEM was added to the flask and mixed well. The DMEM containing the cells was then pipetted from the flask and placed into a 20ml tube. The cell mixture was centrifuged at 700rpm for 5 minutes at room temperature. The supernatant medium was pipetted out from the tube and placed into the waste reservoir. The cell pellet was resuspended in 8mls of DMEM and then using a haemocytometer and further DMEM the cell concentration was diluted to 50,000 cells per ml of DMEM. 370µl of the diluted cell suspension was placed into 6 of the 8 wells in an 8 chamber slide. In three of the wells 3µl of Rapamycin was added to give a final Rapamycin concentration of 0.2µg/ml. The cells were then incubated for 24 hours at 37°C in an atmosphere with 5% CO_2 and a relative humidity of 95%.

After 24 hours the DMEM ± Rapamycin was aspirated from the wells and the cells washed with PBS at room temperature for 5 minutes. The PBS was then aspirated from the wells and the cells washed again with PBS at room temperature for 5 minutes. The cells were then fixed using 0.3mls 3% glutaraldehyde in 0.1M cacodylate buffer, pH 7.2

at room temperature. The chamber slide with the cells on the coverslips in fixative were then taken to the electron microscopy department where the cells were post fixed in 1% osmium tetroxide, dehydrated through ascending grades of ethanol and embedded in Spurr's resin. Ultrathin sections were cut and stained with uranyl acetate and Reynold's lead citrate.

4.3.3.1.2. Cell preparation for electron microscopy Oleate DMEM ± Rapamycin experiment

The cells were prepared as detailed for the DMEM experiment above in sections 4.3.3.1.1. with the exception of Oleate DMEM being used instead of DMEM for the experiment.

4.3.3.2. Electron microscopy and analysis

The cells were examined using transmission electron microscopy on a Hitachi H-7650 transmission electron microscope. Photomicrograph images were taken for each experiment and assessed in conjunction with Dr Jill Moss, Head of Electron Microscopy at Imperial College Healthcare NHS Trust. The particular areas of interest within the cells were the lipid droplets, autophagolysosomes and autolipophagosomes.

4.3.4. Oil Red-O digital image analysis experiment

4.3.4.1. Cell culture methods for Oil Red-O digital image analysis experiment

HUH7 cells were grown in a 6 well plate with three chambers containing HUH7 cells grown in DMEM with Rapamycin (0.2µg/ml) added for 24 hours. The remaining three chambers were controls with HUH7 cells grown in DMEM with no Rapamycin added. This was repeated for HUH7 cells grown in an Oleate DMEM (35.3µg/ml), see the schematic 6 well plate below, **Figure 32.**

Therefore in total 4 experimental groups were examined

1) DMEM only
2) DMEM and Rapamycin
3) Oleate DMEM
4) Oleate and Rapamycin

DMEM only	HUH7 Cells	HUH7 Cells	HUH7 Cells
DMEM & Rapamycin	HUH7 Cells	HUH7 Cells	HUH7 Cells

Oleate DMEM	HUH7 Cells	HUH7 Cells	HUH7 Cells
Oleate & Rapamycin	HUH7 Cells	HUH7 Cells	HUH7 Cells

Figure 32. Schematic 6 well plates for the Oil Red-O digital image analysis experiment.

4.3.4.1.1. Cell preparation for Oil Red-O DMEM ± Rapamycin experiment

The DMEM from the 25cm^3 flask containing HUH7 cells was discarded into the waste reservoir. The HUH7 cells were washed twice with 3mls PBS at room temperature and the PBS then discarded into the waste reservoir. 1ml of trypsin at room temperature was placed into the flask and mixed well. The flask was then placed in the incubator for 2 minutes at 37°C in an atmosphere with 5% CO_2 and a relative humidity of 95%. Then the flask was assessed under the microscope and once all the cells were detached 10mls of room temperature DMEM was added to the flask and mixed well. The DMEM containing the cells was then pipetted from the flask and placed into a 20ml tube. The cell mixture was centrifuged at 700rpm for 5 minutes at room temperature. The supernatant medium was pipetted out from the tube and placed into the waste reservoir. The cell pellet was resuspended in 8mls of DMEM and then using a haemocytometer and further DMEM the cell concentration was diluted to 100,000 cells per ml of DMEM. 1ml of the diluted cell suspension was placed into each of the six wells in the 6 well plate. In three of the wells Rapamycin was added to give a final Rapamycin concentration of 0.2µg/ml. The cells were then incubated for 24 hours at 37°C in an atmosphere with 5% CO_2 and a relative humidity of 95%.

After 24 hours the DMEM ± Rapamycin was aspirated from the wells and the cells washed with PBS at room temperature for 5 minutes. The PBS was then aspirated from the wells and the cells washed again with PBS at room temperature for 5 minutes. 750µl of trypsin at room temperature was placed into each of the six wells. The 6 well plate was

then placed in the incubator for 2 minutes at 37°C in an atmosphere with 5% CO_2 and a relative humidity of 95%. Then the plate was assessed under the microscope and once all the cells were detached 1mls of room temperature DMEM was added to each well in the plate and mixed well. The DMEM containing the cells was then pipetted into a labelled 15mls conical tube and centrifuged at 700rpm for 5 minutes at room temperature. The supernatant was disposed in the waste reservoir and the remaining cell pellet was resuspended in 1ml of PBS at room temperature. This was then centrifuged at 700rpm for 5 minutes at room temperature, the supernatant discarded into the waste reservoir and the remaining cell pellet resuspended in 1ml of PBS at room temperature to ensure no DMEM was left. The cell suspensions were then centrifuged in the cytology department and the cytospins placed on coated slides and stained with ORO.

4.3.4.1.2. Cell preparation for Oil Red-O Oleate DMEM ± Rapamycin experiment

The cells were prepared as detailed for the DMEM experiment above in sections 4.3.4.1.1. with the exception of Oleate DMEM being used instead of DMEM for the experiment.

4.3.4.2. Oil Red-O digital image analysis

DIA was performed using Nikon NIS-Elements BR Software Basic Research. Three random images at x400 magnification for each cell suspension were taken to ensure a representative sample for each specimen. The percentage steatosis by area in the cells for each sample was calculated on ORO stained slides using the same three colour

differentiation system for each case. Prior to starting the analysis at least 20 points on a representative ORO stained slide were identified for each colour (red-fat, blue-cells, and white-background) so that the DIA system learnt how to classify an ORO stained slide. **Figure 33** shows the colour differentiation scatter graph used for the ORO stained slides, each dot on the graph represents a point on the slide that the investigator has identified so the DIA system learnt how to classify an ORO stained slide. This shows that the fat, cells and background on an ORO stained slide can be differentiated into three distinct categories with no overlap between them.

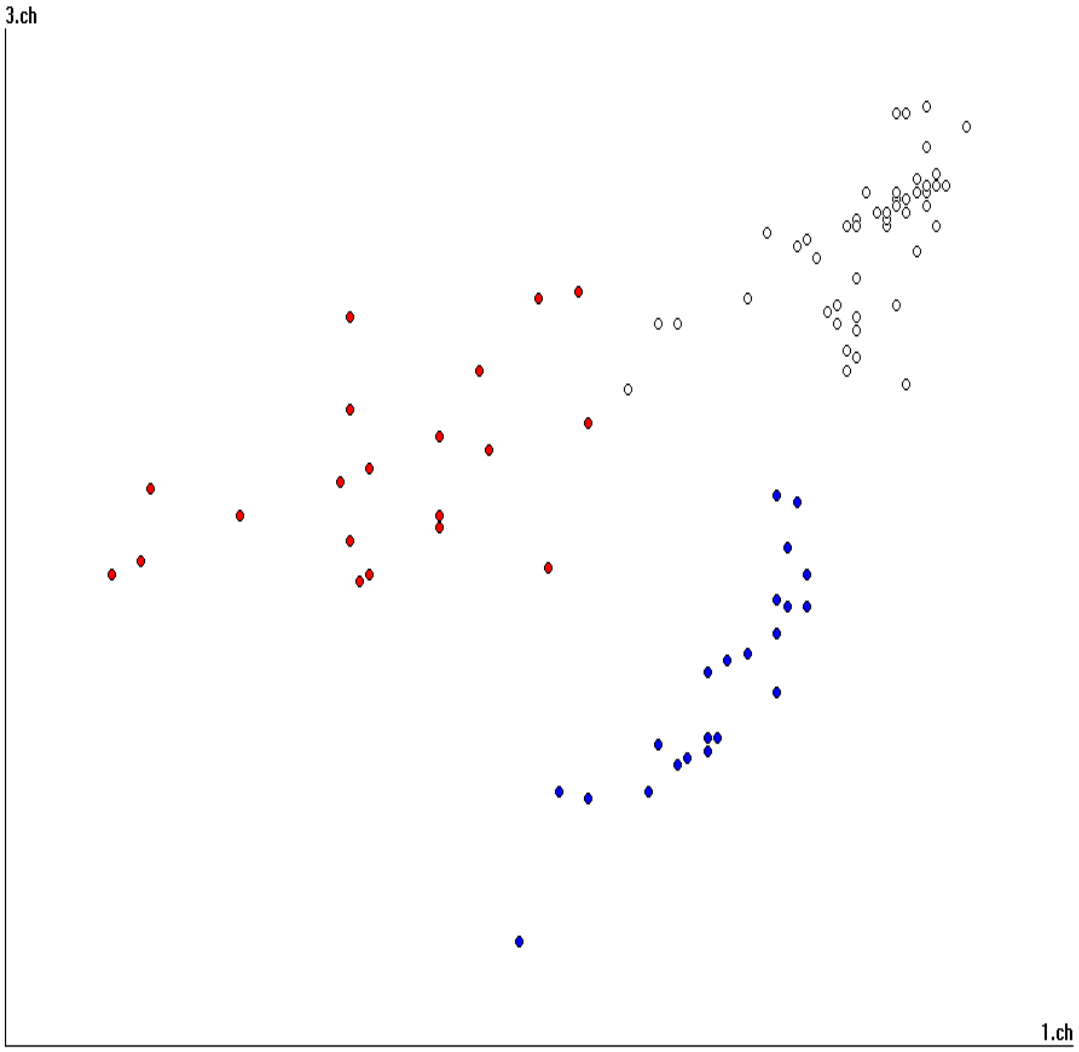


Figure 33. Scatter graph of the three colour differentiation used in ORO DIA (red =fat, blue=cells, white=background)

4.3.5. Triglyceride assay

4.3.5.1. Cell culture methods for triglyceride assay

HUH7 cells were grown in a 6 well plate with three chambers containing HUH7 cells grown in DMEM with Rapamycin (0.2µg/ml) added for 24 hours. The remaining three chambers were controls with HUH7 cells grown in DMEM with no Rapamycin added.

This was repeated for HUH7 cells grown in an Oleate DMEM (35.3µg/ml), see the schematic 6 well plate below, **Figure 34.**

Therefore in total 4 experimental groups were examined

1) DMEM only
2) DMEM and Rapamycin
3) Oleate DMEM
4) Oleate and Rapamycin

DMEM only	HUH7 Cells	HUH7 Cells	HUH7 Cells
DMEM & Rapamycin	HUH7 Cells	HUH7 Cells	HUH7 Cells

Oleate DMEM	HUH7 Cells	HUH7 Cells	HUH7 Cells
Oleate & Rapamycin	HUH7 Cells	HUH7 Cells	HUH7 Cells

Figure 34. Schematic 6 well plates for the triglyceride assay experiment.

4.3.5.1.1. Cell preparation for triglyceride DMEM and Oleate DMEM ± Rapamycin assay

The cells were prepared as detailed for the Oil Red-O experiment above in sections 4.3.4.1.1. and 4.3.4.1.2. The final cell suspension in 1ml PBS was centrifuged and the supernatant discarded to give a cell pellet which was used for triglyceride quantification.

4.3.5.2. Triglyceride quantification

Triglyceride concentrations per well were measured using a commercially available assay by spectrophotometry (Abcam;ab65336). The triglyceride quantification assay gives a

sensitive measure of triglyceride concentration using a colorimetric (spectrophotometry at OD = 570 nm) method. In the assay, triglycerides are converted to free fatty acids and glycerol. The glycerol is then oxidised to generate a product which reacts with a probe to produce colour.

The cell pellet from the experiment had 250µl 5% Triton-X100 in water added and the number of cells per ml was counted using a haemocytometer. The sample was then homogenised and slowly heated to 80°C and incubated for five minutes, then slowly cooled down to room temperature. The heating was repeated once more to solubilise all the triglyceride into solution. The sample was then centrifuged at 14,000rpm for five minutes and any insoluble material removed.

Using a 96 well plate 50µl of each sample was placed into a well, this was performed in duplicate. A standard curve was calculated using the triglyceride standard provided with the assay, and this was again performed in duplicate. 2 µl of lipase was added to each standard and sample well. This was mixed and incubated for 20 minutes at room temperature to convert triglyceride to glycerol and fatty acid. 50µl of triglyceride reaction mix (46 µl Triglyceride Assay Buffer, 2 µl Triglyceride Probe, 2 µl Triglyceride Enzyme Mix) was added to each standard and sample well. This was mixed and incubated for 60minutes at room temperature and protected from the light. Spectrophotometry at O.D. 570nm was measured using a plate reader. Using the absorbance values and standard curve the triglyceride concentration in nmol/well standardised for the number of cells per well was calculated.

4.3.6. Fluorescence activated cell sorting experiments

4.3.6.1. Cell culture methods for fluorescence activated cell sorting for reactive oxygen species detection

HUH7 cells were grown in a 6 well plate with two chambers containing HUH7 cells grown in DMEM with Rapamycin (0.2µg/ml) added for 24 hours, one of these chambers also had the intracellular fluorescent reactive oxygen species marker, carboxy-H2DFFDA added. Three chambers were controls with HUH7 cells grown in DMEM with no Rapamycin added. One of these chambers was a negative control, one had carboxy-H2DFFDA added and the final chamber had carboxy-H2DFFDA and 100µM hydrogen peroxide added to act as a positive control. This was repeated for HUH7 cells grown in an Oleate DMEM (35.3µg/ml), see the schematic 6 well plate, **Figure 35.**

Therefore in total 4 experimental groups were examined

1) DMEM only
2) DMEM and Rapamycin
3) Oleate DMEM
4) Oleate and Rapamycin

DMEM only	No carboxy-H2DFFDA added	Carboxy-H2DFFDA added	Carboxy-H2DFFDA added and 100µM H_2O_2
DMEM & Rapamycin	No carboxy-H2DFFDA added	Carboxy-H2DFFDA added	Empty

Oleate DMEM	No carboxy-H2DFFDA added	Carboxy-H2DFFDA added	Carboxy-H2DFFDA added and 100µM H_2O_2
Oleate & Rapamycin	No carboxy-H2DFFDA added	Carboxy-H2DFFDA added	Empty

Figure 35. Schematic 6 well plates for the fluorescence activated cell sorting reactive oxygen species experiment.

4.3.6.1.1. Cell preparation for fluorescence activated cell sorting reactive oxygen species detection DMEM ± Rapamycin experiment

The DMEM from the 25cm^3 flask containing HUH7 cells was discarded into the waste reservoir. The HUH7 cells were washed twice with 3mls PBS at room temperature and the PBS then discarded into the waste reservoir. 1ml of trypsin at room temperature was placed into the flask and mixed well. The flask was then placed in the incubator for 2 minutes at 37°C in an atmosphere with 5% CO_2 and a relative humidity of 95%. Then the flask was assessed under the microscope and once all the cells were detached 10mls of room temperature DMEM was added to the flask and mixed well. The DMEM containing the cells was then pipetted from the flask and placed into a 20ml tube. The cell mixture was centrifuged at 700rpm for 5 minutes at room temperature. The supernatant medium was pipetted out from the tube and placed into the waste reservoir. The cell pellet was resuspended in 6mls of DMEM, 1mls was placed into the chamber with DMEM only and

1ml into the DMEM Rapamycin only chamber. The remaining 4mls of cells were centrifuged at 700 rpm for 5 minutes at room temperature. The supernatant medium was pipetted out from the tube and placed into the waste reservoir. The cell pellet was re-suspended in 6mls of pre-warmed PBS containing 50µmol/l of the intracellular, fluorescent, reactive oxygen species marker, carboxy-H2DFFDA. This suspension was left for 10 minutes at 37ºC. The sample was then centrifuged at 700rpm for 5 minutes and the supernatant medium was pipetted out from the tube and placed into the waste reservoir. The cells were resuspended in 4mls of pre-warmed DMEM and 1mls was placed into the three chambers, DMEM plus carboxy-H2DFFDA, DMEM plus carboxy-H2DFFDA and 100µM H_2O_2 and DMEM Rapamycin plus carboxy-H2DFFDA. The chambers with Rapamycin had 1mls of DMEM with Rapamycin added to give a final concentration of Rapamycin of 0.2µg/ml. The chambers without Rapamycin had 1mls of DMEM added to make the total volume up to 2mls. The cells were then incubated for 24 hours at 37°C in an atmosphere with 5% CO_2 and a relative humidity of 95%.

30 minutes before the end of the 24 hours, 1ml of DMEM was removed from the DMEM, carboxy-H2DFFDA, H_2O_2 chamber and 1ml of H_2O_2 in DMEM was added to give a concentration of 100µM H_2O_2 within the chamber for 30 minutes.

The media from each well of HUH7 cells was transferred to a separate 15 ml conical tube. The cells adherent to each chamber were gently washed with 2mls PBS and the PBS then removed. 1ml of trypsin at room temperature was placed into each chamber and mixed well. The 6 chamber plate was then placed in the incubator for 2 minutes at 37°C

in an atmosphere with 5% CO_2 and a relative humidity of 95%. Then the flask was assessed under the microscope and once all the cells were detached the cells were resuspended in the original media which was kept in the 15ml conical tubes. The cell suspension was then transferred to a 15ml conical tube and centrifuged at 700rpm for 5 minutes at room temperature. The supernatant medium was pipetted out from the tube and placed into the waste reservoir. The cell pellet was resuspended in 500µl PBS with 0.05% Tween and transferred to a 1.5ml eppendorf ready for FACS analysis.

4.3.6.1.2. Cell preparation for fluorescence activated cell sorting reactive oxygen species detection Oleate DMEM ± Rapamycin experiment

The cells were prepared as detailed for the DMEM experiment above in sections 4.3.6.1.1. with the exception of Oleate DMEM being used instead of DMEM for the experiment.

4.3.6.2. Cell culture methods for fluorescence activated cell sorting for apoptosis and necrosis detection

HUH7 cells were grown in a 6 well plate with four chambers being used in each experiment. The experiment was performed in triplicate. The chambers contain HUH7 cells grown in DMEM ± Rapamycin (0.2µg/ml) added for 24 hours. One of the chambers was a negative control, one had PI added, one of the chambers had AV-FITC added and one had both PI and AV-FITC. This was repeated for HUH7 cells grown in an Oleate DMEM (35.3µg/ml), see the schematic 6 well plate, **Figure 36.**

Therefore in total 4 experimental groups were examined

1) DMEM only
2) DMEM and Rapamycin
3) Oleate DMEM
4) Oleate and Rapamycin

DMEM only	Negative control	PI	AV-FITC
	PI and AV-FITC	Empty	Empty

DMEM & Rapamycin	Negative control	PI	AV-FITC
	PI and AV-FITC	Empty	Empty

Oleate DMEM	Negative control	PI	AV-FITC
	PI and AV-FITC	Empty	Empty

Oleate & Rapamycin	Negative control	PI	AV-FITC
	PI and AV-FITC	Empty	Empty

Figure 36. Schematic 6 well plates for the fluorescence activated cell sorting apoptosis detection experiment.

4.3.6.2.1. Cell preparation for fluorescence activated cell sorting apoptosis and necrosis detection DMEM ± Rapamycin experiment

The DMEM from the 25cm^3 flask containing HUH7 cells was discarded into the waste reservoir. The HUH7 cells were washed twice with 3mls PBS at room temperature and the PBS then discarded into the waste reservoir. 1ml of trypsin at room temperature was placed into the flask and mixed well. The flask was then placed in the incubator for 2 minutes at 37°C in an atmosphere with 5% CO_2 and a relative humidity of 95%. Then the

flask was assessed under the microscope and once all the cells were detached 10mls of room temperature DMEM was added to the flask and mixed well. The DMEM containing the cells was then pipetted from the flask and placed into a 20ml tube. The cell mixture was centrifuged at 700rpm for 5 minutes at room temperature. The supernatant medium was pipetted out from the tube and placed into the waste reservoir. The cell pellet was resuspended in 8mls of DMEM, 1mls was placed into each of the 8 chambers being used in the experiment. The four chambers with Rapamycin had 1mls of DMEM with Rapamycin added to give a final concentration of Rapamycin of 0.2µg/ml. The four chambers without Rapamycin had 1mls of DMEM added to make the total volume up to 2mls. The cells were then incubated for 24 hours at 37°C in an atmosphere with 5% CO_2 and a relative humidity of 95%.

4.3.6.2.2. Cell preparation for fluorescence activated cell sorting apoptosis and necrosis detection Oleate DMEM ± Rapamycin experiment

The cells were prepared as detailed for the DMEM experiment above in sections 4.3.6.2.1. with the exception of Oleate DMEM being used instead of DMEM for the experiment.

4.3.6.2.3. Protocol for the addition of Annexin V and Propidium Iodide immunofluorescent markers

The media from each well of HUH7 cells was transferred to a separate 15 ml conical tube and placed on ice. The cells adherent to each chamber were gently washed with 2mls PBS and the PBS then removed. 1ml of trypsin at room temperature was placed into each

chamber and mixed well. The 6 chamber plate was then placed in the incubator for 2 minutes at 37°C in an atmosphere with 5% CO_2 and a relative humidity of 95%. Then the flask was assessed under the microscope and once all the cells were detached the cells were resuspended in the original media which was kept in the 15ml conical tubes. The cell suspension was then transferred to a 15ml conical tube and centrifuged at 700rpm for 5 minutes at room temperature. The supernatant medium was pipetted out from the tube and placed into the waste reservoir. The cell pellet was resuspended in 500µl of DMEM (Oleate DMEM for Oleate experiment), mixed well and transferred to a 1.5ml eppendorf. 10µl of media binding reagent was then added (Merck – PF032 Annexin V Apoptosis Detection Kit I), then 1.25µl of AV-FITC to the chambers with AV in. The sample was then incubated in the dark for 15 minutes at room temperature. The sample was then centrifuged at 1000rpm for 5mins at room temperature and the supernatant was pipetted out from the tube and placed into the waste reservoir. The cells were then gently resuspended in 0.5mls cold 1x binding buffer with 0.05% Tween, then 10µl of PI was added to the chambers with PI in. The samples were placed on ice away from the light and immediately analysed by FACS.

4.3.6.3. Fluorescence activated cell sorting

The cells were analysed on a flow cytometer which emitted an excitation light between 488-495nm to quantify the AV-FITC, PI and carboxy-H2DFFDA signals. The FITC and carboxy-H2DFFDA signals were detected at 518nm by the FITC detector and the PI at 620nm by the phycoerythrin fluorescence detector. The results were controlled to exclude

background noise and cells/cell fragments of abnormal size and shape. The data was analysed using Dako Summit V4.3 software.

4.4. Results

4.4.1. Confocal immunofluorescence

4.4.1.1. Lipid droplet number & area

Images from the confocal immunofluorescence microscopy are shown which demonstrate BODIPY staining of neutral lipids within HUH7 cells grown in Oleate DMEM ± Rapamycin (**Figure 37)** and DMEM ± Rapamycin. (**Figure 38**)

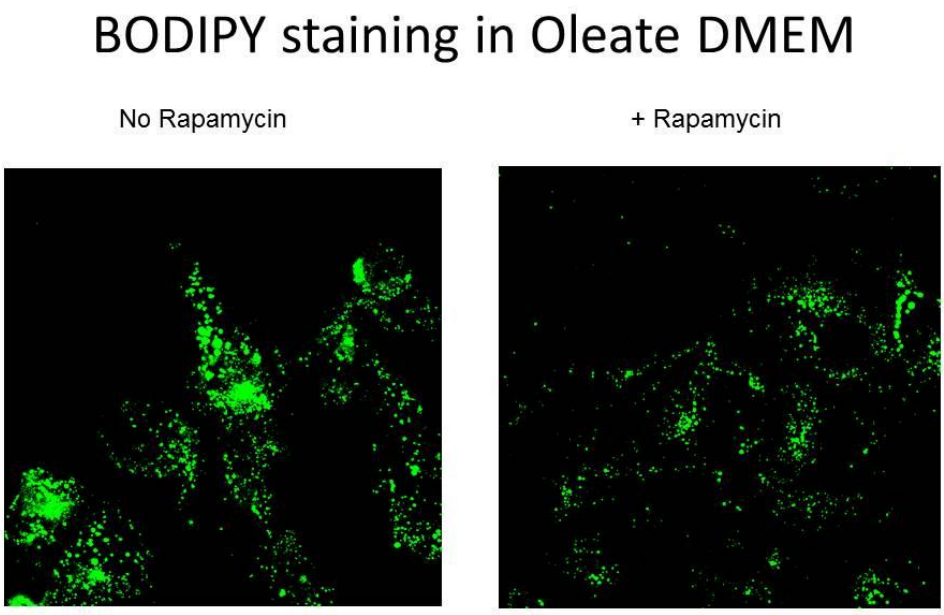


Figure 37. Confocal immunofluorescence images with BODIPY staining in HUH7 cells grown in Oleate DMEM with and without Rapamycin.

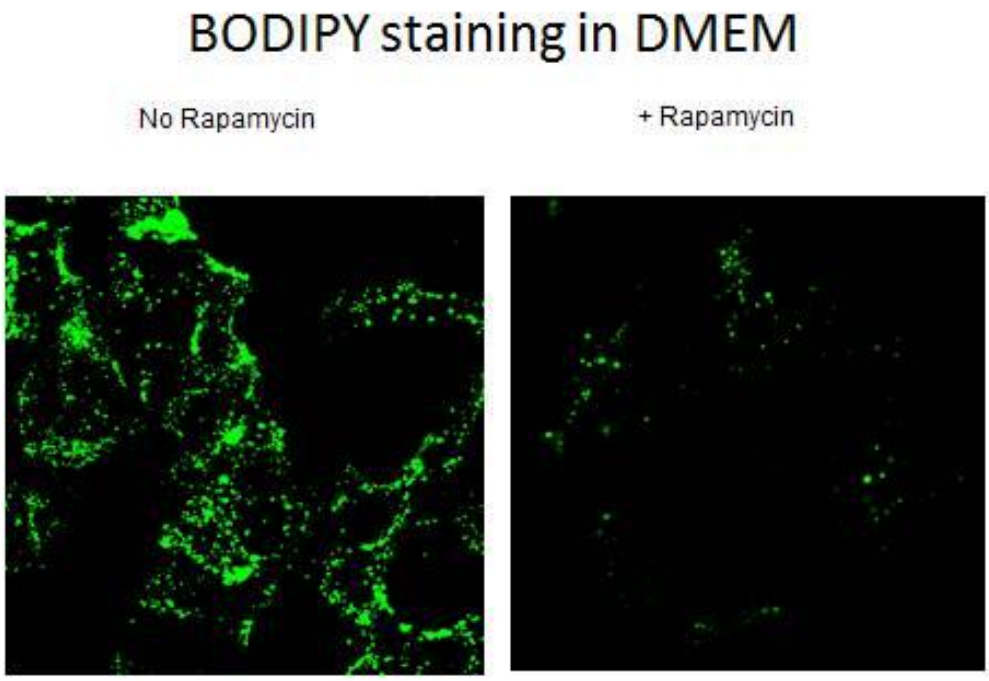


Figure 38. Confocal immunofluorescence images with BODIPY staining in HUH7 cells grown in DMEM with and without Rapamycin.

The number of lipid droplets per HUH7 cell grown in Oleate DMEM ± Rapamycin or DMEM ± Rapamycin and the lipid droplet area per cell (pixels^2) is shown in **Table 27** and **Figures 39-40.**

	Oleate	Oleate Rapamycin	DMEM	DMEM Rapamycin
Mean lipid droplets per cell ± SEM	127.93 ± 23.30	68.16 ± 19.46	78.00 ± 12.38	22.28 ± 2.53
Mean lipid droplet area per cell ± SEM (pixels^2)	529.90 ± 90.02	285.60 ± 36.27	313.38 ± 50.50	93.67 ± 1.67

Table 27. Mean number of lipid droplets and lipid droplet area ± SEM per HUH7 cell, grown in DMEM ± Rapamycin or Oleate DMEM ± Rapamycin.

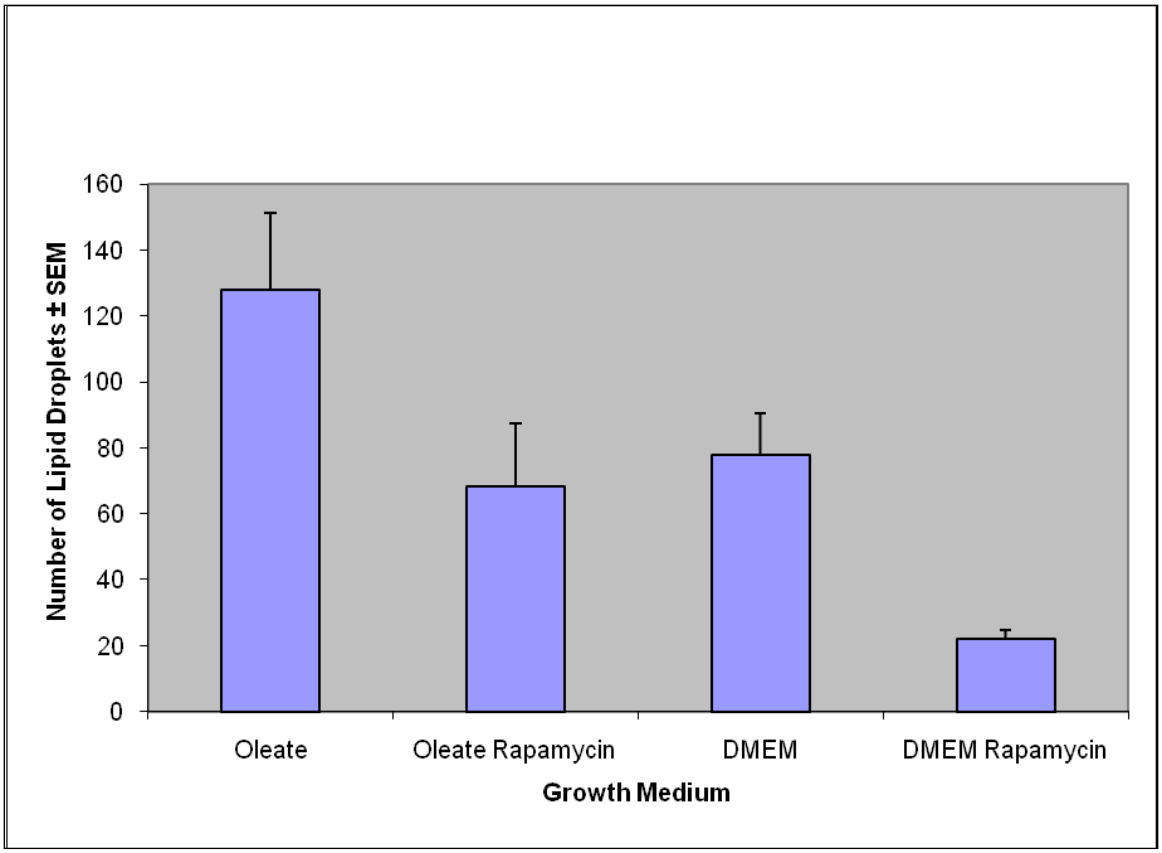


Figure 39. Mean number of lipid droplets ± SEM per HUH7 cell in different growth mediums.

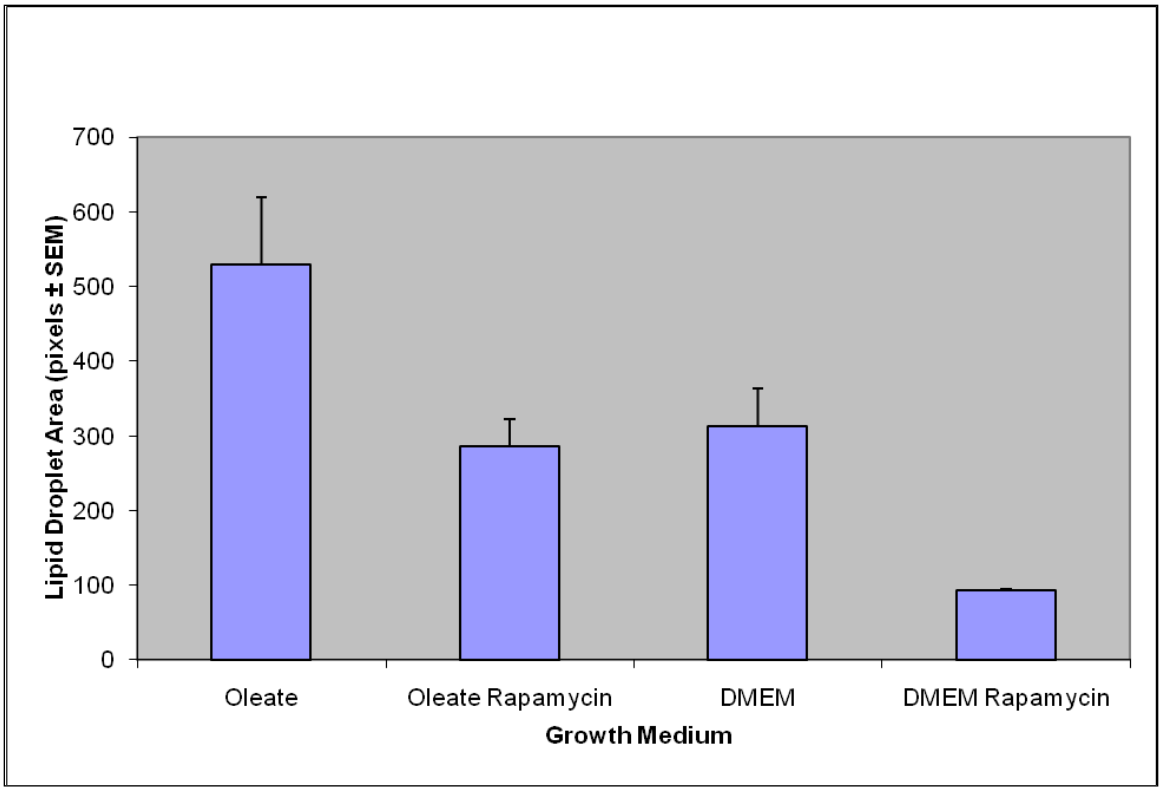


Figure 40. Mean lipid droplet area (pixels^2) ± SEM per HUH7 cell in different growth mediums.

The number of lipid droplets (127.93±23.30 vs. 78.00±12.38) and lipid droplet area (529.90±90.02 vs. 313.38±50.50) per cell is higher in cells grown in Oleate DMEM than in DMEM as would be expected. With the addition of Rapamycin to the growth medium the number and area of lipid droplets per cell decreased. However, none of the results reached statistical significance (all p >0.37) which may have been due to the relatively small number of cells examined.

4.4.1.2. Co-localisation of lysosomes and lipids

Representative images from the confocal immunofluorescence microscopy are shown which demonstrate LAMP1 staining of lysosomes (red), BODIPY staining of neutral lipids (green) and co-localisation (yellow) within HUH7 cells grown in Oleate DMEM ± Rapamycin (**Figures 41-42**) and DMEM ± Rapamycin (**Figures 43-44**).

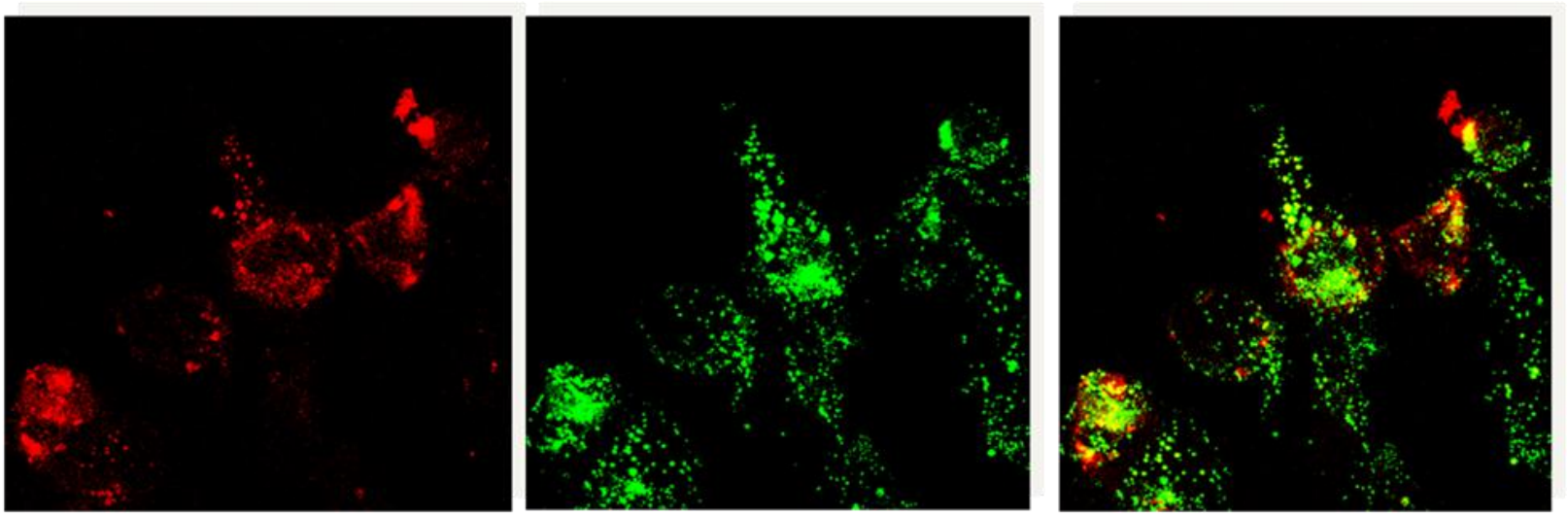


Figure 41. Confocal immunofluorescence in HUH7 cells grown in Oleate DMEM without Rapamycin.

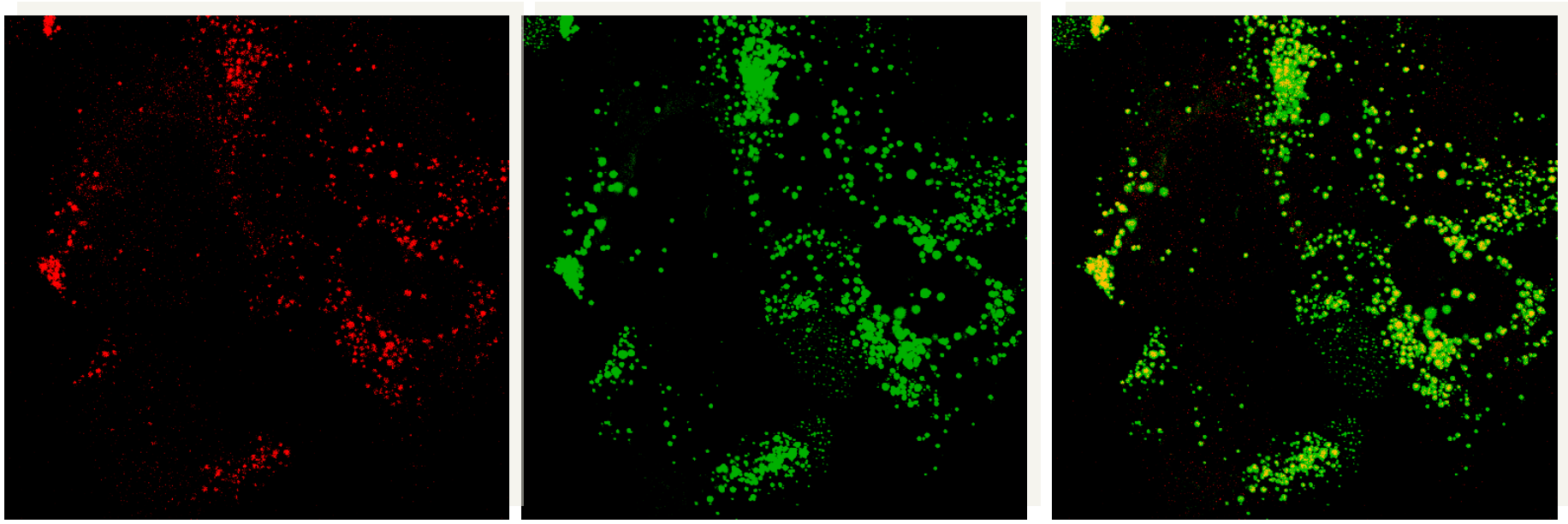


Figure 42. Confocal immunofluorescence in HUH7 cells grown in Oleate DMEM with Rapamycin.

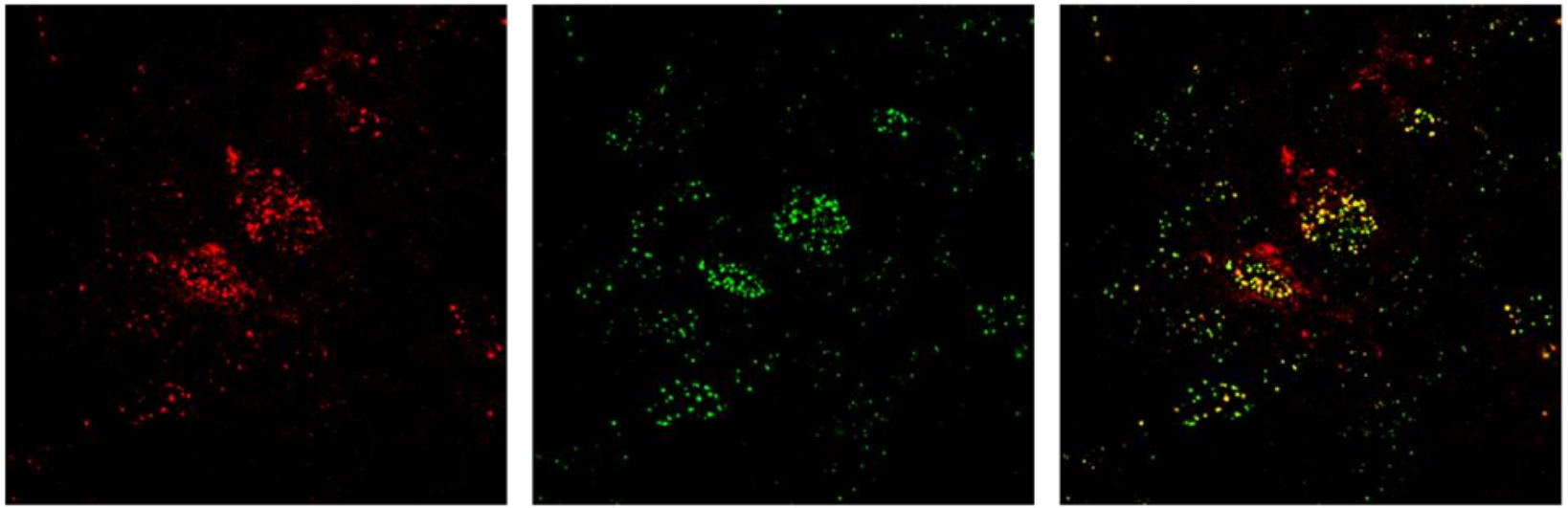


Figure 43. Confocal immunofluorescence in HUH7 cells grown in DMEM without Rapamycin.

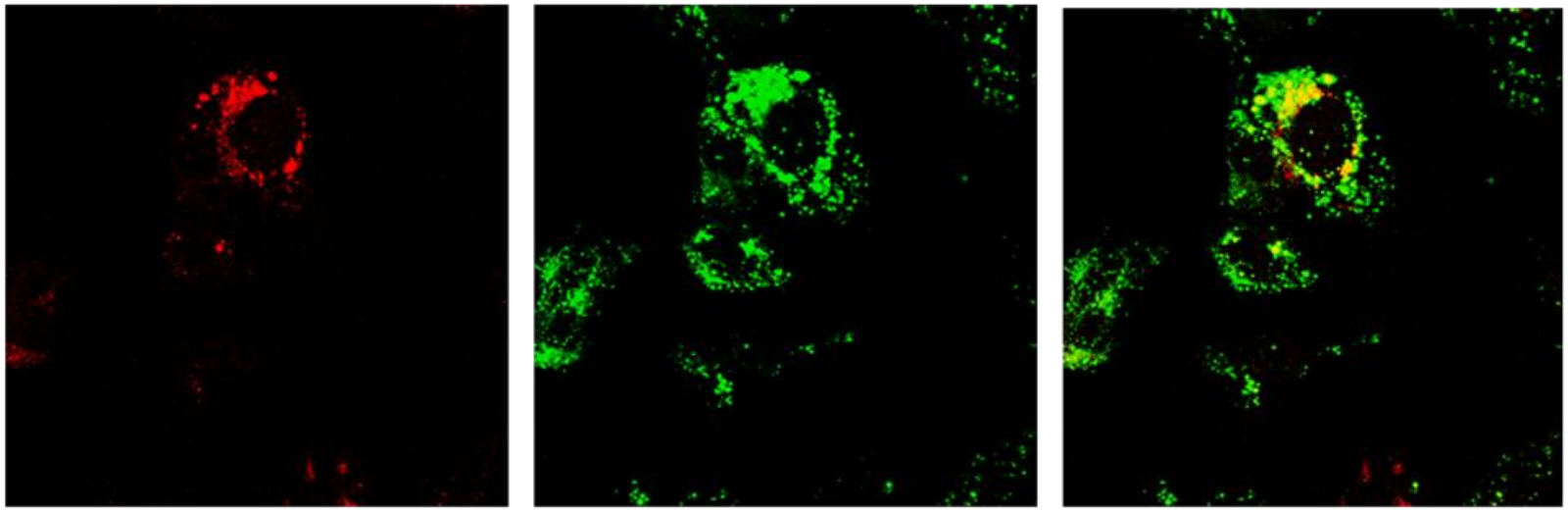


Figure 44. Confocal immunofluorescence in HUH7 cells grown in DMEM with Rapamycin.

The percentage area co-localisation between LAMP1 and BODIPY in HUH7 cells grown in Oleate DMEM ± Rapamycin or DMEM ± Rapamycin is shown in **Table 28** and **Figure 45**.

	Oleate	**Oleate Rapamycin**	**DMEM**	**DMEM Rapamycin**
Mean percentage co-localisation area ± SEM	19.85 ± 0.95	32.85 ± 0.85	10.20 ± 0.60	21.75 ± 0.15

Table 28. Mean percentage area co-localisation between LAMP1 and BODIPY in HUH7 cells grown in different growth mediums.

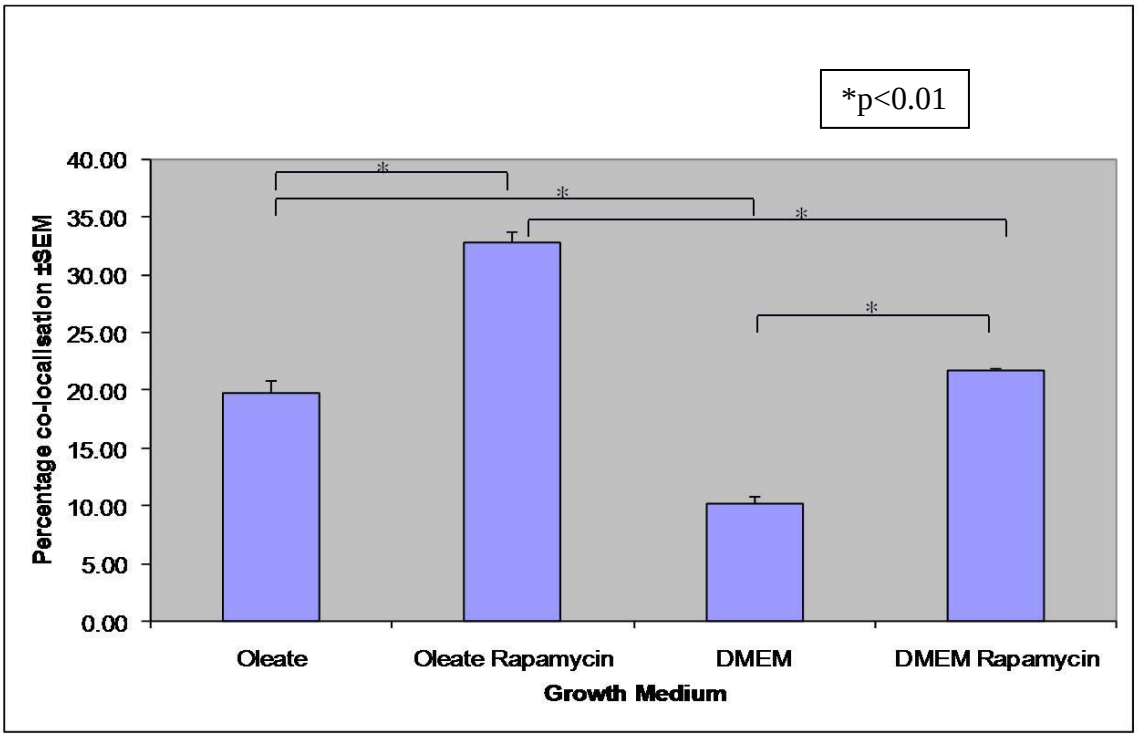


Figure 45. Mean percentage area co-localisation ±SEM between LAMP1 and BODIPY in HUH7 cells grown in different growth mediums.

Confocal immunofluorescence demonstrated a significant increase in co-localisation between lipid droplets and lysosomes in cells grown with Rapamycin compared to those without Rapamycin, $p<0.01$. It also showed a significant increase in co-localisation between lipid droplets and lysosomes in cells grown in Oleate DMEM, 19.85 ± 0.95%, compared to DMEM, 10.20 ± 0.60%, $p<0.01$.

4.4.2. Electron microscopy

Representative images from electron microscopy are shown and labelled with relevant structures. (**Figures 46 – 53)**

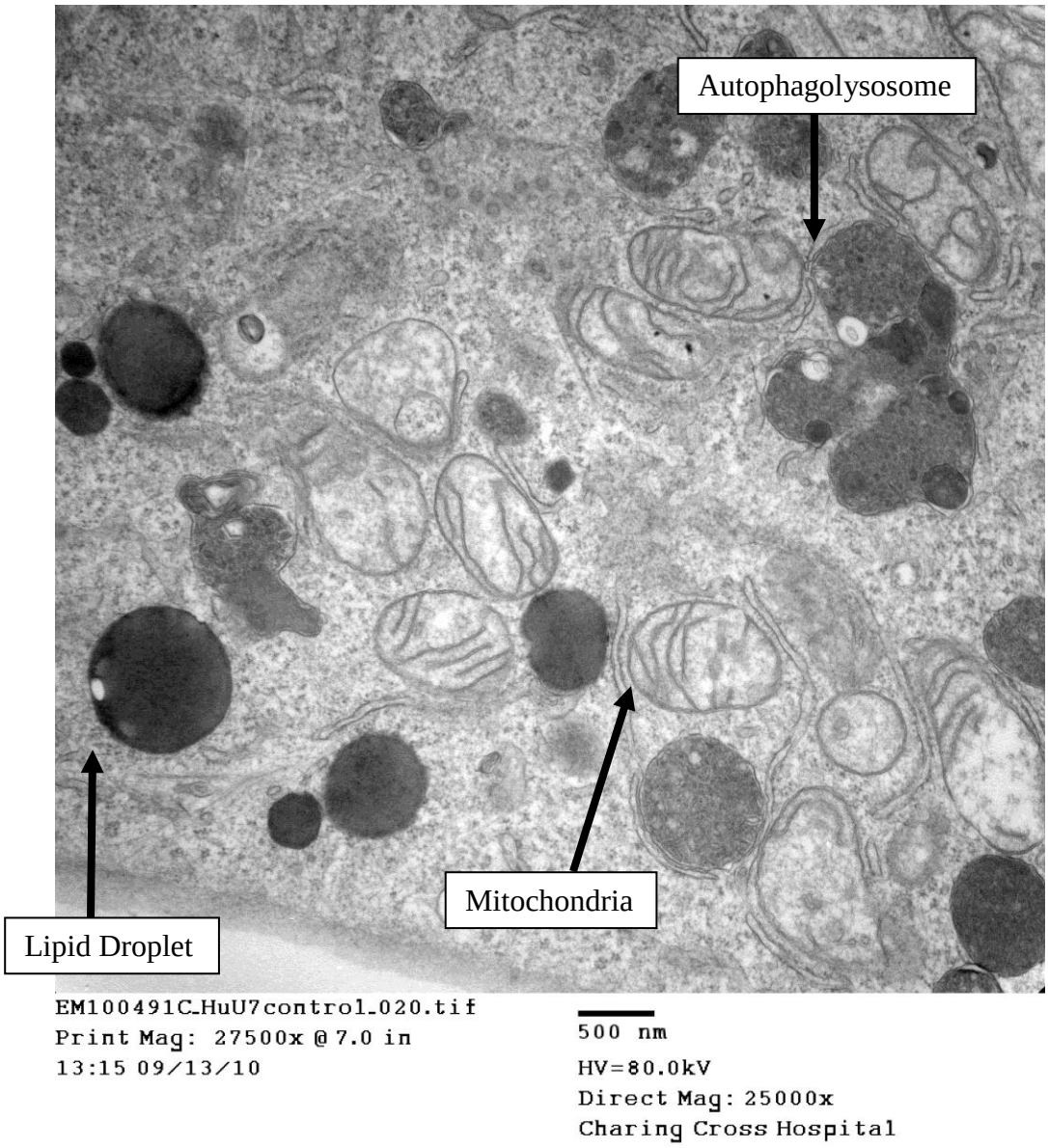


Figure 46. Electron microscopy photomicrograph from an HUH7 cell grown in DMEM only, original magnification x25000.

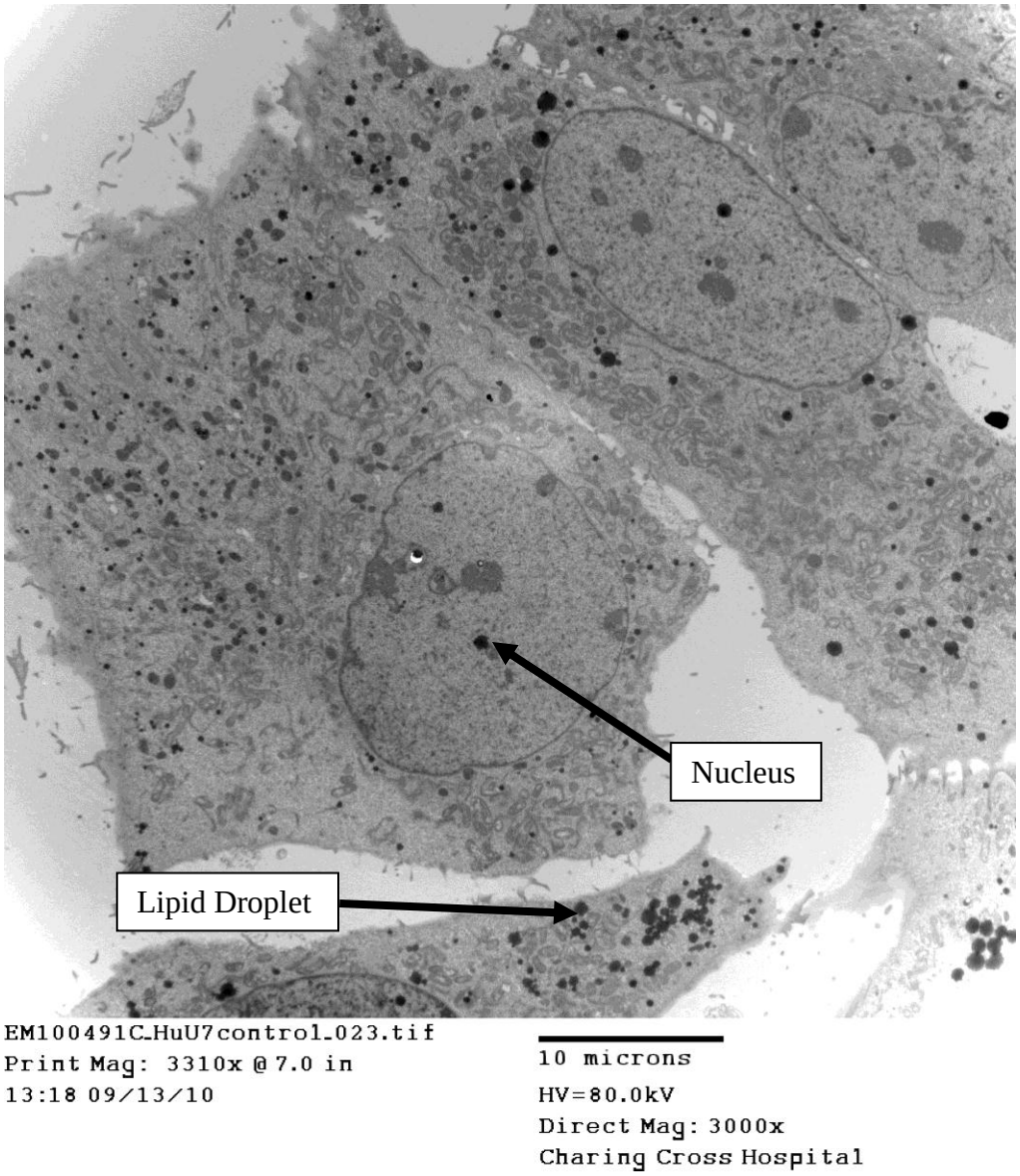


Figure 47. Electron microscopy photomicrograph from an HUH7 cell grown in DMEM only, original magnification x3000.

These figures show that in HUH7 cells grown in standard DMEM there are scattered lipid droplets within the cytoplasm. However, only very occasional autophagolysosomes are seen.

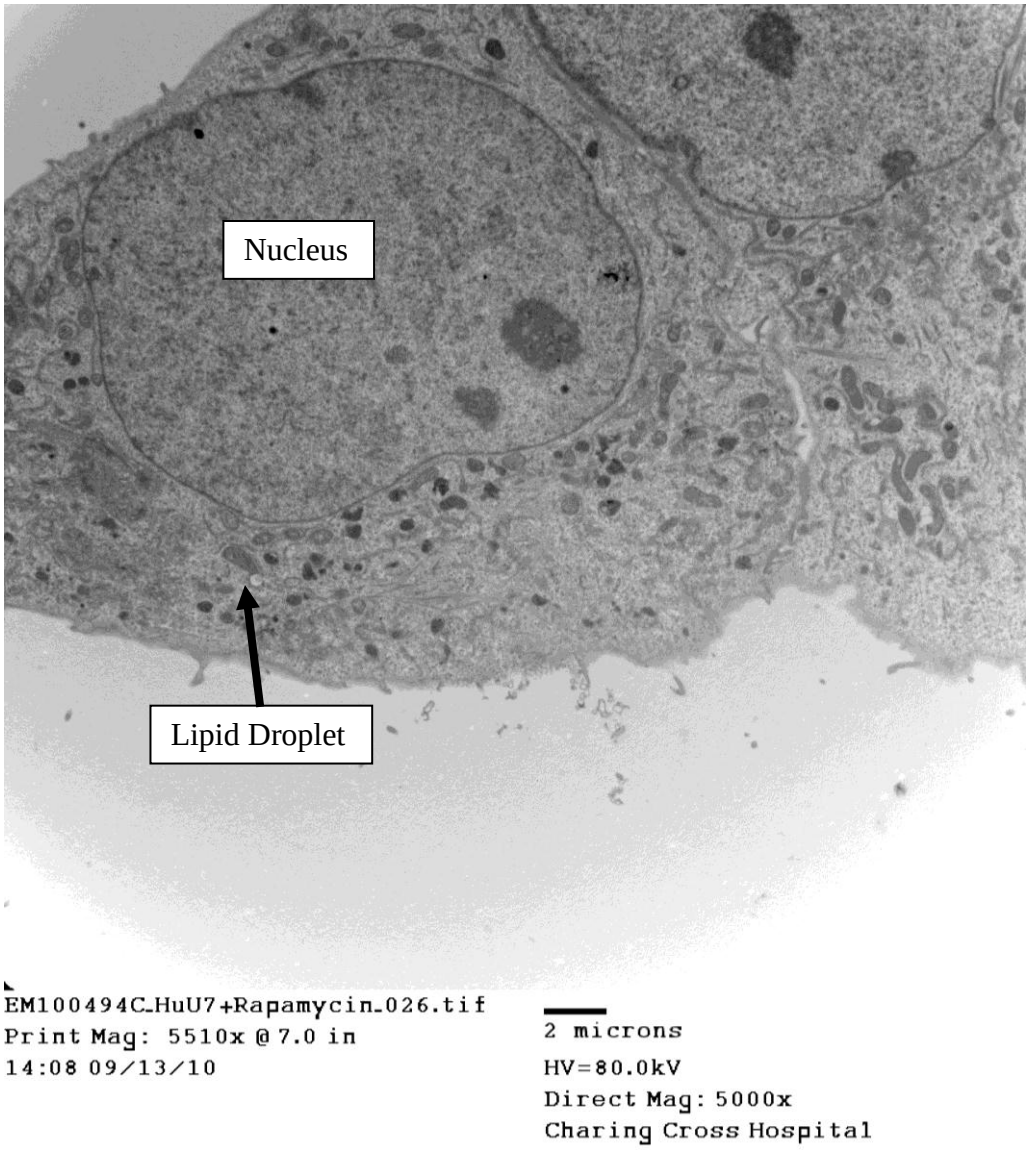


Figure 48. Electron microscopy photomicrograph from an HUH7 cell grown in DMEM with Rapamycin, original magnification x5000.

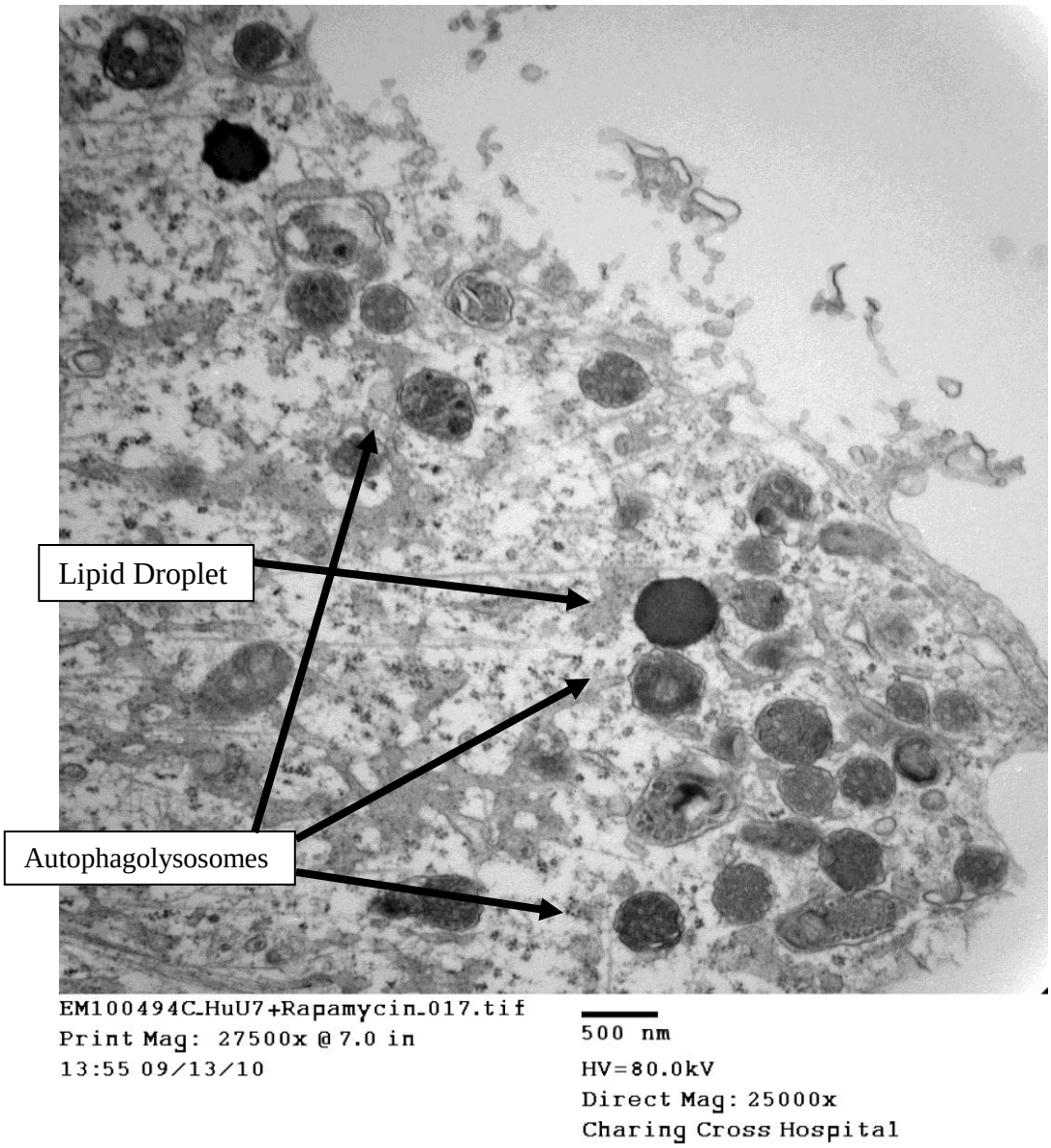


Figure 49. Electron microscopy photomicrograph from an HUH7 cell grown in DMEM with Rapamycin, original magnification x25000.

The images from HUH7 cells grown in DMEM with Rapamycin show decreased numbers of lipid droplets and increased numbers of autophagolysosomes when compared to cells grown in DMEM without Rapamycin.

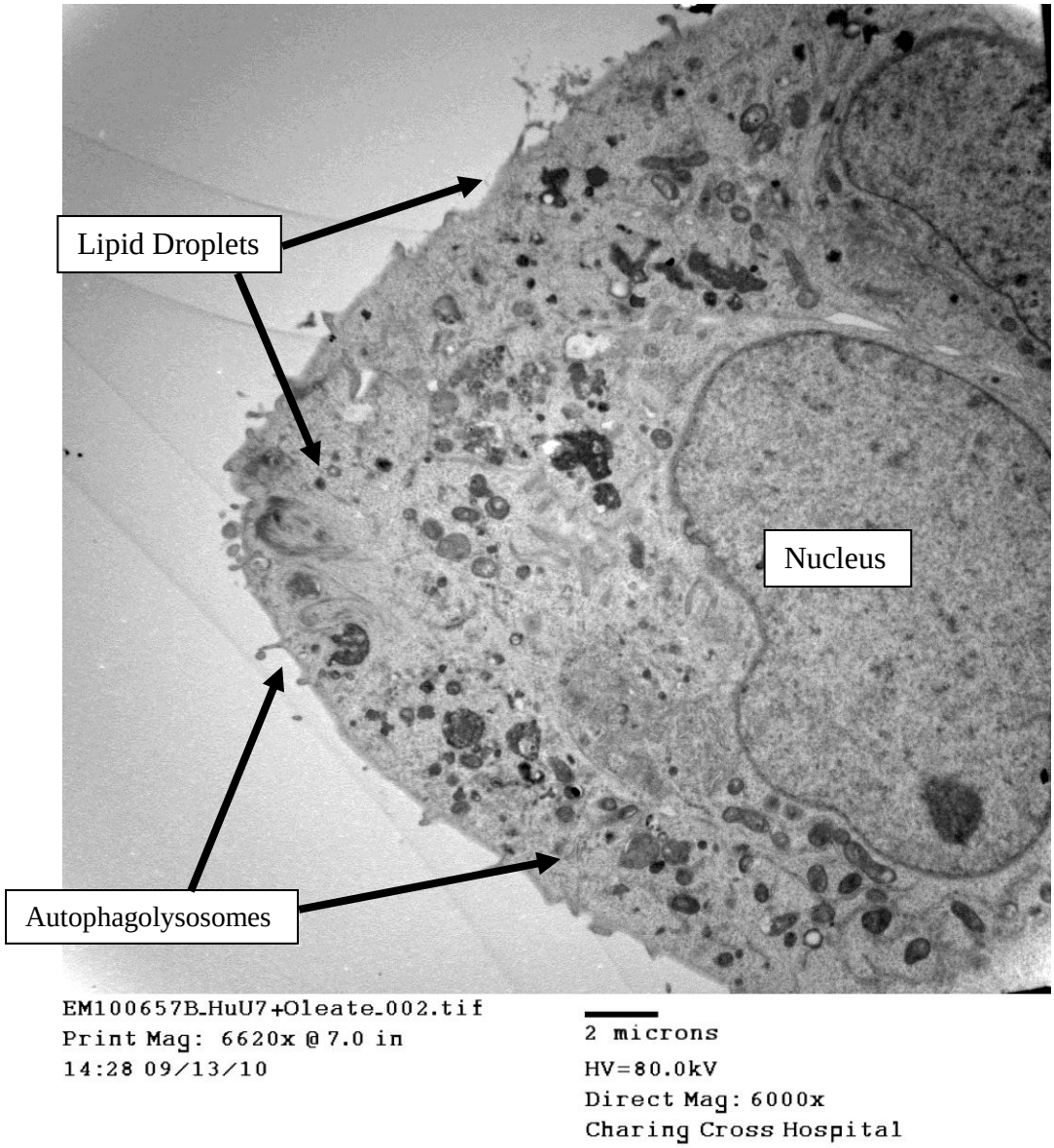


Figure 50. Electron microscopy photomicrograph from an HUH7 cell grown in Oleate DMEM, original magnification x6000.

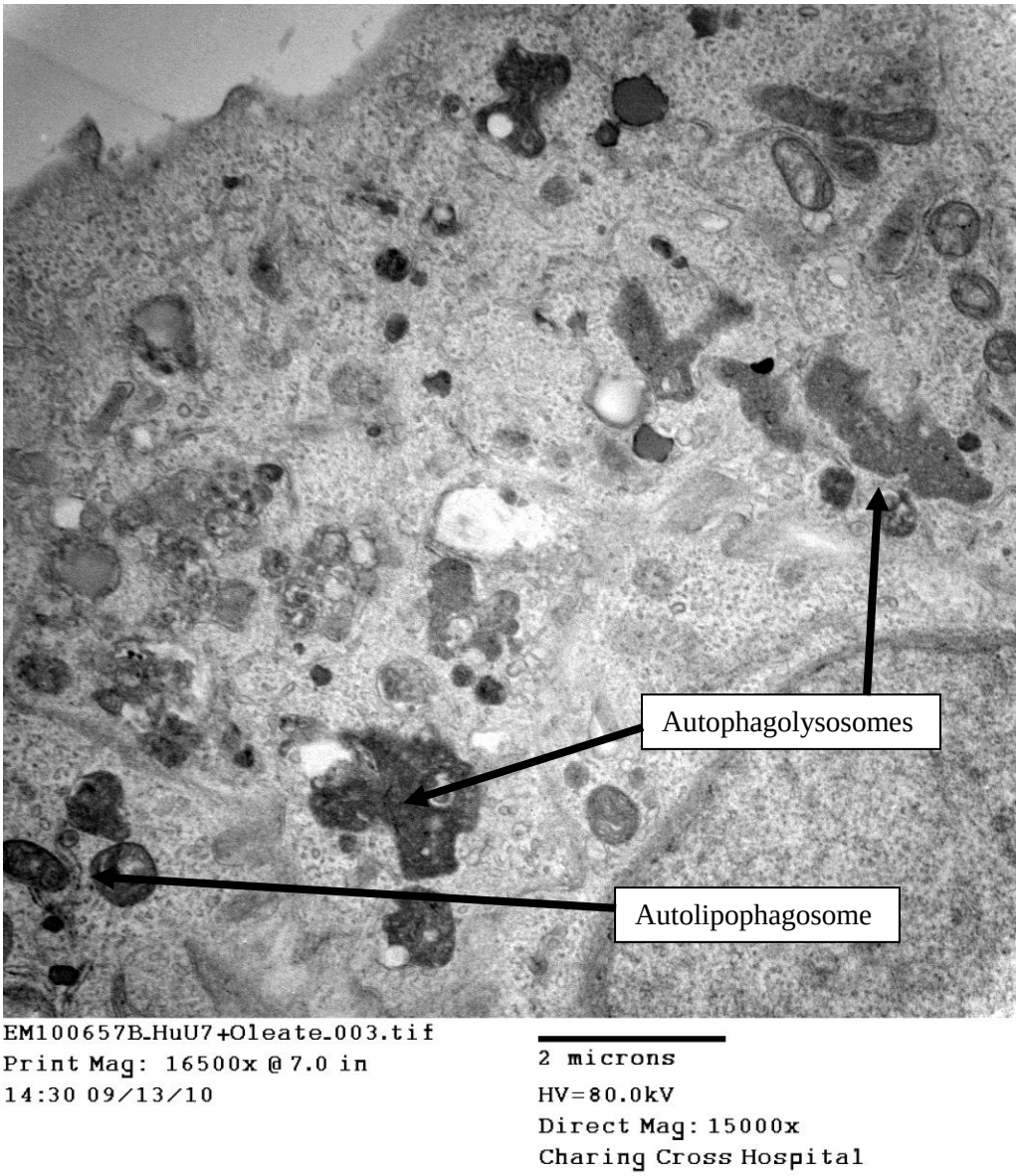


Figure 51. Electron microscopy photomicrograph from an HUH7 cell grown in Oleate DMEM, original magnification x15000.

The images from HUH7 cells grown in Oleate DMEM without Rapamycin show increased lipid droplets and increased numbers of autolipophagosomes and autophagolysosomes in comparison to the cells grown in standard DMEM without Rapamycin.

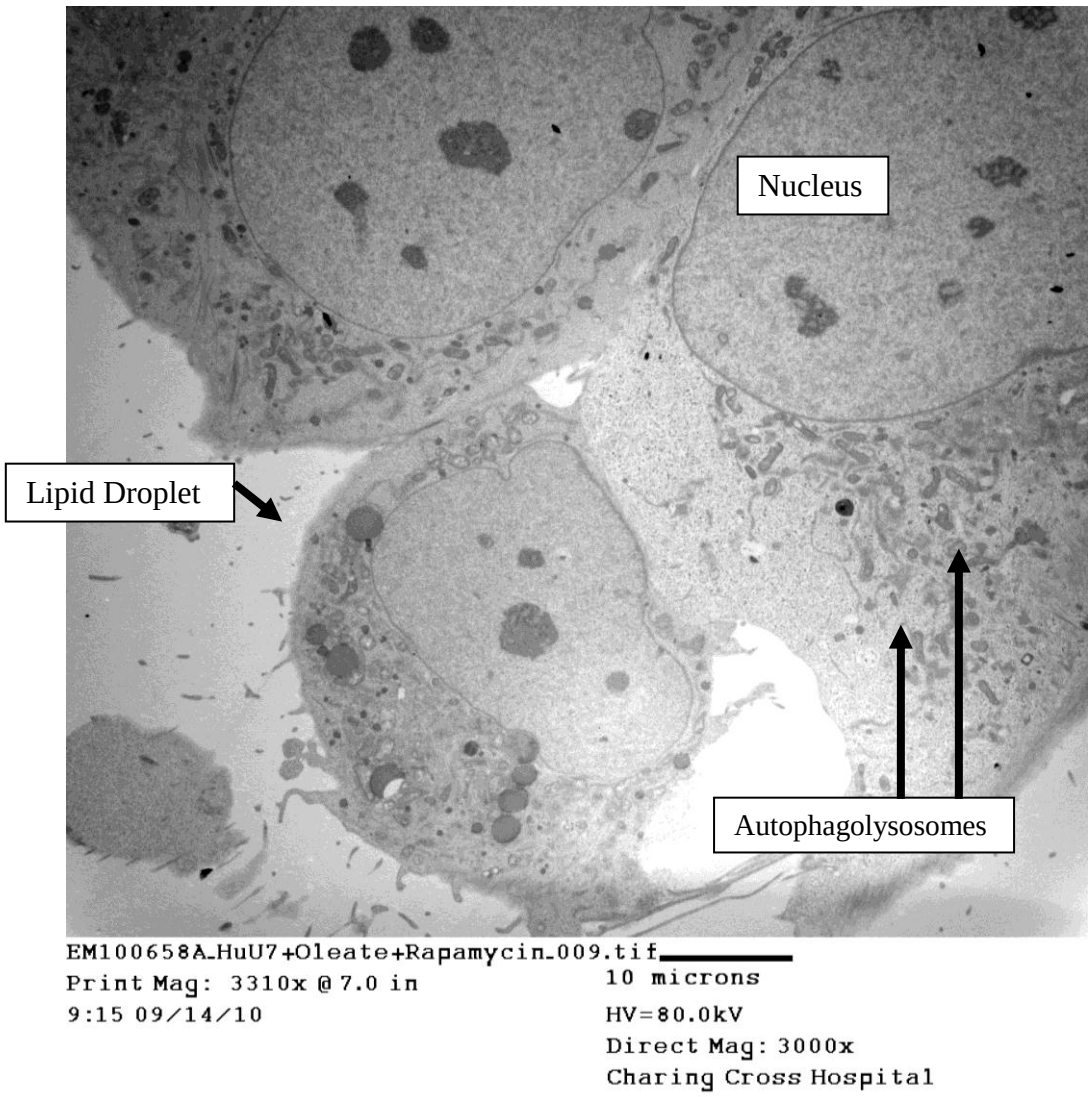


Figure 52. Electron microscopy photomicrograph from an HUH7 cell grown in Oleate DMEM with Rapamycin, original magnification x3000.

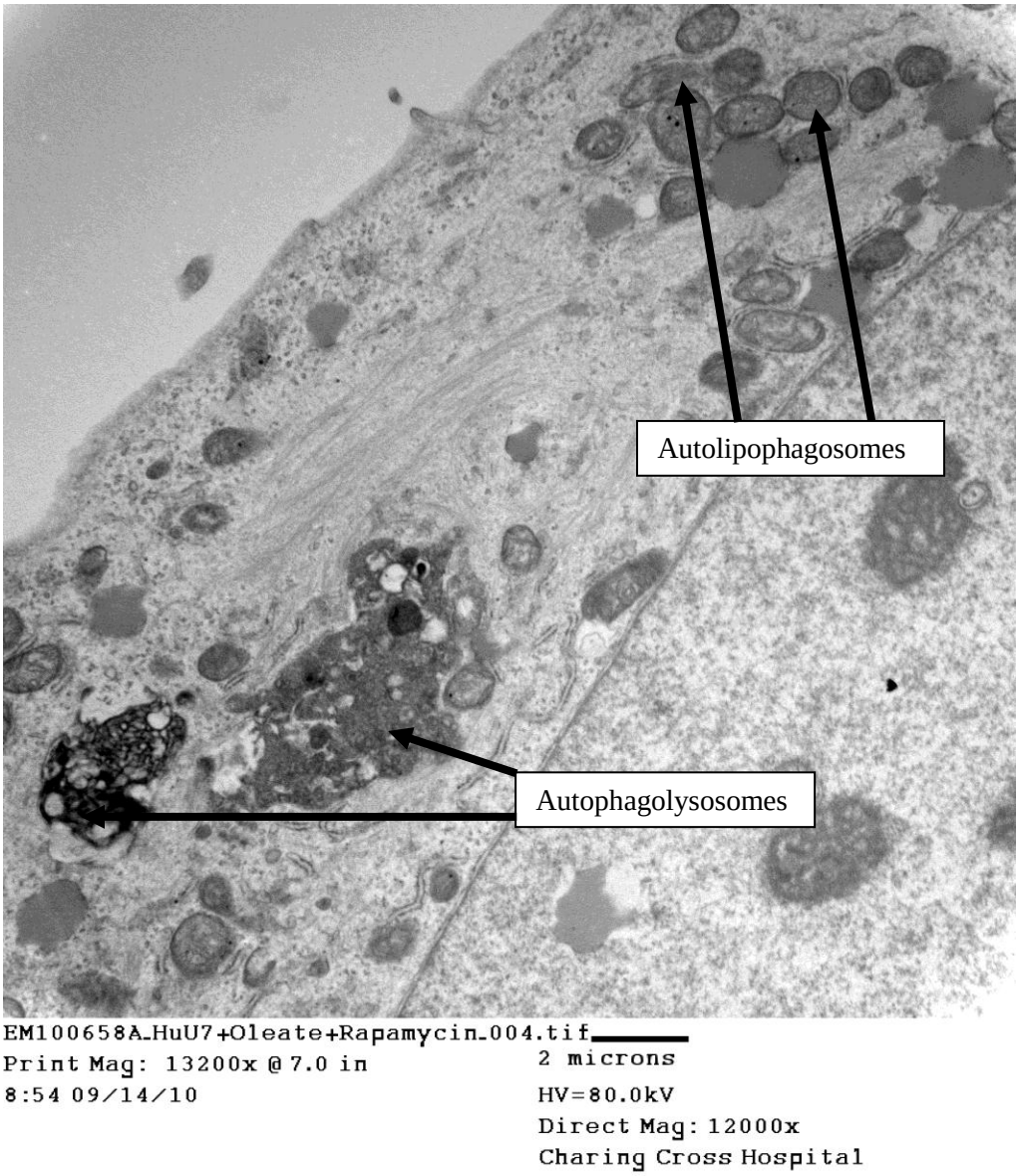


Figure 53. Electron microscopy photomicrograph from an HUH7 cell grown in Oleate DMEM with Rapamycin, original magnification x12000.

The images from HUH7 cells grown in Oleate DMEM with Rapamycin show decreased lipid droplets and increased numbers of autolipophagosomes and autophagolysosomes in comparison to the cells grown in Oleate DMEM without Rapamycin. The

autophagolysosomes in areas are larger and have a more irregular outline such as in **Figure 53.**

4.4.3. Oil Red-O digital image analysis

Representative images from the ORO stained HUH7 cells are shown in **Figure 54** which demonstrate red staining of steatosis within HUH7 cells grown in normal DMEM ± Rapamycin and Oleate DMEM ± Rapamycin.

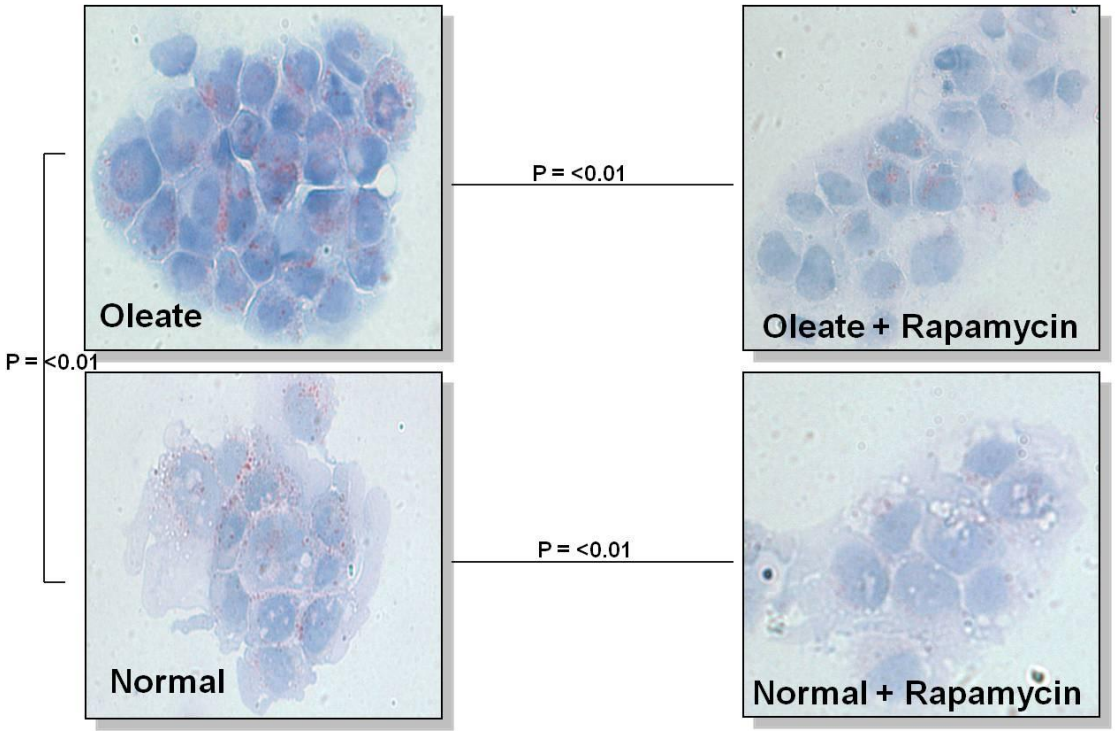


Figure 54. Oil Red-O staining in HUH7 cells grown in Oleate DMEM or Normal DMEM ± Rapamycin.

Table 29 and **Figure 55** show the mean percentage steatosis ± SEM using ORO DIA for each experimental group.

	Oleate	Oleate Rapamycin	DMEM	DMEM Rapamycin
Mean Percentage Steatosis ± SEM	16.79 ± 0.94	6.93 ± 0.69	11.99 ± 0.61	8.27 ± 0.44

Table 29. Oil Red-O digital image analysis mean percentage steatosis ± SEM in HUH7 cells grown in Oleate DMEM ± Rapamycin or DMEM ± Rapamycin.

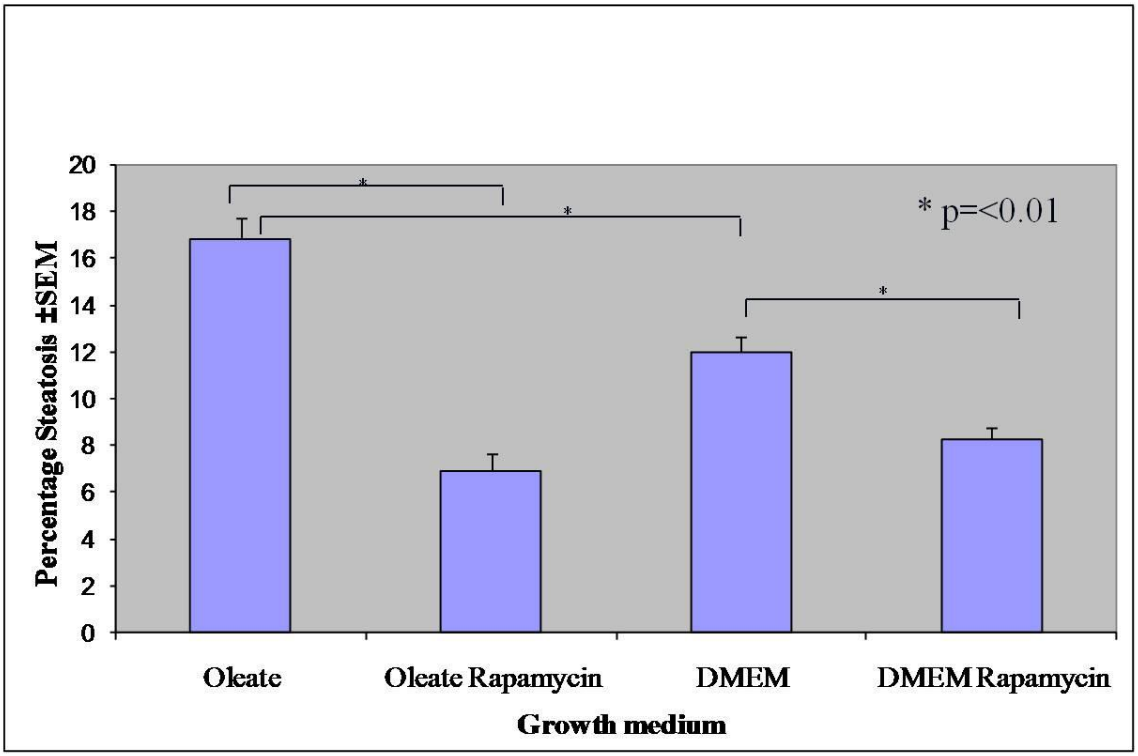


Figure 55. Oil Red-O digital image analysis mean percentage steatosis ± SEM in HUH7 cells grown in Oleate DMEM ± Rapamycin or DMEM ± Rapamycin.

ORO staining identified significantly more steatosis in the cells grown in Oleate DMEM, 16.79 ± 0.94%, compared to DMEM, 11.99 ± 0.61%, ($p<0.01$) and significantly less steatosis in the cells grown with Oleate Rapamycin or DMEM Rapamycin, (both $p<0.01$).

4.4.4 Triglyceride assay analysis

Table 30 and **Figure 56** show the mean triglyceride concentration (nmol per well) ± SEM for HUH7 cells grown in DMEM ± Rapamycin and Oleate DMEM ± Rapamycin.

	Oleate	**Oleate Rapamycin**	**DMEM**	**DMEM Rapamycin**
Mean triglyceride concentration ± SEM (nmol per well)	3.71 ± 0.15	1.96 ± 0.11	2.79 ± 0.11	2.33 ± 0.08

Table 30. Mean triglyceride concentration (nmol per well) ± SEM for HUH7 cells grown in Oleate DMEM ± Rapamycin or DMEM ± Rapamycin.

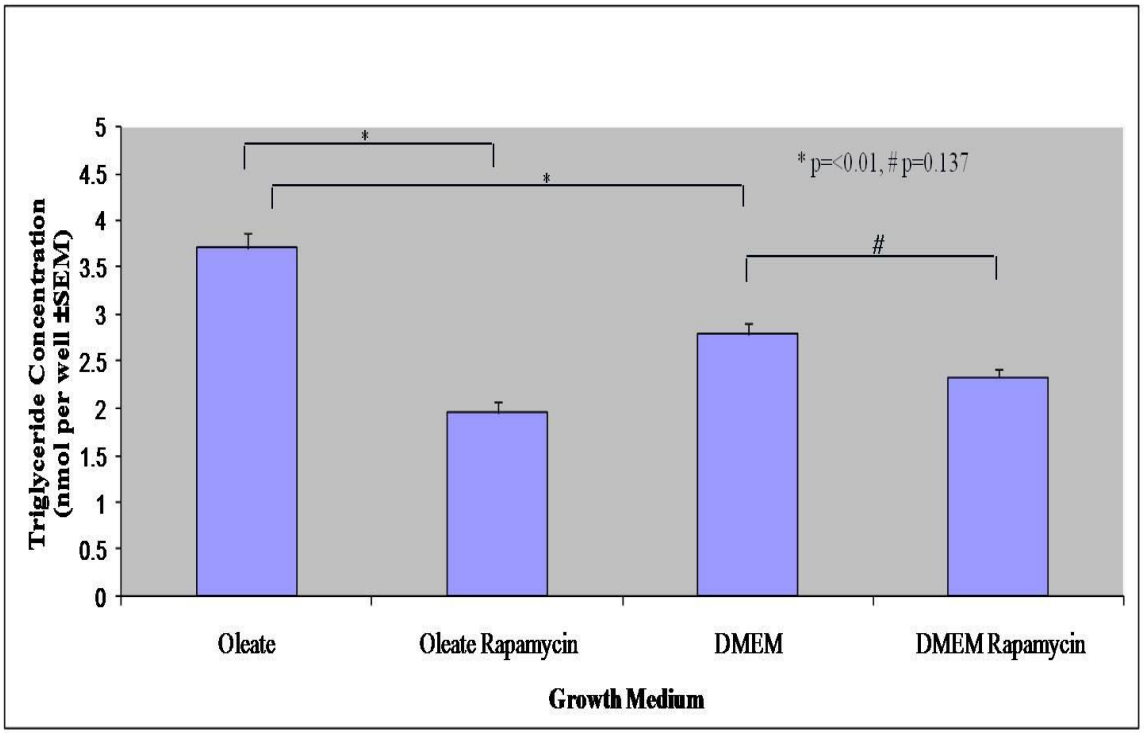


Figure 56. Mean triglyceride concentration (nmol per well) ± SEM for HUH7 cells grown in Oleate DMEM ± Rapamycin or DMEM ± Rapamycin.

The triglyceride assay identified significantly more triglyceride in the cells grown in Oleate DMEM, 3.71 ± 0.15nmol per well, compared to DMEM, 2.79 ± 0.11nmol per well, ($p<0.01$). There was significantly less triglyceride in the cells grown in Oleate DMEM with Rapamycin, 1.96 ± 0.11nmol per well, compared to without Rapamycin, 3.71 ± 0.15nmol per well, ($p<0.01$). Although there was less triglyceride in the cells grown in DMEM with Rapamycin, 2.33 ± 0.08 nmol per well, compared to without Rapamycin, 2.79 ± 0.11nmol per well, this did not reach statistical significance, ($p=0.137$).

The triglyceride results correlated well with the ORO DIA steatosis measurement within the HUH7 cells, Pearson correlation R=0.995, p<0.01.

4.4.5. Fluorescence activated cell sorting analysis

Table 36 shows the percentage of viable, early apoptotic, late apoptotic and necrotic cells and the intracellular ROS levels (median fluorescence intensity) in HUH7 cells grown in Oleate DMEM ± Rapamycin or DMEM ± Rapamycin.

	Oleate	**Oleate Rapamycin**	**DMEM**	**DMEM Rapamycin**
Early Apoptotic Cells (%)	1.52±0.17#	0.83±0.11#	3.69±0.45¬	3.94±0.45¬
Late Apoptotic Cells (%)	2.73±0.36~	0.61±0.12~	1.67±0.19^	1.19±0.12^
Necrotic Cells (%)	10.82±0.78*	5.65±0.13*	6.06±0.27”	7.96±0.88”
Viable Cells (%)	84.93±0.99	92.90±1.15	88.58±1.34	86.91±1.89
Intracellular ROS Levels (median fluorescence intensity)	27.74	26.76	26.76	25.81

Table 31. The percentage of viable, early apoptotic, late apoptotic and necrotic cells and the intracellular ROS levels (median fluorescence intensity) in HUH7 cells grown in Oleate DMEM ± Rapamycin or DMEM ± Rapamycin. (#,~,* p<0.05; ¬,^,” p>0.05).

Statistical analysis was not possible on the intracellular ROS levels as only one median fluorescence intensity result was obtained per experiment, so although based on multiple readings from different cells, the results were not suitable for statistical analysis.

Figures 57-60 are contour diagrams showing the FACS results from the AV and PI experiments demonstrating the percentage viable, early apoptotic, late apoptotic and necrotic HUH7 cells grown in Oleate DMEM ± Rapamycin or DMEM ± Rapamycin. The lower left quadrant of the diagram represents the viable cells (AV−/PI−), the upper right quadrant represents the late apoptotic cells (AV+/PI+), the lower right quadrant represents early apoptotic cells (AV+/PI−) and necrotic cells are in the upper left quadrant (AV−/PI+).

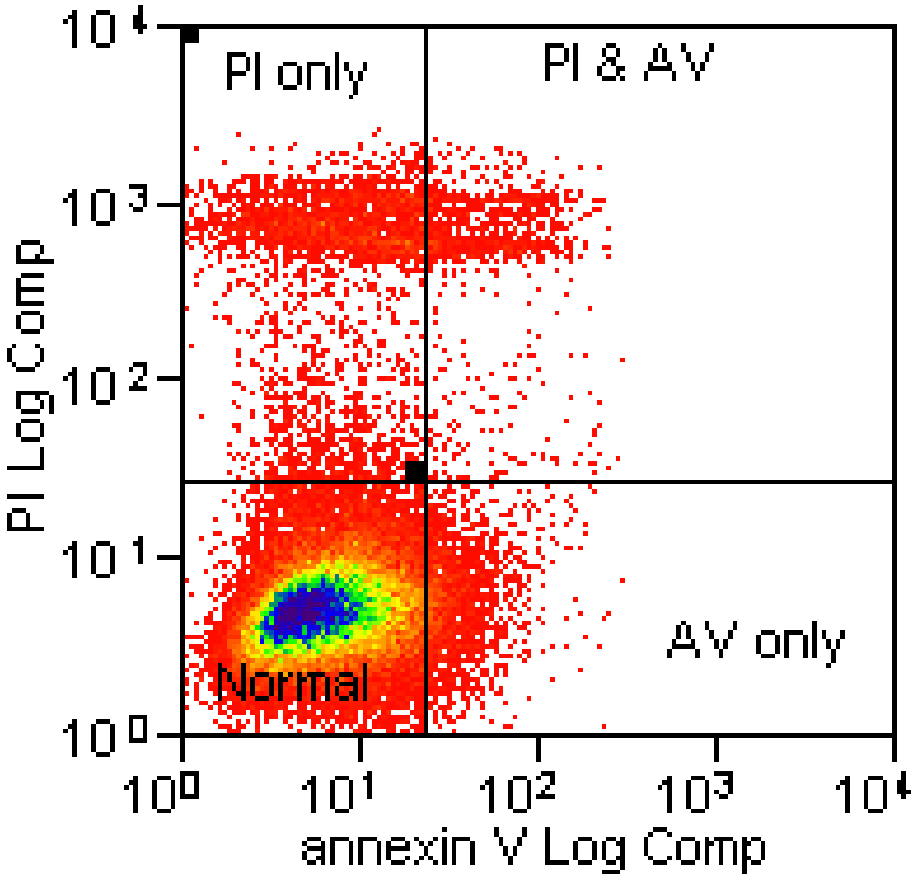


Figure 57. A contour diagram of AV/PI obtained by flow cytometry of HUH7 cells grown in DMEM only. AV fluorescence is presented on the horizontal axis and PI fluorescence on the vertical axis.

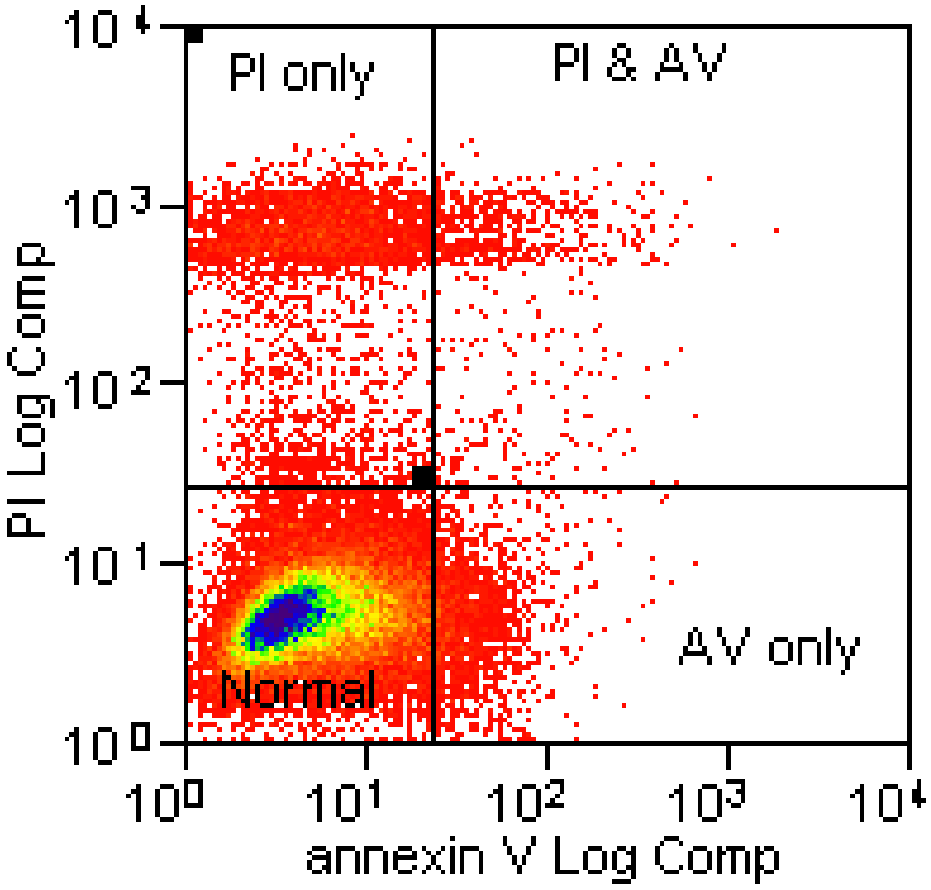


Figure 58. A contour diagram of AV/PI obtained by flow cytometry of HUH7 cells grown in DMEM with Rapamycin. AV fluorescence is presented on the horizontal axis and PI fluorescence on the vertical axis.

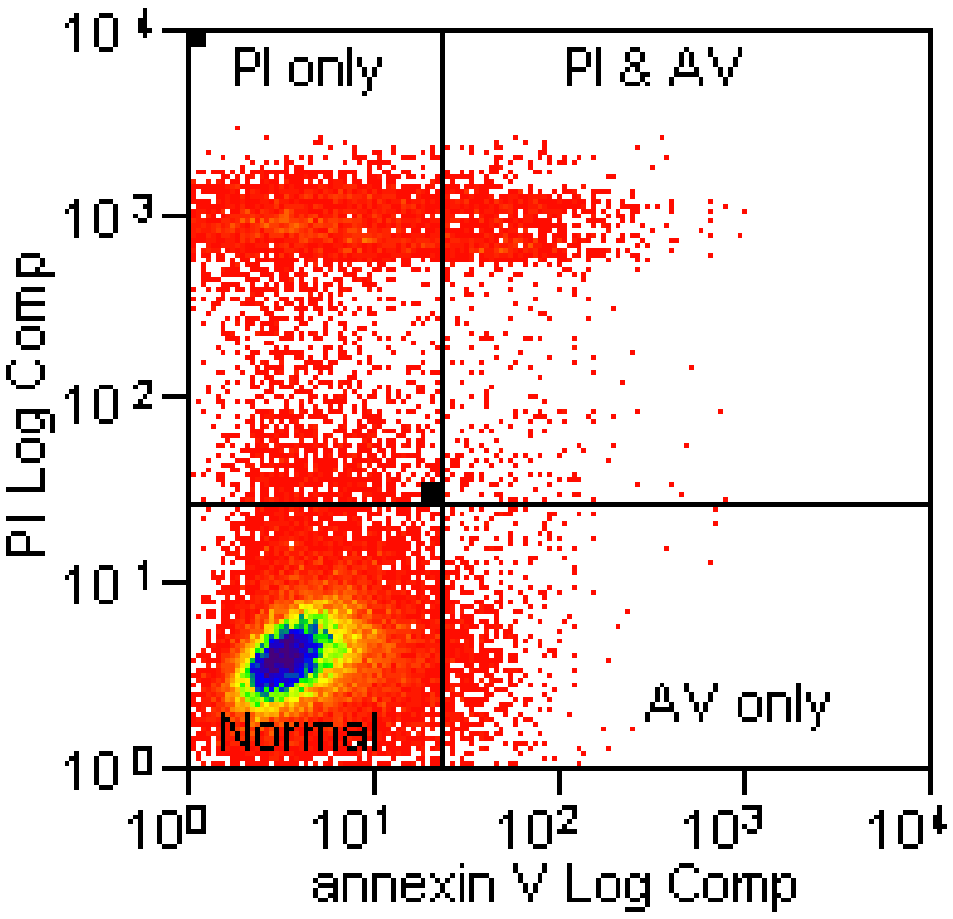


Figure 59. A contour diagram of AV/PI obtained by flow cytometry of HUH7 cells grown in an oleate DMEM only. AV fluorescence is presented on the horizontal axis and PI fluorescence on the vertical axis.

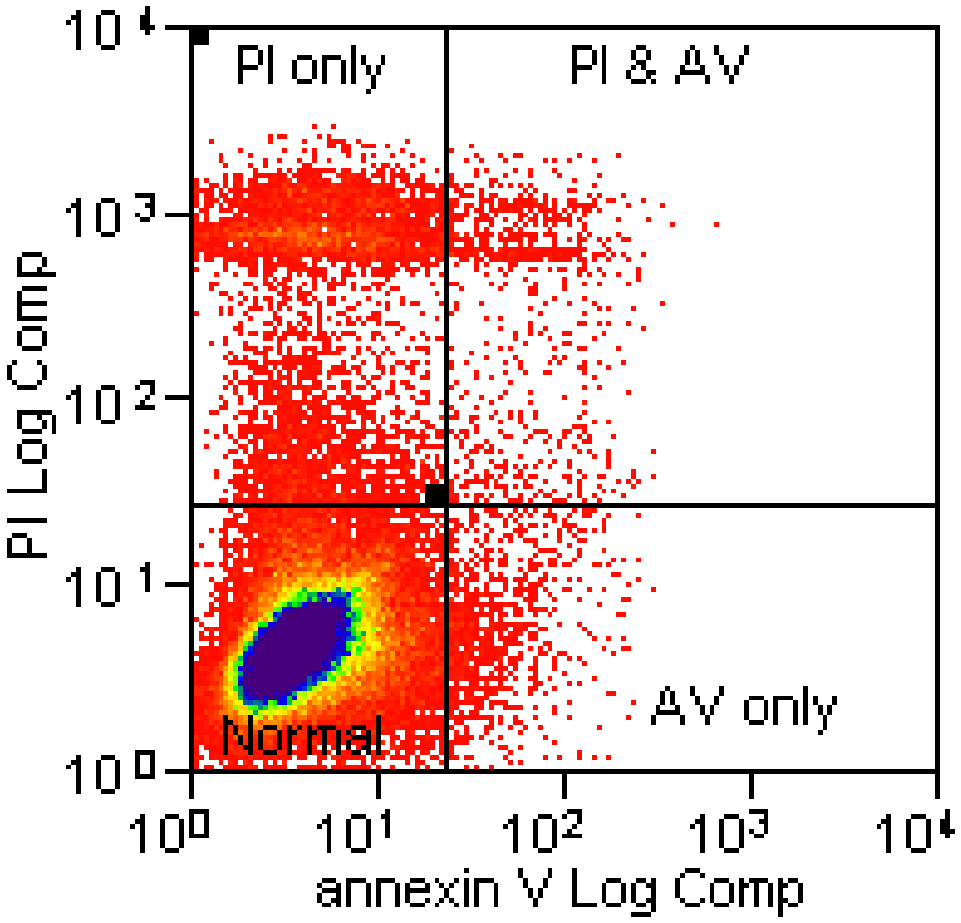


Figure 60. A contour diagram of AV/PI obtained by flow cytometry of HUH7 cells grown in an oleate DMEM with Rapamycin. AV fluorescence is presented on the horizontal axis and PI fluorescence on the vertical axis.

Figures 61-64 are the contour diagrams showing the FACS results from the carboxy-H2DFFDA experiments demonstrating the intracellular ROS levels (median fluorescence intensity).

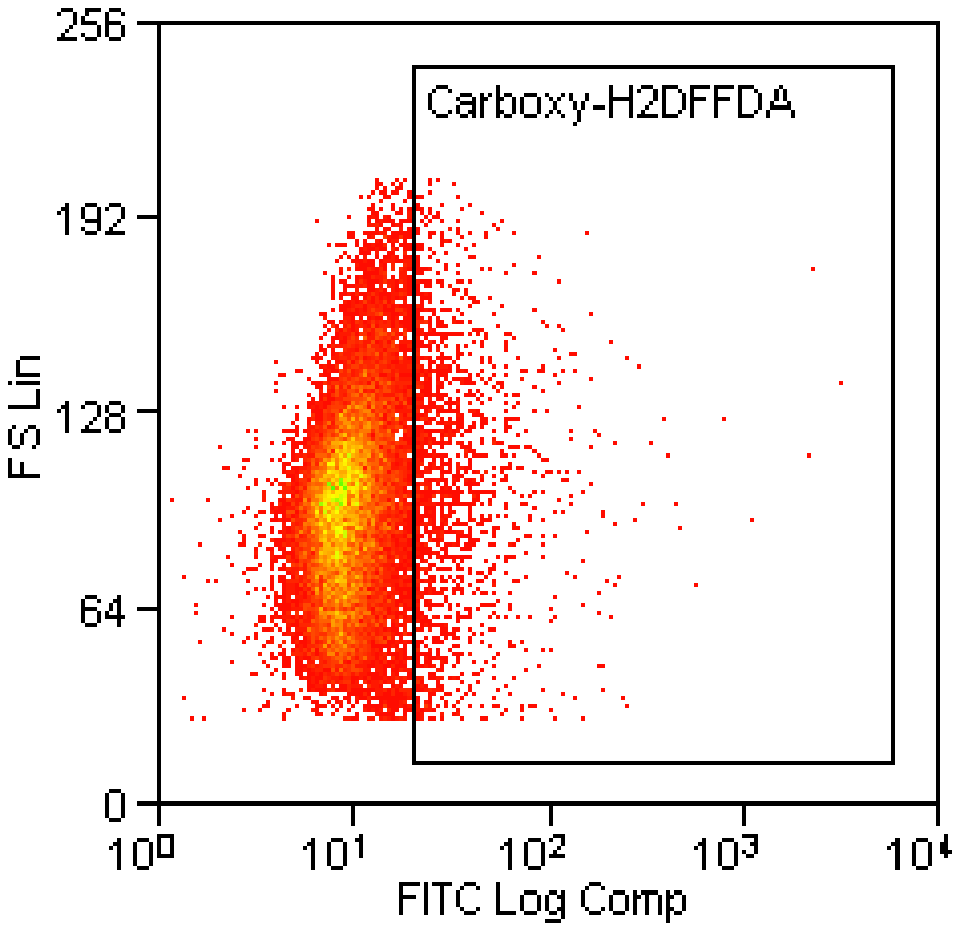


Figure 61. A contour diagram of carboxy-H2DFFDA obtained by flow cytometry of HUH7 cells grown in DMEM only. FITC fluorescence is presented on the horizontal axis and forward scatter on the vertical axis.

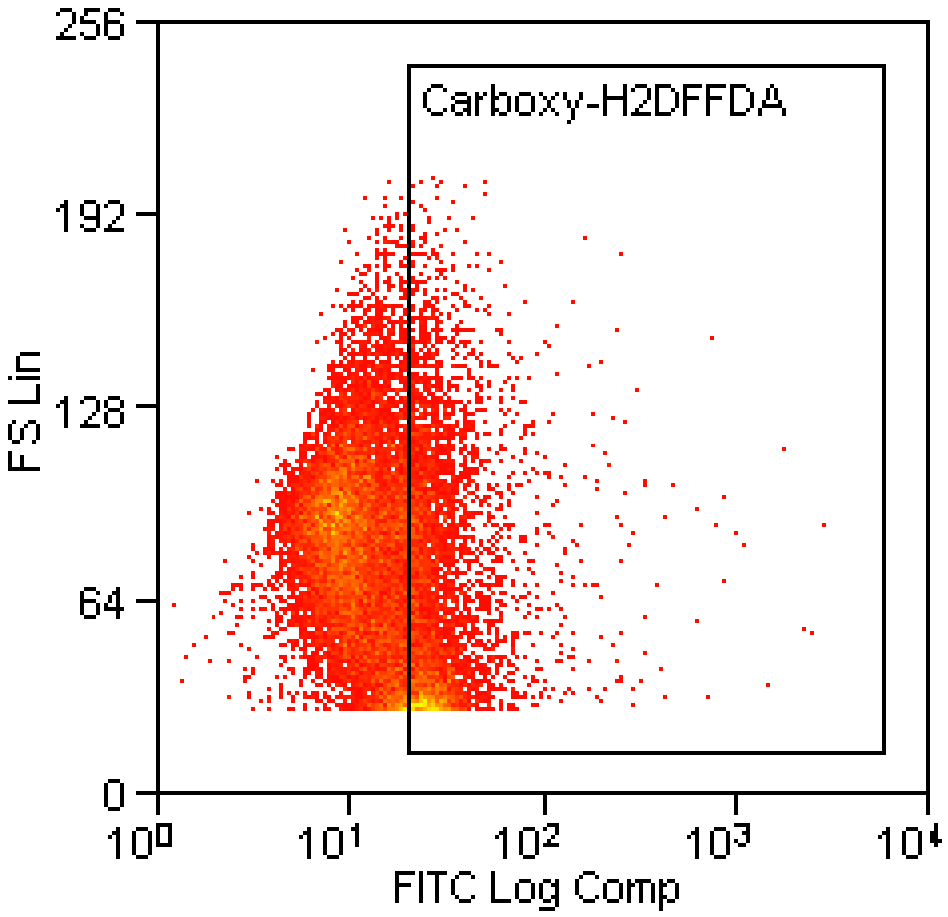


Figure 62. A contour diagram of carboxy-H2DFFDA obtained by flow cytometry of HUH7 cells grown in DMEM with Rapamycin. FITC fluorescence is presented on the horizontal axis and forward scatter on the vertical axis.

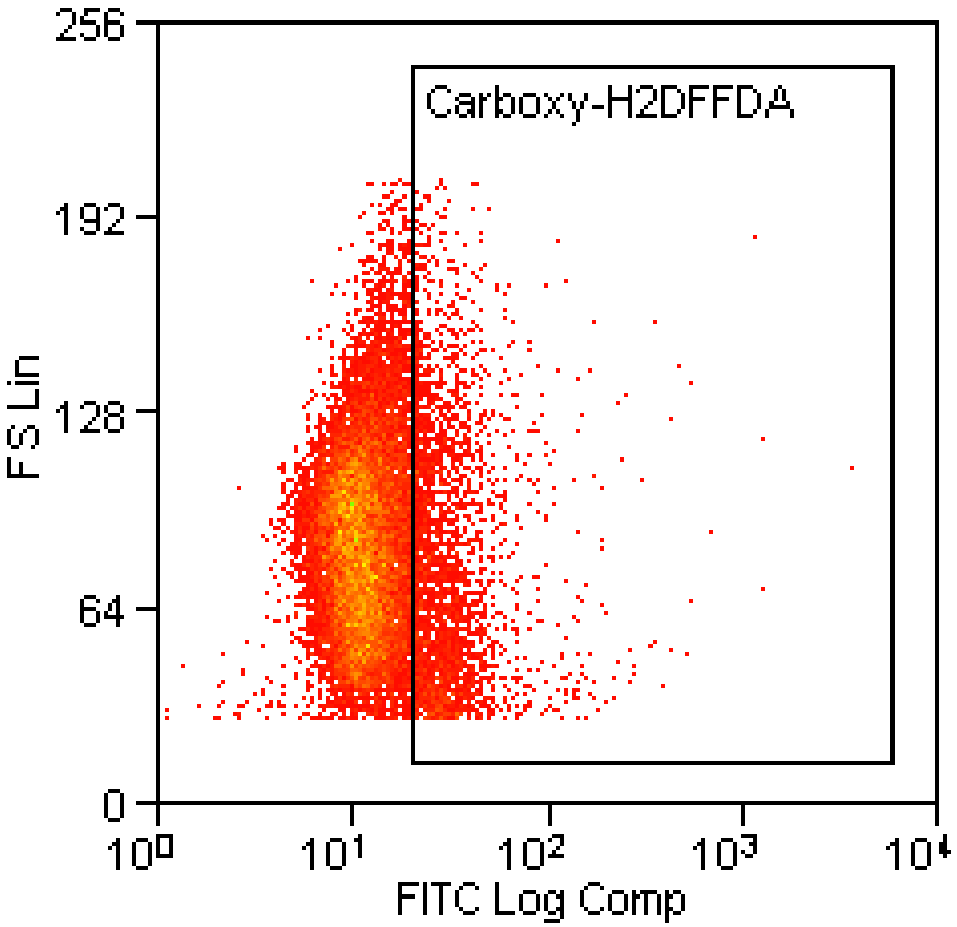


Figure 63. A contour diagram of carboxy-H2DFFDA obtained by flow cytometry of HUH7 cells grown in an Oleate DMEM only. FITC fluorescence is presented on the horizontal axis and forward scatter on the vertical axis.

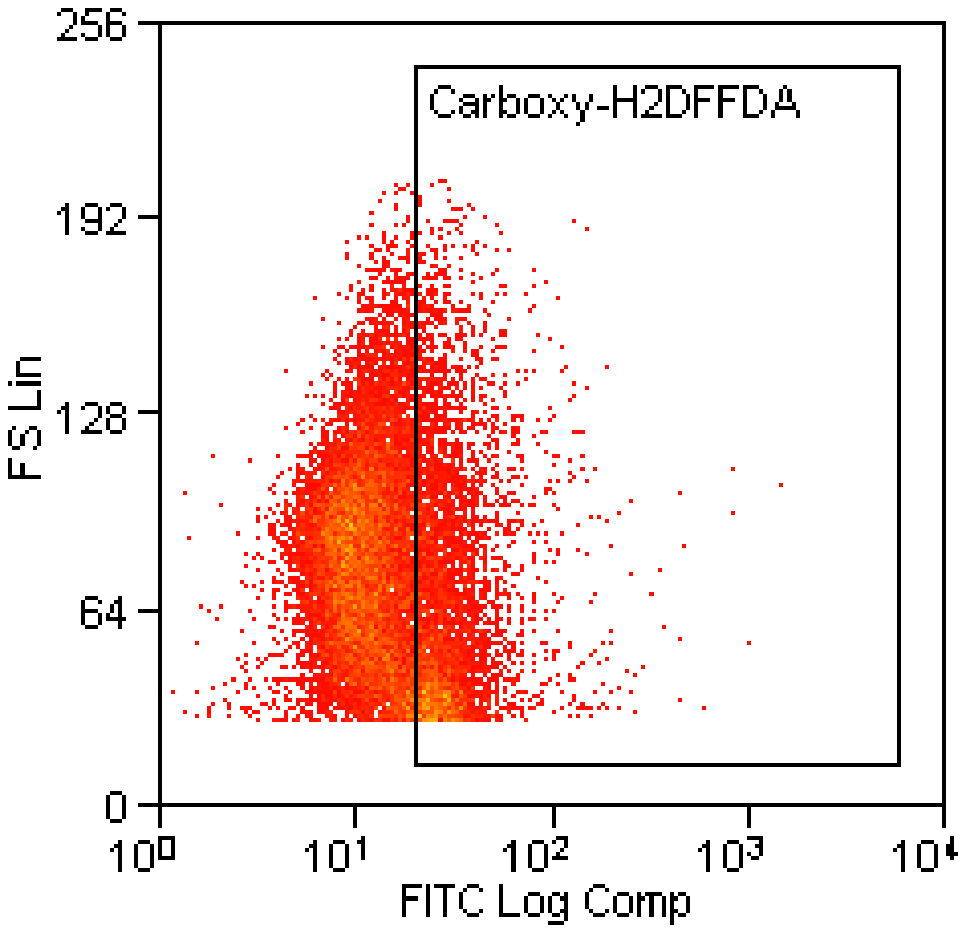


Figure 64. A contour diagram of carboxy-H2DFFDA obtained by flow cytometry of HUH7 cells grown in an Oleate DMEM with Rapamycin. FITC fluorescence is presented on the horizontal axis and forward scatter on the vertical axis.

The FACS results demonstrate that there is significantly increased necrosis (10.82±0.78 vs. 6.06±0.27%; $p<0.05$), late apoptosis (2.73±0.36 vs. 1.67±0.19%; $p<0.05$) and intracellular ROS (27.74 vs. 26.76 median fluorescence intensity) in HUH7 cells grown in an Oleate DMEM compared to those grown in DMEM.

On addition of Rapamycin to the Oleate DMEM there is significantly decreased necrosis (10.82±0.78 vs. 5.65±0.13%; $p<0.05$), late apoptosis (2.73±0.36 vs. 0.61±0.12%; $p<0.05$) and intracellular ROS (27.74 vs. 26.76 median fluorescence intensity). However, in normal DMEM the addition of Rapamycin only led to a decrease in intracellular ROS (26.76 vs. 25.81) and minimal non-significant decrease in late apoptotic cells (1.67±0.19 vs. 1.19±0.12%; $p>0.05$), the necrotic cells showed a non-significant slight increase (6.06±0.27 vs. 7.96±0.88%; $p>0.05$).

4.5. Discussion

This study has shown that HUH7 cells grown in an Oleate DMEM have increased amounts of lipid compared to those grown in normal DMEM as shown by ORO DIA, triglyceride assay and electron microscopy. There was a strong correlation between the ORO DIA and triglyceride assay results confirming the earlier work done in Chapter 2 on tissue samples. This shows that in cell culture work as well as tissue samples the two methods produce results that correlate well with each other and either method could be used in future work. Confocal immunofluorescence showed similar results but they were not statistically significant which may be due to the number of cells examined.

The addition of Rapamycin to Oleate DMEM and normal DMEM led to increased autophagocytosis in HUH7 cells as shown by the increased co-localisation of lysosomes and lipid droplets by confocal immunofluorescence and the increase in autolipophagosomes and autophagolysosomes seen with electron microscopy. The increased macroautophagy causes triglyceride hydrolysis to free fatty acids within

lysosomes.[125] This is likely to have led to the decreased number of lipid droplets seen in HUH7 cells in both Oleate DMEM and normal DMEM with Rapamycin on electron microscopy and ORO DIA. As the triglycerides are hydrolysed to free fatty acids in macroautophagy one would expect the triglyceride concentration in the HUH7 cells to decrease with the addition of Rapamycin to the Oleate DMEM or normal DMEM which is what the triglyceride assay showed.

Similar results were seen in a study in cultured hepatocytes and a mouse model of acute alcohol disease which showed that autophagy protects against liver injury from alcohol.[126] There were increased autolipophagosomes which suggests that the liver may selectively limit lipid accumulation. When autophagy was inhibited there was increased hepatocyte injury suggesting autophagy protects cell from injury. Rapamycin reduced alcohol induced lipid accumulation, which is also shown in the work in this thesis for diet induced lipid accumulation. Inhibition of autophagy worsened steatosis, showing that autophagy regulates hepatic lipid content.

The incidence of the metabolic syndrome, and accompanying NAFLD, increases with age, in parallel with a decrease in autophagy function.[127, 128] Variation in genes that regulate autophagy function or an overall decrease in autophagy, which occurs with increasing age, might in part underlie the pathogenesis of liver steatosis.

One of the features of the metabolic syndrome is hyperinsulinaemia, this could compound the defect in autophagy induced by increasing age. The ability of insulin to

suppress autophagy is retained despite the presence of insulin resistance in liver differentiated cells or mouse liver, indicating that hyperinsulinaemia might contribute to impaired autophagy in the obese state.[129] Interestingly, a decrease in autophagy might impair hepatic insulin signalling. Restoration of autophagy that was decreased in the livers of obese mice increased insulin sensitivity within the liver.[130] These observations suggest that a self-perpetuating cycle might exist within the liver in the metabolic syndrome where insulin resistance impairs autophagy, which then in combination with obesity worsens hepatic steatosis and insulin resistance which further impairs autophagy. This decrease in autophagy within the liver may in part explain physiologic changes that lead to the clinical manifestations of the metabolic syndrome.

The FACS results demonstrate that when HUH7 cells have increased amounts of lipid after being grown in an oleate DMEM there is an increase in necrosis, late apoptosis and intracellular ROS compared to cells with normal amounts of lipid grown in normal DMEM. This is consistent with triglycerides and lipid droplets having a role in increased lipid peroxidation and ROS production which subsequently causes increased DNA damage, apoptosis and necrosis.[118]

If macroautophagy is stimulated by Rapamycin in the HUH7 cells with increased lipids grown in an Oleate DMEM there is a decrease in necrosis, apoptosis and intracellular ROS as shown by the FACS results. This could be consistent with decreased ROS causing less death of HUH7 cells by necrosis or apoptosis. Another possibility is with

Rapamycin increasing macroautophagy the increased supply of free fatty acids may help to maintain cellular levels of ATP which would decrease cell death.

The decrease in ROS is consistent with a decrease in triglycerides and lipid droplets leading to decreased lipid peroxidation and ROS production.[118] One may not have expected this with the increased free fatty acids produced by the lysosomes undergoing beta or omega oxidation within the cells which would normally produce glucose and be associated with ROS formation.[30] However, the decrease in lipid droplets present causing decreased lipid peroxidation and ROS production is likely to be greater than the amount of ROS produced during free fatty acid oxidation. Another possibility is that the free fatty acids produced by macroautophagy may not be involved in oxidation, for example they could be exported from the cell and therefore the decreased lipid burden within the cell and therefore lipid peroxidation could causes a decrease in ROS levels in comparison to cells with less autophagocytosis which have increased lipids within the cell. The decrease in ROS levels could also be due to another effect of autophagocytosis independent of fat metabolism. Rapamycin also affects other cellular pathways in addition to autophagy because mTOR regulates many cellular pathways so the decreased ROS could be due to an effect on a pathway independent of autophagy. The exact mechanism for the decrease in ROS is unclear.

The decreased apoptosis and necrosis seen in the cells grown in the Oleate DMEM with Rapamycin, with stimulation of autophagocytosis was not seen in cells grown in a normal DMEM even though there was a decrease in intracellular ROS. The reason for there

being no decrease in necrosis and apoptosis with autophagocytosis stimulation in cells grown in a normal DMEM could be because there is little excess fat in these cells and therefore stimulating autophagocytosis will not decrease the lipid burden as much in these cells. ORO DIA and triglyceride assay both showed a smaller decrease in lipid burden with Rapamycin addition in cells grown in normal DMEM compared to those grown in oleate DMEM. Another possible explanation for there being no decrease in necrosis and apoptosis in the cells grown in normal DMEM with autophagocytosis stimulation may be that this is the basal level of turnover seen in cells and not related to the amount of fat within the cell.

The exact role of autophagy in cell death is unclear in the literature, in certain situations it can cause cell death; however, it has also been shown to have survival effects after stresses that would normally induce cell death.[119-121] Some components of autophagy are directly involved in apoptosis which further complicates the role of autophagy in cell death.[131]

One of the situations where autophagy may mediate cell death is when autophagy is overactivated. This may explain why the HUH7 cells grown in DMEM with Rapamycin show a slight increase in cell death compared to HUH7 cells in DMEM with no Rapamycin. A possible explanation why this does not occur in the HUH7 cells in Oleate DMEM may be because there are more lipid droplets in the cells, the increase in autophagy caused by Rapamycin is able to supply lipid droplets and subsequently free fatty acids for energy in the cells rather than mediate cell death.

These results suggest that autophagocytosis is a pathway which could be activated by human hepatocytes to deal with increased lipids such as triglycerides which are a large component of the metabolic syndrome and NAFLD.[68] It could also potentially improve insulin sensitivity another component of the metabolic syndrome. The results also suggest that autophagy may limit hepatocyte cell death when there are increased lipids present by one of two methods either alone or in combination. Firstly, by reducing levels of intracellular lipids and ROS that promote cellular injury and secondly, by having a direct inhibitory effect on cell death pathways.

Cell culture models do not reflect the complicated pathophysiology of NAFLD but these results raise the possibility that autophagocytosis could prevent the development of NAFLD and potentially provide a therapeutic target for NAFLD patients in the future. If people have genetic variation in their ability to activate autophagocytosis and deal with increased lipids it could also explain why some patients develop NAFLD and others do not despite similar lifestyles and risk factors.

Chapter 5.

Overall Conclusions

In the studies undertaken, current clinical methods and a novel technique for assessing NAFLD have been investigated along with the role of autophagocytosis in NAFLD.

The data in Chapter 2 has shown that ORO DIA is the most accurate way of assessing steatosis within the liver of mouse models and human liver biopsies. Importantly for clinical practice, ORO DIA is more accurate than MRI measurements of liver steatosis. The increased accuracy of steatosis measurement and the additional information regarding lipid droplet size and the zonation of steatosis should encourage the use of ORO DIA in all mouse models of NAFLD. ORO DIA should also have a role in clinical trials of NAFLD treatments where changes in steatosis are anticipated.

As described in Chapters 1, 2 and 3, the diagnosis of NASH is usually made or at least confirmed by liver biopsy in conjunction with a NAS of ≥5. The use of multi-excitation fluorescence spectroscopy as an alternative diagnostic tool in NAFLD via an optical probe was shown to work well in livers from mouse models of NAFLD and also worked in the small number of liver biopsies examined. The tool is unlikely to replace liver biopsies for routine NAFLD diagnosis and assessment but in the future but does have the potential for real-time diagnosis of NAFLD in the transplant and bariatric surgery settings where it could change the future management of patients. Such studies are currently being planned.

Chapter 4 has shown that stimulating autophagocytosis within cultured liver differentiated cells with increased steatosis leads to decreased steatosis, necrosis, apoptosis and intracellular ROS. Although these results are based on cell culture work they do raise the possibility of a future therapeutic target for NAFLD.

5.1. Future work

Steatosis quantification using ORO DIA needs further work in human liver biopsies to increase the number of samples studied and confirm the results seen in this work. It would be interesting to look at the potential reasons for the increase in macrovesicular steatosis seen in zones 2 and 3 in the HFD/fructose mouse model of NAFLD as in humans steatosis often starts in zone 3. Possible reasons could include fat being metabolised first in zone 1 where there is increased blood flow and oxygen.

In the multi-excitation fluorescence spectroscopy study, it would be useful to measure Vitamin A and NAD(P)H levels in the liver tissue using high performance liquid chromatography. This would confirm the photobleaching data that the probe is measuring changes in the level of specific fluorophores. After further work in human liver biopsies confirming the data presented in this study, the probe should be trialled in bariatric surgery patients and pilot studies are currently being planned. This would allow the use of the probe in a patient population with an increased incidence of NAFLD who were already undergoing a surgical procedure. This would help further refine the probe and ensure its suitability for further clinical use in this setting and also the transplant setting.

The autophagocytosis study has the potential to lead to many different future areas of work. For example, the information regarding ROS production and autophagocytosis could be expanded to look at where in the autophagocytosis/fat metabolism pathway ROS are produced and which ROS are produced.

It would be interesting to look at the effects of stimulating/inhibiting autophagocytosis in different mouse models of NAFLD to see if the cell culture results are replicated. As well as using Rapamycin it would be useful to try and develop more specific autophagocytosis activators as mTOR has many roles within cells beyond autophagocytosis. This would enable future drug trials into the effect of increasing autophagy in NAFLD and in other manifestations of the metabolic syndrome, initially in animal models and, if successful, in patients.

Chapter 6.

Publications & Presentations Derived from the Thesis

6.1. Original research papers & review articles

- **Levene A.P.,** Kudo H., Armstrong M.J., Gedroyc W., Thursz M.R., Anstee Q.M., Goldin R.D. Quantifying Hepatic Steatosis - More Than Meets The Eye. (Histopathology. Accepted for publication July 2011. Online early view, DOI: 10.1111/j.1365-2559.2012.04193.x)

- **Levene A.P.,** Goldin R.D. The Epidemiology, Pathogenesis and Histopathology of Fatty Liver Disease. (Histopathology. Accepted for publication January 2011. Online early view, DOI: 10.1111/j.1365-2559.2011.04145.x)

- Sauvage V.R., **Levene A.P.,** Nguyen H.T., Kudo H., Wood T., Concas D., Thomas H., Thursz M., Goldin R.D., Anstee Q.M., Elson D. Multi-Excitation Fluorescence Spectroscopy for Analysis of Non-Alcoholic Fatty Liver Disease. (Lasers in Surgery & Medicine, 2011;**43**: 392-400.)

- **Levene A.P.,** Kudo H., Thursz M.R., Anstee Q.M., Goldin R.D. Is Oil Red-O and Digital Image Analysis the Gold Standard for Quantifying Steatosis in the Liver? (Hepatology, 2010;**51**(5): 1859-1860.)

- Anstee Q.M., Concass D., Kudo H., **Levene A.,** et al. Impact of Pan-Caspase Inhibition in Animal Models of Established Steatosis and Non-Alcoholic Steatohepatitis. (Journal of Hepatology, 2010;**53**:542-550.)

6.2. Published abstracts

- **Levene A.P.,** Kudo H., Thursz M., Anstee Q.M., Goldin R.D. Activating Autophagocytosis Decreases Fat Within the Liver. (The Journal of Pathology, 2011;**224** (S1): 4.)
- **Levene A.P.,** Anstee Q.M., Kudo H., Ladva S., Thanh Hoa N., Sauvage V., Concas D., Thursz M.R., Elson D.S., Goldin R.D. Autofluorescence Spectroscopy – Developing a Tool for the Assessment of Steatohepatitis in the Liver. (The Journal of Pathology, 2010**;220** (S1):11.)
- **Levene A.P.,** Kudo H., Thursz M.R., Anstee Q.M., Goldin R.D. Is Oil Red-O and Digital Image Analysis the Gold Standard for Quantifying Steatosis in the Liver? (Journal of Hepatology, 2010;**52** (S1):147-148.)

6.3. Oral presentations at conferences

- **Levene A.P.,** Kudo H., Thursz M., Anstee Q.M., Goldin R.D. Activating Autophagocytosis Decreases Fat Within the Liver.

  Plenary oral presentation: Pathological Society of Great Britain & Ireland 199th Meeting, January 2011, Cambridge, UK.
- **Levene A.P.**, Kudo H., Thursz M.R., Anstee Q.M., Goldin R.D. Is Oil Red-O and Digital Image Analysis the Gold Standard for Quantifying Steatosis in the Liver?

1st Prize oral presentation: The School of Pathology Inaugural Trainee Conference, March 2010, London, UK.

6.4. Poster presentations at conferences

- **Levene A.P.**, Kudo H., Thursz M.R., Anstee Q.M., Goldin R.D. Is Oil Red-O and Digital Image Analysis the Gold Standard for Quantifying Steatosis in the Liver?

  45th Annual Meeting European Association for the Study of the Liver, April 2010, Vienna, Austria.

- **Levene A.P.,** Anstee Q.M., Kudo H., Ladva S., Thanh Hoa N., Sauvage V., Concas D., Thursz M.R., Elson D.S., Goldin R.D. Autofluorescence Spectroscopy – Developing a Tool for the Assessment of Steatohepatitis in the Liver.

  Pathological Society of Great Britain & Ireland 197th Meeting, January 2010, London, UK.

- Anstee Q.M., **Levene A.P.,** Thanh Hoa N., Sauvage V., Concas D., Thomas H., Thursz M.R., Elson D., Goldin R. Autofluorescence: modelling a tool for assessment of steatotic marginal grafts in liver transplantation.

  60th AGM American Association for the Study of Liver Diseases, November 2009, Boston, USA.

- Sauvage V., Nguyen H.T., **Levene A.P.**, Hill R., Concas D., Thursz M.R., Goldin R., Anstee Q.M. Multi-excitation fluorescence spectroscopy for analysis of non-alcoholic fatty liver disease.

  Biomedical Optics & Photonics AGM 2010, San Francisco, USA.

Acknowledgements

I would like to thank my wife, Danielle, for her continuous support throughout the many hours I have spent carrying out the work and then writing up my thesis. I would also like to acknowledge my newborn son Zane, who was born just before the viva, whose first smiles have encouraged me at the final stages.

My supervisor, Professor Robert Goldin, for his constant guidance, support and expert supervision throughout the project, his help went far beyond what one would expect from their supervisor.

Dr Quentin Anstee, for his help and thoughtful opinions, which have continued even after his move to Newcastle. Mrs Hiromi Kudo and the other scientists, who generously gave me their time and taught me the laboratory techniques I used in this project. Dr Vincent Sauvage & Dr Daniel Elson, for their help with the technical elements of the autofluorescence spectroscopy system. Mr Suresh Ladva for his help with the ORO staining at Imperial College Healthacre NHS Trust. Professor Wady Gedroyc, for his help with the MRI steatosis assessment at Imperial College Healthcare NHS Trust. Dr Jill Moss, for her help with the electron microscopy at Imperial College Healthcare NHS Trust. Professor Mark Thursz, for his useful comments regarding the work at our regular laboratory meetings.

References

1. Ratziu V, Bellentani S, Cortez-Pinto H, Day C, Marchesini G. A position statement on NAFLD/NASH based on the EASL 2009 special conference. *J Hepatol* 2010;**53**;372-384.
2. Gholam PM, Flancbaum L, Machan JT, Charney DA, Kotler DP. Nonalcoholic fatty liver disease in severely obese subjects. *Am J Gastroenterol* 2007;**102**;399-408.
3. Balkau B, Charles MA, Drivsholm T *et al.* Frequency of the WHO metabolic syndrome in European cohorts, and an alternative definition of an insulin resistance syndrome. *Diabetes & metabolism* 2002;**28**;364-376.
4. Adams LA, Lymp JF, St Sauver J *et al.* The natural history of nonalcoholic fatty liver disease: a population-based cohort study. *Gastroenterology* 2005;**129**;113-121.
5. Targher G, Bertolini L, Poli F *et al.* Nonalcoholic fatty liver disease and risk of future cardiovascular events among type 2 diabetic patients. *Diabetes* 2005;**54**;3541-3546.
6. Hamaguchi M, Kojima T, Takeda N *et al.* Nonalcoholic fatty liver disease is a novel predictor of cardiovascular disease. *World J Gastroenterol* 2007;**13**;1579-1584.
7. Wieckowska A, Feldstein AE. Diagnosis of nonalcoholic fatty liver disease: invasive versus noninvasive. *Semin Liver Dis* 2008;**28**;386-395.
8. Berasain C, Betes M, Panizo A *et al.* Pathological and virological findings in patients with persistent hypertransaminasaemia of unknown aetiology. *Gut* 2000;**47**;429-435.
9. Wanless IR, Lentz JS. Fatty liver hepatitis (steatohepatitis) and obesity: an autopsy study with analysis of risk factors. *Hepatology* 1990;**12**;1106-1110.
10. Bedogni G, Miglioli L, Masutti F, Tiribelli C, Marchesini G, Bellentani S. Prevalence of and risk factors for nonalcoholic fatty liver disease: the Dionysos nutrition and liver study. *Hepatology* 2005;**42**;44-52.
11. Browning JD, Szczepaniak LS, Dobbins R *et al.* Prevalence of hepatic steatosis in an urban population in the United States: impact of ethnicity. *Hepatology* 2004;**40**;1387-1395.
12. Ruhl CE, Everhart JE. Determinants of the association of overweight with elevated serum alanine aminotransferase activity in the United States. *Gastroenterology* 2003;**124**;71-79.
13. Lazo M, Clark JM. The epidemiology of nonalcoholic fatty liver disease: a global perspective. *Semin Liver Dis* 2008;**28**;339-350.
14. Skelly MM, James PD, Ryder SD. Findings on liver biopsy to investigate abnormal liver function tests in the absence of diagnostic serology. *J Hepatol* 2001;**35**;195-199.
15. Daniel S, Ben-Menachem T, Vasudevan G, Ma CK, Blumenkehl M. Prospective evaluation of unexplained chronic liver transaminase abnormalities in asymptomatic and symptomatic patients. *Am J Gastroenterol* 1999;**94**;3010-3014.
16. Ong JP, Younossi ZM. Epidemiology and natural history of NAFLD and NASH. *Clin Liver Dis* 2007;**11**;1-16, vii.
17. McCullough AJ. The clinical features, diagnosis and natural history of nonalcoholic fatty liver disease. *Clin Liver Dis* 2004;**8**;521-533, viii.

18. Ekstedt M, Franzen LE, Mathiesen UL *et al.* Long-term follow-up of patients with NAFLD and elevated liver enzymes. *Hepatology* 2006;**44**;865-873.
19. Bugianesi E, Leone N, Vanni E *et al.* Expanding the natural history of nonalcoholic steatohepatitis: from cryptogenic cirrhosis to hepatocellular carcinoma. *Gastroenterology* 2002;**123**;134-140.
20. Ratziu V, Bonyhay L, Di Martino V *et al.* Survival, liver failure, and hepatocellular carcinoma in obesity-related cryptogenic cirrhosis. *Hepatology* 2002;**35**;1485-1493.
21. Marrero JA, Fontana RJ, Su GL, Conjeevaram HS, Emick DM, Lok AS. NAFLD may be a common underlying liver disease in patients with hepatocellular carcinoma in the United States. *Hepatology* 2002;**36**;1349-1354.
22. Shimada M, Hashimoto E, Taniai M *et al.* Hepatocellular carcinoma in patients with non-alcoholic steatohepatitis. *J Hepatol* 2002;**37**;154-160.
23. Hanley AJ, Karter AJ, Festa A *et al.* Factor analysis of metabolic syndrome using directly measured insulin sensitivity: The Insulin Resistance Atherosclerosis Study. *Diabetes* 2002;**51**;2642-2647.
24. Bullock RE, Zaitoun AM, Aithal GP, Ryder SD, Beckingham IJ, Lobo DN. Association of non-alcoholic steatohepatitis without significant fibrosis with hepatocellular carcinoma. *J Hepatol* 2004;**41**;685-686.
25. Davila JA, Morgan RO, Shaib Y, McGlynn KA, El-Serag HB. Diabetes increases the risk of hepatocellular carcinoma in the United States: a population based case control study. *Gut* 2005;**54**;533-539.
26. Welzel TM, Graubard BI, Zeuzem S, El-Serag HB, Davila JA, McGlynn KA. Metabolic syndrome increases the risk of primary liver cancer in the United States: a study in the SEER-Medicare database. *Hepatology* 2011;**54**;463-471.
27. Marchesini G, Brizi M, Morselli-Labate AM *et al.* Association of nonalcoholic fatty liver disease with insulin resistance. *Am J Med* 1999;**107**;450-455.
28. Day CP, James OF. Steatohepatitis: a tale of two "hits"? *Gastroenterology* 1998;**114**;842-845.
29. Day CP. Pathogenesis of steatohepatitis. *Best Pract Res Clin Gastroenterol* 2002;**16**;663-678.
30. Yamaguchi K, Yang L, McCall S *et al.* Inhibiting triglyceride synthesis improves hepatic steatosis but exacerbates liver damage and fibrosis in obese mice with nonalcoholic steatohepatitis. *Hepatology* 2007;**45**;1366-1374.
31. Chitturi S, Abeygunasekera S, Farrell GC *et al.* NASH and insulin resistance: Insulin hypersecretion and specific association with the insulin resistance syndrome. *Hepatology* 2002;**35**;373-379.
32. James O, Day C. Non-alcoholic steatohepatitis: another disease of affluence. *Lancet* 1999;**353**;1634-1636.
33. Utzschneider KM, Kahn SE. Review: The role of insulin resistance in nonalcoholic fatty liver disease. *J Clin Endocrinol Metab* 2006;**91**;4753-4761.
34. Tsochatzis E, Papatheodoridis GV, Archimandritis AJ. The evolving role of leptin and adiponectin in chronic liver diseases. *Am J Gastroenterol* 2006;**101**;2629-2640.
35. Tilg H, Hotamisligil GS. Nonalcoholic fatty liver disease: Cytokine-adipokine interplay and regulation of insulin resistance. *Gastroenterology* 2006;**131**;934-945.

36. Browning JD, Horton JD. Molecular mediators of hepatic steatosis and liver injury. *J Clin Invest* 2004;**114**;147-152.
37. Feldstein AE, Canbay A, Angulo P *et al.* Hepatocyte apoptosis and fas expression are prominent features of human nonalcoholic steatohepatitis. *Gastroenterology* 2003;**125**;437-443.
38. Neuschwander-Tetri BA, Caldwell SH. Nonalcoholic steatohepatitis: summary of an AASLD Single Topic Conference. *Hepatology* 2003;**37**;1202-1219.
39. Nonalcoholic steatohepatitis clinical research network. *Hepatology* 2003;**37**;244.
40. Etgen GJ, Oldham BA, Johnson WT *et al.* A tailored therapy for the metabolic syndrome: the dual peroxisome proliferator-activated receptor-alpha/gamma agonist LY465608 ameliorates insulin resistance and diabetic hyperglycemia while improving cardiovascular risk factors in preclinical models. *Diabetes* 2002;**51**;1083-1087.
41. Kleiner DE, Brunt EM, Van Natta M *et al.* Design and validation of a histological scoring system for nonalcoholic fatty liver disease. *Hepatology* 2005;**41**;1313-1321.
42. Goodman ZD. Grading and staging systems for inflammation and fibrosis in chronic liver diseases. *J Hepatol* 2007;**47**;598-607.
43. Bedossa P, Poynard T. An algorithm for the grading of activity in chronic hepatitis C. The METAVIR Cooperative Study Group. *Hepatology* 1996;**24**;289-293.
44. Ishak K, Baptista A, Bianchi L *et al.* Histological grading and staging of chronic hepatitis. *J Hepatol* 1995;**22**;696-699.
45. Ratziu V, Charlotte F, Heurtier A *et al.* Sampling variability of liver biopsy in nonalcoholic fatty liver disease. *Gastroenterology* 2005;**128**;1898-1906.
46. Banner BF, Savas L, Zivny J, Tortorelli K, Bonkovsky HL. Ubiquitin as a marker of cell injury in nonalcoholic steatohepatitis. *Am J Clin Pathol* 2000;**114**;860-866.
47. Zatloukal K, Stumptner C, Fuchsbichler A *et al.* p62 Is a common component of cytoplasmic inclusions in protein aggregation diseases. *Am J Pathol* 2002;**160**;255-263.
48. Lackner C, Gogg-Kamerer M, Zatloukal K, Stumptner C, Brunt EM, Denk H. Ballooned hepatocytes in steatohepatitis: the value of keratin immunohistochemistry for diagnosis. *J Hepatol* 2008;**48**;821-828.
49. Brunt EM, Janney CG, Di Bisceglie AM, Neuschwander-Tetri BA, Bacon BR. Nonalcoholic steatohepatitis: a proposal for grading and staging the histological lesions. *Am J Gastroenterol* 1999;**94**;2467-2474.
50. Levene AP, Goldin RD. Physiological hepatic nuclear vacuolation--how long does it persist? *Histopathology* 2010;**56**;426-429.
51. Abrams GA, Kunde SS, Lazenby AJ, Clements RH. Portal fibrosis and hepatic steatosis in morbidly obese subjects: A spectrum of nonalcoholic fatty liver disease. *Hepatology* 2004;**40**;475-483.
52. Brunt EM, Kleiner DE, Wilson LA *et al.* Portal chronic inflammation in nonalcoholic fatty liver disease (NAFLD): a histologic marker of advanced NAFLD-Clinicopathologic correlations from the nonalcoholic steatohepatitis clinical research network. *Hepatology* 2009;**49**;809-820.
53. Richardson MM, Jonsson JR, Powell EE *et al.* Progressive fibrosis in nonalcoholic steatohepatitis: association with altered regeneration and a ductular reaction. *Gastroenterology* 2007;**133**;80-90.
54. Mazhar SM, Shiehmorteza M, Sirlin CB. Noninvasive assessment of hepatic steatosis. *Clin Gastroenterol Hepatol* 2009;**7**;135-140.

55. Sharma P, Martin DR, Pineda N *et al.* Quantitative analysis of T2-correction in single-voxel magnetic resonance spectroscopy of hepatic lipid fraction. *J Magn Reson Imaging* 2009;**29**;629-635.
56. Brunt EM. Nonalcoholic steatohepatitis. *Semin Liver Dis* 2004;**24**;3-20.
57. Abdelmalek MF, Sanderson SO, Angulo P *et al.* Betaine for nonalcoholic fatty liver disease: results of a randomized placebo-controlled trial. *Hepatology* 2009;**50**;1818-1826.
58. Anstee QM, Goldin RD. Mouse models in non-alcoholic fatty liver disease and steatohepatitis research. *Int J Exp Pathol* 2006;**87**;1-16.
59. Anstee QM, Concas D, Kudo H *et al.* Impact of pan-caspase inhibition in animal models of established steatosis and non-alcoholic steatohepatitis. *J Hepatol* 2010;**53**;542-550.
60. Bancroft JD, Gamble M. *Theory and Practice of Histological Techniques.*: Churchill Livingstone, 2007.
61. Zaitoun AM, Al Mardini H, Awad S, Ukabam S, Makadisi S, Record CO. Quantitative assessment of fibrosis and steatosis in liver biopsies from patients with chronic hepatitis C. *J Clin Pathol* 2001;**54**;461-465.
62. Bley TA, Wieben O, Francois CJ, Brittain JH, Reeder SB. Fat and water magnetic resonance imaging. *J Magn Reson Imaging* 2010;**31**;4-18.
63. El-Badry AM, Breitenstein S, Jochum W *et al.* Assessment of hepatic steatosis by expert pathologists: the end of a gold standard. *Annals of surgery* 2009;**250**;691-697.
64. De Gottardi A, Vinciguerra M, Sgroi A *et al.* Microarray analyses and molecular profiling of steatosis induction in immortalized human hepatocytes. *Lab Invest* 2007;**87**;792-806.
65. Raptis DA, Fischer MA, Graf R *et al.* MRI: the new reference standard in quantifying hepatic steatosis? *Gut* 2012;**61**;117-127.
66. Bradbury MW. Lipid metabolism and liver inflammation. I. Hepatic fatty acid uptake: possible role in steatosis. *Am J Physiol Gastrointest Liver Physiol* 2006;**290**;G194-198.
67. Ran J, Hirano T, Adachi M. Angiotensin II type 1 receptor blocker ameliorates overproduction and accumulation of triglyceride in the liver of Zucker fatty rats. *Am J Physiol Endocrinol Metab* 2004;**287**;E227-232.
68. Reaven GM. Insulin resistance: a chicken that has come to roost. *Ann N Y Acad Sci* 1999;**892**;45-57.
69. Whorwood CB, Donovan SJ, Flanagan D, Phillips DI, Byrne CD. Increased glucocorticoid receptor expression in human skeletal muscle cells may contribute to the pathogenesis of the metabolic syndrome. *Diabetes* 2002;**51**;1066-1075.
70. Morris AA. Mitochondrial respiratory chain disorders and the liver. *Liver* 1999;**19**;357-368.
71. Scheuer PJ, Lefkowitch JH. *Liver Biopsy Interpretation*: Saunders, 2006.
72. Selzner N, Selzner M, Jochum W, Amann-Vesti B, Graf R, Clavien PA. Mouse livers with macrosteatosis are more susceptible to normothermic ischemic injury than those with microsteatosis. *J Hepatol* 2006;**44**;694-701.
73. Ahmed U, Redgrave TG, Oates PS. Effect of dietary fat to produce non-alcoholic fatty liver in the rat. *J Gastroenterol Hepatol* 2009;**24**;1463-1471.

74. Marsman H, Matsushita T, Dierkhising R *et al.* Assessment of donor liver steatosis: pathologist or automated software? *Hum Pathol* 2004;**35**;430-435.
75. Arnault I, Bao YM, Sebagh M *et al.* Beneficial effect of pentoxifylline on microvesicular steatotic livers submitted to a prolonged cold ischemia. *Transplantation* 2003;**76**;77-83.
76. Garcia-Ruiz I, Rodriguez-Juan C, Diaz-Sanjuan T, Martinez MA, Munoz-Yague T, Solis-Herruzo JA. Effects of rosiglitazone on the liver histology and mitochondrial function in ob/ob mice. *Hepatology* 2007;**46**;414-423.
77. Shi Z, Taylor AW, Hu G, Gill T, Wittert GA. Rice intake, weight change and risk of the metabolic syndrome development among Chinese adults: the Jiangsu Nutrition Study (JIN). *Asia Pacific journal of clinical nutrition* 2012;**21**;35-43.
78. Ellingrod VL, Taylor SF, Dalack G *et al.* Risk factors associated with metabolic syndrome in bipolar and schizophrenia subjects treated with antipsychotics: the role of folate pharmacogenetics. *Journal of clinical psychopharmacology* 2012;**32**;261-265.
79. Cuda C, Badawi A, Karmali M, El-Sohemy A. Effects of polymorphisms in nucleotide-binding oligomerization domains 1 and 2 on biomarkers of the metabolic syndrome and type II diabetes. *Genes & nutrition* 2012.
80. Rasic-Milutinovic Z, Perunicic-Pekovic G, Jovanovic D, Gluvic Z, Cankovic-Kadijevic M. Association of blood pressure and metabolic syndrome components with magnesium levels in drinking water in some Serbian municipalities. *Journal of water and health* 2012;**10**;161-169.
81. Jialal I, Huet BA, Kaur H, Chien A, Devaraj S. Increased Toll-Like Receptor Activity in Patients With Metabolic Syndrome. *Diabetes care* 2012.
82. Agyemang C, van Valkengoed IG, van den Born BJ, Bhopal R, Stronks K. Heterogeneity in sex differences in the metabolic syndrome in Dutch white, Surinamese African and South Asian populations. *Diabet Med* 2012.
83. Lao XQ, Zhang YH, Sang Wong MC *et al.* The prevalence of metabolic syndrome and cardiovascular risk factors in adults in southern China. *BMC public health* 2012;**12**;64.
84. Wu PY, Hung CC, Liu WC *et al.* Metabolic syndrome among HIV-infected Taiwanese patients in the era of highly active antiretroviral therapy: prevalence and associated factors. *The Journal of antimicrobial chemotherapy* 2012.
85. Hamaguchi M, Kojima T, Ohbora A, Takeda N, Fukui M, Kato T. Protective effect of alcohol consumption for fatty liver but not metabolic syndrome. *World J Gastroenterol* 2012;**18**;156-167.
86. Ogawa T, Tateno C, Asahina K *et al.* Identification of vitamin A-free cells in a stellate cell-enriched fraction of normal rat liver as myofibroblasts. *Histochem Cell Biol* 2007;**127**;161-174.
87. Puttonen S, Viitasalo K, Harma M. The relationship between current and former shift work and the metabolic syndrome. *Scandinavian journal of work, environment & health* 2012.
88. Luczynski W, Wawrusiewicz-Kurylonek N, Bossowski A *et al.* Transformation of conventional T cells into regulatory T cells in children with metabolic syndrome. *Kardiologia polska* 2011;**69**;1221-1226.
89. Hernandez MI, Mericq V. Metabolic syndrome in children born small-for-gestational age. *Arquivos brasileiros de endocrinologia e metabologia* 2011;**55**;583-589.

90. Janszky I, Vatten L, Romundstad P *et al.* Metabolic syndrome in Poland - the PONS Study. *Annals of agricultural and environmental medicine : AAEM* 2011;**18**;270-272.
91. Anstee QM. Animal models in nonalcoholic steatohepatitis research: utility and clinical translation. *Liver Int* 2011;**31**;440-442.
92. Khan SR. Is oxidative stress, a link between nephrolithiasis and obesity, hypertension, diabetes, chronic kidney disease, metabolic syndrome? *Urological research* 2012.
93. Yokochi M, Watanabe T, Ida K, Yoshida K, Sato Y. Effects of physical exercise prescribed by a medical support team on elderly lower extremity osteoarthritis combined with metabolic syndrome and/or type 2 diabetes. *Geriatrics & gerontology international* 2011.
94. Wender-Ozegowska E, Zawiejska A, Michalowska-Wender G, Iciek R, Wender M, Brazert J. Metabolic syndrome in type 1 diabetes mellitus. Does it have any impact on the course of pregnancy? *Journal of physiology and pharmacology : an official journal of the Polish Physiological Society* 2011;**62**;567-573.
95. Takada-Watanabe A, Yokote K, Takemoto M *et al.* A case of Werner syndrome without metabolic abnormality: implications for the early pathophysiology. *Geriatrics & gerontology international* 2012;**12**;140-146.
96. Sahai A, Malladi P, Melin-Aldana H, Green RM, Whitington PF. Upregulation of osteopontin expression is involved in the development of nonalcoholic steatohepatitis in a dietary murine model. *Am J Physiol Gastrointest Liver Physiol* 2004;**287**;G264-273.
97. Collins S, Martin TL, Surwit RS, Robidoux J. Genetic vulnerability to diet-induced obesity in the C57BL/6J mouse: physiological and molecular characteristics. *Physiol Behav* 2004;**81**;243-248.
98. Deng QG, She H, Cheng JH *et al.* Steatohepatitis induced by intragastric overfeeding in mice. *Hepatology* 2005;**42**;905-914.
99. Feldstein AE, Canbay A, Guicciardi ME, Higuchi H, Bronk SF, Gores GJ. Diet associated hepatic steatosis sensitizes to Fas mediated liver injury in mice. *J Hepatol* 2003;**39**;978-983.
100. Rinella ME, Green RM. The methionine-choline deficient dietary model of steatohepatitis does not exhibit insulin resistance. *J Hepatol* 2004;**40**;47-51.
101. Pais R, Pascale A, Fedchuck L, Charlotte F, Poynard T, Ratziu V. Progression from isolated steatosis to steatohepatitis and fibrosis in nonalcoholic fatty liver disease. *Gastroenterol Clin Biol* 2010.
102. Krishnapuram B, Carin L, Figueiredo MA, Hartemink AJ. Sparse multinomial logistic regression: fast algorithms and generalization bounds. *IEEE Trans Pattern Anal Mach Intell* 2005;**27**;957-968.
103. Tibshirani R. Regression shrinkage and selection via the Lasso. *J Roy Stat Soc B Met* 1996;**58**;267-288.
104. Giral P, Ratziu V, Couvert P *et al.* Plasma bilirubin and gamma-glutamyltransferase activity are inversely related in dyslipidemic patients with metabolic syndrome: relevance to oxidative stress. *Atherosclerosis* 2010;**210**;607-613.
105. Zeng H, MacAulay C, McLean DI, Palcic B, Lui H. The dynamics of laser-induced changes in human skin autofluorescence--experimental measurements and theoretical modeling. *Photochem Photobiol* 1998;**68**;227-236.

106. Wagnieres GA, Star WM, Wilson BC. In vivo fluorescence spectroscopy and imaging for oncological applications. *Photochem Photobiol* 1998;**68**;603-632.
107. Mehrpour M, Esclatine A, Beau I, Codogno P. Autophagy in health and disease. 1. Regulation and significance of autophagy: an overview. *Am J Physiol Cell Physiol* 2010;**298**;C776-785.
108. Harada M, Hanada S, Toivola DM, Ghori N, Omary MB. Autophagy activation by rapamycin eliminates mouse Mallory-Denk bodies and blocks their proteasome inhibitor-mediated formation. *Hepatology* 2008;**47**;2026-2035.
109. Orenstein SJ, Cuervo AM. Chaperone-mediated autophagy: molecular mechanisms and physiological relevance. *Semin Cell Dev Biol* 2010;**21**;719-726.
110. Levine B, Klionsky DJ. Development by self-digestion: molecular mechanisms and biological functions of autophagy. *Dev Cell* 2004;**6**;463-477.
111. Cuervo AM. Autophagy: in sickness and in health. *Trends Cell Biol* 2004;**14**;70-77.
112. Qu X, Zou Z, Sun Q *et al.* Autophagy gene-dependent clearance of apoptotic cells during embryonic development. *Cell* 2007;**128**;931-946.
113. Komatsu M, Waguri S, Ueno T *et al.* Impairment of starvation-induced and constitutive autophagy in Atg7-deficient mice. *J Cell Biol* 2005;**169**;425-434.
114. Mizushima N, Levine B, Cuervo AM, Klionsky DJ. Autophagy fights disease through cellular self-digestion. *Nature* 2008;**451**;1069-1075.
115. Neufeld TP. TOR-dependent control of autophagy: biting the hand that feeds. *Curr Opin Cell Biol* 2010;**22**;157-168.
116. Suzuki K, Kubota Y, Sekito T, Ohsumi Y. Hierarchy of Atg proteins in pre-autophagosomal structure organization. *Genes Cells* 2007;**12**;209-218.
117. Noda T, Ohsumi Y. Tor, a phosphatidylinositol kinase homologue, controls autophagy in yeast. *J Biol Chem* 1998;**273**;3963-3966.
118. Lonardo A, Adinolfi LE, Loria P, Carulli N, Ruggiero G, Day CP. Steatosis and hepatitis C virus: mechanisms and significance for hepatic and extrahepatic disease. *Gastroenterology* 2004;**126**;586-597.
119. Gozuacik D, Kimchi A. Autophagy and cell death. *Curr Top Dev Biol* 2007;**78**;217-245.
120. Maiuri MC, Zalckvar E, Kimchi A, Kroemer G. Self-eating and self-killing: crosstalk between autophagy and apoptosis. *Nat Rev Mol Cell Biol* 2007;**8**;741-752.
121. Pua HH, Dzhagalov I, Chuck M, Mizushima N, He YW. A critical role for the autophagy gene Atg5 in T cell survival and proliferation. *J Exp Med* 2007;**204**;25-31.
122. Wang Y, Singh R, Xiang Y, Czaja MJ. Macroautophagy and chaperone-mediated autophagy are required for hepatocyte resistance to oxidant stress. *Hepatology* 2010;**52**;266-277.
123. Moore A, Donahue CJ, Bauer KD, Mather JP. Simultaneous measurement of cell cycle and apoptotic cell death. *Methods Cell Biol* 1998;**57**;265-278.
124. Jelluma N, Yang X, Stokoe D, Evan GI, Dansen TB, Haas-Kogan DA. Glucose withdrawal induces oxidative stress followed by apoptosis in glioblastoma cells but not in normal human astrocytes. *Mol Cancer Res* 2006;**4**;319-330.
125. Martin S, Parton RG. Lipid droplets: a unified view of a dynamic organelle. *Nat Rev Mol Cell Biol* 2006;**7**;373-378.

126. Ding WX, Li M, Chen X *et al.* Autophagy reduces acute ethanol-induced hepatotoxicity and steatosis in mice. *Gastroenterology* 2010;**139**;1740-1752.
127. Ford ES, Giles WH, Dietz WH. Prevalence of the metabolic syndrome among US adults: findings from the third National Health and Nutrition Examination Survey. *JAMA* 2002;**287**;356-359.
128. Cuervo AM, Bergamini E, Brunk UT, Droge W, Ffrench M, Terman A. Autophagy and aging: the importance of maintaining "clean" cells. *Autophagy* 2005;**1**;131-140.
129. Liu HY, Han J, Cao SY *et al.* Hepatic autophagy is suppressed in the presence of insulin resistance and hyperinsulinemia: inhibition of FoxO1-dependent expression of key autophagy genes by insulin. *J Biol Chem* 2009;**284**;31484-31492.
130. Yang L, Li P, Fu S, Calay ES, Hotamisligil GS. Defective hepatic autophagy in obesity promotes ER stress and causes insulin resistance. *Cell Metab* 2010;**11**;467-478.
131. Yousefi S, Perozzo R, Schmid I *et al.* Calpain-mediated cleavage of Atg5 switches autophagy to apoptosis. *Nat Cell Biol* 2006;**8**;1124-1132.